

Dissertation

Submitted to the

Combined Faculty of Natural Sciences and Mathematics

Heidelberg University, Germany

for the degree of

Doctor of Natural Sciences (Dr. rer. nat.)

Presented by

M. Sc. Wei Huang

Oral examination: June 14th, 2019

**Novel Conjugated Polymers: Synthesis and
Application as Sensor Arrays for Detection and
Discrimination of Nitroaromatics**

Gutachter: Prof. Dr. Uwe H. F. Bunz

Prof. Dr. Milan Kivala

Acknowledgement

Firstly, I would like to show my best regards to my super talented supervisor, Prof. Dr. Uwe H. F. Bunz, such a respectable, responsible and resourceful scholar. Working in AK Bunz is not just a job, actually it is a wonderful adventure in my life. Prof. Bunz has support me with the most valuable guidance in every stage of the working and writing of this thesis. Without his genius instruction, impressive kindness and patience, it could so hard to finish my thesis. His keen and vigorous academic observation enlightens me not only in this thesis but also in my future study. I also want to express my deep gratitude to Dr. Kai Seehafer for his open attitude and kind help during the time of my research. His professional and smart advices contribute a lot to my works. I would like to thank Prof. Dr. Milan Kivala for his kindness as my second evaluator for this dissertation.

Prof. Rasmus R. Schröder, Dr. Irene Wacker and Mr. Ernest Ronald Curticean (Cryo Electron Microscopy, BioQuant, Universitätsklinikum Heidelberg) have my sincere gratitude as my collaborators. Their very professional work allows my comprehensive and convincing. Especially, Dr. Irene Wacker encourages me with her super enthusiasm to work and the spirit of seeking truth, which leads me to be a better researcher.

I would like to thank Mrs. Kerstin Windisch, Kerstin Brödner and Olena Tverskoy, Mr. Holger Lambert for their kindly help and effective organization to provide us a highly ordered and organized working circumstance. I would also like to thank all employees of the OCI for their kind help in chemicals and measurements, including Chemikalienausgabe, MS analysis, NMR spectra and elemental analysis, and also administration departments.

I would like to thank my intelligent colleagues, Dr. Markus Bender, Dr. Benhua Wang, Dr. Jinsong Han, Gaozhan Xie, Hao Zhang, Dr. Yury Kozhemyakin, Sebastian Hahn, Soh Kushida, Emanuel Smarsly, Dr. Jan Freudenberg, Maximilian Bojanowski and Dr. Allan Bastos for their kind advices and valuable discussions during my research. It is a joy to communicate with Dr. Markus Bender. He stunned me with his intelligence, extensive knowledge and also handsome appearance. It's such a pleasure to know him. I also want to extend my thanks to the whole working group members for the friendly cooperation and

general guidance that build the foundation for finishing this dissertation. I'm so lucky to have these very great persons as my colleagues. I also want to thanks Jua, my Zumba dance teacher. He is such a talent and gives me such a good time during the hard research life.

I would especially like to thank my dear friends, Weiwei Chen, Benhua Wang, Jing Liang, Shuaichen Jin and Simin Fang who are always there to support and encourage me. Weiwei, my dearest friend, is so patient to hear about all my complaining and give me the deepest understood. Having her as my friend is one of the best things I have ever done in my life. I'm so lucky to have these wonderful females as my friends. Benhua, as my friend and colleague, accompany me over the three long and lonely years. I'm so grateful to her.

Finally, my beloved family. My great parents are so open-minded, tolerant and lovely. Their support, care and love make me stand on the solid ground and keep optimistic whatever I come through. The love of my life, my husband Shengliang Zhang, is the person I owe the most. However three years separated life test our true love. Distance only makes the hearts grow fonder. With his love and tolerance, I feel safe to go anywhere and be the person I want to be. Because I know whenever I look back he will be always there for me. I have a home called him. Thanks to his selfless and endless love and company.

I am very grateful to the CSC (Chinese Scholarship Council) for their financial support of my Ph.D. research.

Abstract

This thesis evaluates three novel synthesized conjugated polymer series with respect to their sensitivity and selectivity in the detection of nitroaromatic analytes, especially in aqueous environments.

Central building blocks of the polymers are functionalized truxene or tetraphenylethene centers, which are polycondensed with different diethynylaromatics by Sonogashira cross-coupling.

In a first explorative study, Truxene-based hyper-branched polymers (**HCPs**) were compared with related linear rod-shaped poly(*p*-phenylenethynylenes) (**PPEs**) with respect to their sensor performance of nitroaromatics (Chapter 2). By encapsulation with amphiphilic **F-127** in water-soluble micelles, 14 nitroaromatics could be distinguished with 100% accuracy in fluorescence quenching experiments. The **HCPs** display a better sensor performance than the sensor system for nitroaromatics previously known from **PPE** (Chapter 2). To increase the sensor performance, tetraphenylethene cores (**TPEs**) replaced the truxene units in the polymers in a follow-up study (Chapter 3). **TPEs** use aggregate-induced emission to detect the analytes. A sensor field based on four **TPE** polymers was able to detect and distinguish nitroaromatics in water with excellent sensitivity (ppm range) compared to **HCP** or **PPE** systems (Chapter 3). This improved system is able to detect the regioisomers of nitroaromatics in a specific way. Finally, the performance of the **TPE** system was improved by varying the **TPE** moiety with amino or nitro groups for aqueous detection (Chapter 4). The functional **TPE** polymers (**F-TPEPs**) also exhibit aggregate-induced emission, with enhanced pH-specific (amino groups) or solvatochrome (nitro groups) sensor sensitivity. The presence of amino groups improves the sensory properties of **F-TPEPs** in the aqueous nitroaromatic system. The challenge of the detection of nitroaromatics in water could be mastered by the systematic development of **F-TPEPs** sensor system from the well-known **PPE** sensor.

Zusammenfassung

Diese Arbeit evaluiert zwei neuartig synthetisierte, konjugierte Polymererien hinsichtlich ihrer Sensitivität und Selektivität bei der Detektion von nitroaromatischen Analyten, v.a. im wässrigen Milieu.

Zentrale Bausteine der Polymere bilden funktionalisierte Truxen- bzw. Tetraphenylethenzentren, die mit verschiedenen Diethinylaromaten durch Sonogashira Kreuzkuppelung polykondensiert wurden.

In einer ersten explorativen Studie wurden hoch verzweigte Truxen-basierte Polymere (**HCPs**) mit den verwandten, linearen stabförmigen Poly(*p*-phenylenethinyl)en (**PPEs**) hinsichtlich ihrer Sensorleistung von Nitroaromaten verglichen (Kap.2). Durch Verkapselung mit amphiphilen **F-127** in wasserlösliche Mizellen konnten 14 Nitroaromaten bei Fluoreszenzlöschexperimenten mit 100% Genauigkeit unterschieden werden. Die **HCPs** weisen eine bessere Sensorleistung als die bisher von **PPE** bekannte Sensorik zu Nitroaromaten auf (Kap. 2). Zur Steigerung der Sensorleistung ersetzten Tetraphenylethenkerne (**TPEs**) in einer Folgestudie die Truxeneinheiten in den Polymeren (Kap. 3). **TPEs** nutzen Aggregat-induzierte Emission zur Detektion der Analyten. Ein Sensorfeld auf Basis von vier **TPE**-Polymeren konnte Nitroaromaten in Wasser mit ausgezeichneter Empfindlichkeit (ppm-Bereich) im Vergleich zu **HCP** bzw. **PPE**-Systemen erkennen und unterscheiden (Kap. 3). Dieses verbesserte System kann Regioisomere der Nitroaromaten gezielt detektieren. Abschließend wurde die Leistung des **TPE**-Systems durch Variation der **TPE**-Kerne mit Amino- bzw. Nitro-Gruppen für die wässrige Detektion verbessert (Kap. 4). Die funktionellen **TPE**-Polymere (**F-TPEPs**) weisen weiterhin Aggregat-induzierte Emission auf, die pH-Wert-spezifische (Aminogruppen) oder solvatochrome (Nitrogruppen) Sensorempfindlichkeitssteigerungen zeigen. Das Vorhandensein von Aminogruppen verbessert die Sensorik von **F-TPEPs** im wässrigen System für die Nitroaromatik. Die Herausforderung der Detektion von Nitroaromaten in Wasser konnten durch gezielte Entwicklung des **F-TPEPs** Sensorsystems vom bekannten **PPE**-Sensor.

Publications

Wei Huang, Emanuel Smarsly, Jinsong Han, Markus Bender, Kai Seehafer, Irene Wacker, Rasmus R. Schröder, and Uwe H. F. Bunz, Truxene-Based Hyperbranched Conjugated Polymers: Fluorescent Micelles Detect Explosives in Water. *ACS Appl. Mater. Interfaces* **2017**, 9, 3068-3074.

Wei Huang, Markus Bender, Kai Seehafer, Irene Wacker, Rasmus R. Schröder and Uwe H. F. Bunz, A Tetraphenylethene-Based Polymer Array Discriminates Nitroarenes. *Macromolecules* **2018**, 51, 1345–1350.

Wei Huang, Markus Bender, Kai Seehafer, Irene Wacker, Rasmus R. Schröder and Uwe H. F. Bunz, Novel Functional TPE Polymers: Aggregation-Induced Emission, pH Response, and Solvatochromic Behavior. *Macromol. Rapid Commun.* **2018**, DOI: 10.1002/marc.201800774.

Jinsong Han, Benhua Wang, Markus Bender, Jessica Pfisterer, **Wei Huang**, Kai Seehafer, Mahdiah Yazdani, Vincent M. Rotello, Caren M. Rotello and Uwe H. F. Bunz, Fingerprinting antibiotics with PAE-based fluorescent sensor arrays. *Polym. Chem.* **2017**, 8, 2723-2732.

Jinsong Han, Haoran Cheng, Benhua Wang, Markus Santhosh Braun, Xiaobo Fan, Markus Bender, **Wei Huang**, Cornelius Domhan, Walter Mier, Thomas Lindner, Kai Seehafer, Michael Wink and Uwe H. F. Bunz, Han J, Cheng H, Wang B, et al. A Polymer/Peptide Complex- Based Sensor Array That Discriminates Bacteria in Urine. *Angew. Chem. Int. Ed* **2017**, 56, 15246-15251.

Abbreviations

AIE	aggregation induced emission
CDNB	1-chloro-2,4-nitrobenzene
CPEs	conjugated polyelectrolytes
CPs	conjugated polymers
CV	cyclic voltammetry
DET	Dexter energy transfer
DNT	dinitrotoluene
FRET	Förster Resonance Energy Transfer
GC-MS	gas chromatography-mass spectrometry
GPC	gel permeation chromatography
HCPs	hyperbranched conjugated polymers
HPLC	high-performance liquid chromatography
HR-MS	high resolution mass spectra
HCA	hierarchical cluster analysis
ICT	intermolecular charge transfer
LDA	linear discriminant analysis
MANOVA	multivariate analysis of variance
mCNB	3-chloro-2-nitrobenzene
mDNB	1,3-dinitrobenzene
mNA	3-nitroaniline
MS	mass spectrometry
NACs	nitroaromatic compounds
NA	nitroaniline
NB	nitrobenzene
NIR	near-infrared spectroscopy
NMR	Nuclear magnetic resonance
NP	nanoparticle
oCNB	1-chloro-2-nitrobenzene
oDNB	1,2-dinitrobenzene
oNA	2-nitroaniline

ONCB 2-nitrochlorobenzene
oNP 2-nitrophenol
pNP 4-nitrophenol
PA polyacetylene (Chapter 1); Picric acid(Chapter 2-4)
PCA principal component analysis
PDI polydispersities
PET photo-induced electron transfer
PF poly(fluorene)
PFP polyfluorene-1,4-phenylene
PPE poly(*para*-phenyleneethynylene)
PPP poly(*para*-phenylene)
PPV poly(*para*-phenylenevinylene)
PPy polypyrrole
PT polythiophene
RT room temperature
SW swallowtail (oligoethyleneglycol side-chains)
TLC thin layer chromatography
TMS Trimethylsilyl
TNT 2,4,6-trinitrotoluene
TPEPs Tetraphenylethene based polymers
UV-Vis ultraviolet-visible spectrophotometry
calcd. calculated
d days
h hours
min minutes
 Φ fluorescence quantum yields
 τ fluorescence lifetime
 δ chemical shift

Table of Contents

Abstract.....	V
Publications	VII
Abbreviations	VIII
Table of Contents	X
Chapter 1. Introduction	1
1.1 Conjugated Polymers.....	2
1.1.1 Introduction of Conjugated Polymers.....	2
1.1.2 Synthesis of Conjugated Polymers	3
1.1.3 Optical and Electronic Properties of Conjugated polymers	4
1.2 Application of Conjugated Polymers as Sensors.....	6
1.2.1 Introduction of Sensors	6
1.2.2 Single Sensors and Sensor Arrays.....	7
1.2.3 Conjugated Polymers in Sensor Application.....	8
1.2.4 Sensor Array based on Fluorescent Conjugated Polymers.....	10
1.3 Nitroaromatics: Detection and Discrimination	13
1.3.1 Nitroaromatics and Their Detection Approach	14
1.3.2 Polymeric Sensors for Nitroaromatics Detecion and Discrimination.....	15
1.4 Sensing Mechanism of Conjugated Polymers to Nitroaromatics	18
1.4.1 Fluorescence Quenching Mechanism.....	18
1.4.2 Fluorescence Quenching Theory	19
1.5 Objective	21
Chapter 2. Truxene-Based Conjugated Polymers and Fluorescent Micelles Detect Nitroaromatics	22
2.1 Truxene-based Polymers	24
2.2 Hyperbranched Truxene Polymers and Poly(<i>para</i>-phenylene-ethynylene)s	26

2.2.1 Synthesis of Monomers, HCPs and PPEs	26
2.2.2 Molecular and Photophysical Properties of the Polymers	27
2.3 Detection and Discrimination in Organic and Water Milieus	29
2.3.1 Detection and Discrimination of Nitroaromatics in Organic Solvents.....	29
2.3.2 Detection and Discrimination Nitroaromatics in Water by Fluorescent Micelles.....	36
2.4 Conclusion.....	44
Chapter 3. A Tetraphenylethene-Based Polymer Array: Detect and Discriminate Nitroaromatics	45
3.1 Aggregation-Induced Emission and TPE Moiety.....	47
3.2 Synthesis and Characterization of TPEPs	50
3.3 Detection of Nitroaromatics by the TPEPs	55
3.4 Discrimination of Nitroaromatics by TPEPs	62
3.5 Conclusion.....	65
Chapter 4. Functional TPE Polymers: Aggregation-Enhanced Emission, pH Response, Solvatochromic and Nitroaromatics Sensing	67
4.1 Functionalization on the TPE moiety	69
4.2 Synthesis and Characterization of Functional Polymers	70
4.3 AIE effect of P1-P4 and Solvatochromism of P4.....	75
4.4 pH Response of P1-P3	78
4.5 Detection of Nitroaromatics based on P1-P4	80
4.6 Discrimination of Nitroaromatics based on P1-P3.....	86
4.7 Conclusion.....	89
Chapter 5. Summary and Outlook.....	90
5.1 Summary	91
5.2 Outlook.....	92

Chapter 6. Experimental Section	94
6.1 General Remarks.....	95
6.2 Synthesis Details and Analytical Data	100
6.2.1 Synthesis of HCPs and PPEs (Chapter 2).....	100
6.2.2 Synthesis of TPEPs (Chapter 3).....	104
6.2.3 Synthesis of F-TPEPs (Chapter 4).....	106
6.3 NMR Spectra	111
6.3.1 ¹ H NMR spectra (Chapter 2)	111
6.3.2 ¹ H NMR spectra (Chapter 3)	115
6.3.3 ¹ H NMR spectra (Chapter 4)	124
6.4 Linear Discriminant Analysis	131
6.4.1 LDA Calculation (Chapter 2)	131
6.4.2 LDA Calculation (Chapter 3)	136
6.4.3 LDA Calculation (Chapter 4)	140
References	144

Chapter 1. Introduction

1.1 Conjugated Polymers

1.1.1 Introduction of Conjugated Polymers

Conjugated polymers (CPs) are organic macromolecules characterized by a backbone of alternating single- and double- or triple-bonds. The overlapping π -orbitals of CPs create a system of delocalised π -electrons. Over the past decades, CPs have emerged as one of the most important classes of transduction materials.¹ They transform a chemical signal into an easily detected electrical or optical signal. CPs have been widely applied into organic light-emitting diodes (OLEDs)²⁻⁴, field effect transistors⁵, solar cells⁶⁻⁷, and fluorescent chemical and biological sensors.⁸⁻¹⁰ Based on the difference of their backbones, various types of CPs have been designed and studied. Structures of the most reported CPs are shown in Figure 1, including poly(*para*-phenylene) (PPP), poly(*para*-phenylenevinylene)(PPV), poly(*para*-phenyleneethynylene) (PPE), polythiophene (PT), polypyrrole (PPy), polyaniline (PANI), poly(fluorene) (PF) and polyacetylene (PA). In addition, tremendous numbers of CPs with unique, tunable electronic and optical properties were designed and synthesized for specific application. To improve the chemical and physical properties, constructing of new CPs is quite attractive.

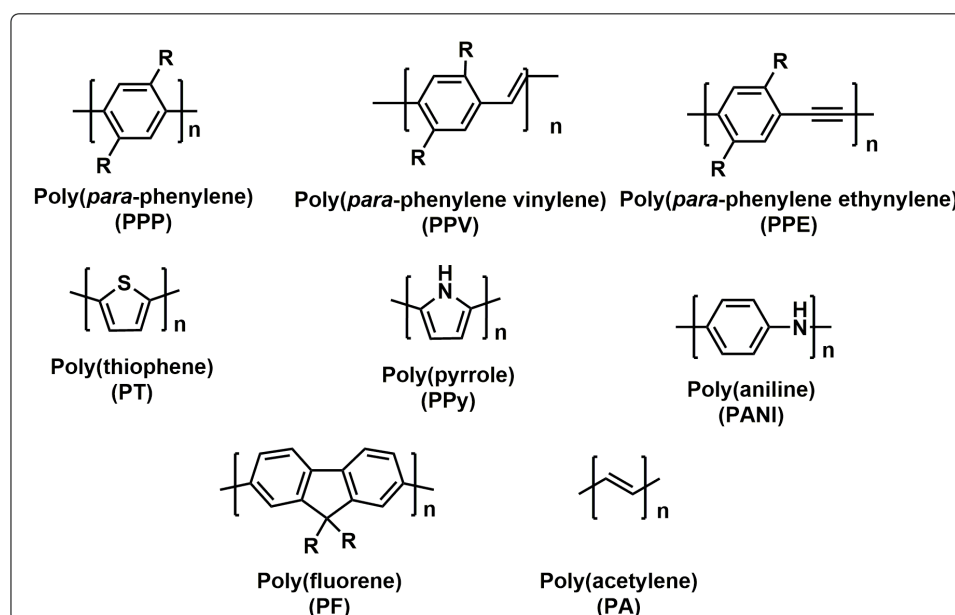


Figure 1. Molecular structures and backbones of typical conjugated polymers.

1.1.2 Synthesis of Conjugated Polymers

The constructions of CPs rely on the efficient carbon-carbon single bond formation between two unsaturated carbons in aromatic units. Polymers with structural variety can be easily accessed by diverse synthetic routes. Oxidative polymerizations have been extensively used to synthesize heteroaromatic ring polymers such as polythiophene and polypyrrole.¹¹ However, this method suffers from an inevitable defect, that the structures of polymer are undirected and undefined. It's usually very hard to control linkage position or the degree of branching or cross-linking.¹²⁻¹⁴ Transition-metal-catalyzed cross-coupling reactions provide a huge scope for polymerization.¹⁵ In general, the reaction involves a transition-metal-catalyzed oxidative addition reaction across the C-X bond of an electrophile and then transmetalation with a main group organometallic nucleophile, followed by a reductive elimination step leading to the carbon-carbon bond formation.¹⁶ The well-known coupling reaction includes Grignard reaction, Kumada coupling, Yamamoto coupling, Sonogashira coupling, Stille cross coupling, Suzuki reaction, Buchwald-Hartwig reaction and so on.¹⁷⁻²⁰ One of the most common methods for the polymerization is palladium catalyzed Sonogashira coupling. The mechanism of Sonogashira coupling is shown in Figure 2. The advantage of Sonogashira coupling includes mild reaction conditions, the tolerance to functional groups, and capability to produce different backbone structures. It is employed in synthesis of conjugated polymers in this work.

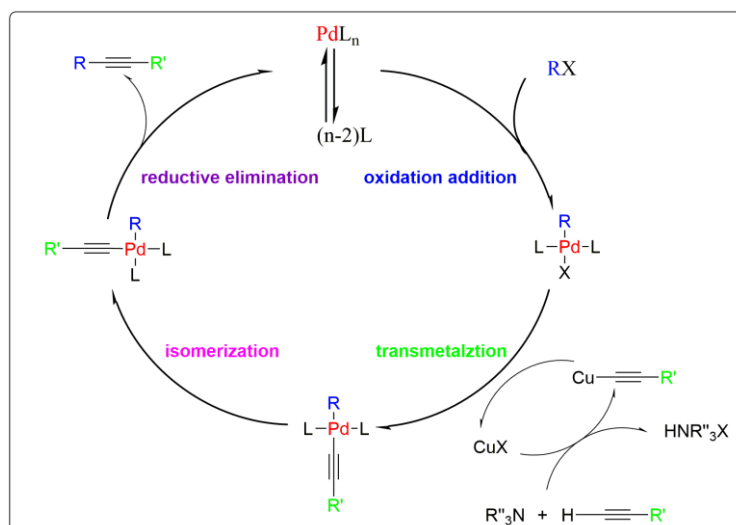


Figure 2. Mechanism of Sonogashira coupling.

1.1.3 Optical and Electronic Properties of Conjugated polymers

CPs have a backbone with a delocalized electronic structure. In comparison to small molecule counterparts, the excitation energy along the whole backbone of the CPs transferring to lower energy electron/energy acceptor sites over long distances results in the high conductivity and amplified fluorescence signal.²¹ The nature of conjugated system, the conjugation length, regio-regularity and the substituent(s), inter alia, may all influence the optical and electronic properties of conjugated polymers.¹⁵

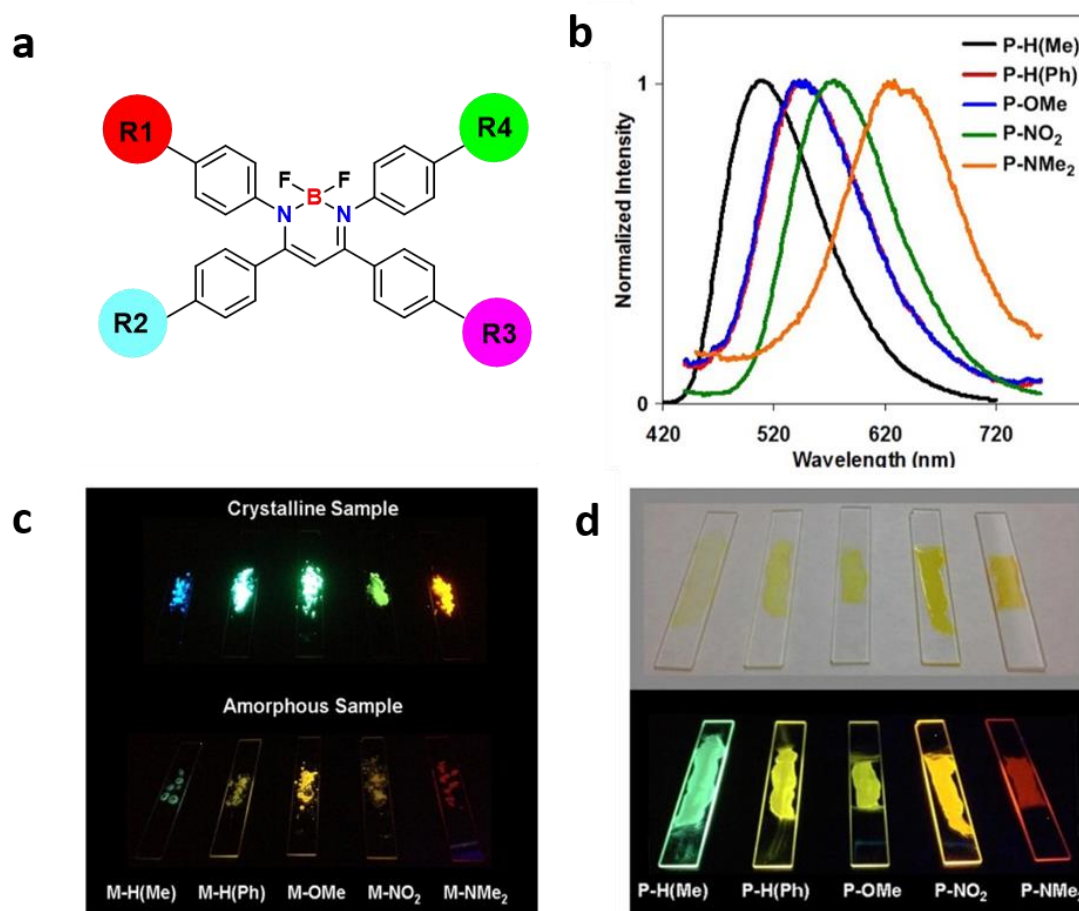


Figure 3. a) The structure of boron diiminates derivatives with different side groups. b) PL spectra of the synthesized polymers in the thin-film state upon excitation at each absorption maximum. c) photographs of boron diiminates in crystalline and amorphous states under UV irradiation. d) photographs of the synthesized polymers in the film state under the UV irradiation. Reproduced with permission from ref.22 © 2014 American Chemical Society.

The optical properties of conjugated polymers are depending on their molecular conformation and aggregation (in film or solvent). For optical applications, the emission color of the

material is basically determined by the construction of polymer, thus the color tuning and efficiency can be controlled by changing molecular structures. One example of fine color tuning is shown in Figure 3. The boron diimines derivatives exhibit aggregation-induced emission (AIE) and crystallization-induced emission enhancement (CIEE) properties.²² The emission spectra of resulting molecules were efficiently modulated by introducing different substituents. Dimethylamino group (strong electron-donating substituents) induces a large red-shifted emission (from 478 nm to 645 nm). A variety of the molecules' conformations results in diverse optical and electrical properties. Looking into the rules for how the properties relate to the structure is one of the most interesting and profound topic in organic material science.

The fluorescence etc. properties of the polymers are changed by the surrounding environment, such as temperature, humidity, pH values or the reaction with other substances. By changing those factors, a variety of chemical properties of the CPs will take place, revealing as a mutative chemical signal. The chemical signal of CPs can be transformed into an optical or electrical signal, which is easily measured. Therefore, CPs are super sensory materials, which are sensitive to the surrounding environment. Fluorescent conjugated polymers have been reported as effective sensory materials according to their fluorescent changes to targeted analytes. They have been applied successfully in detecting and discriminating small molecules, complexed samples, such as foods, beverages, medicines or even biological species such as proteins or cells.

1.2 Application of Conjugated Polymers as Sensors

1.2.1 Introduction of Sensors

From the touching screen on the smart phone, to the meters for blood glucose tips, sensors are indispensable in our daily lives. Invention of good sensors with high sensitivity, accuracy and quick-response are always hot topics to the scientists and engineers. The function of a sensor is to provide information about the chemical, physical or biological environment (shown in Figure 4).²³ The response to the environment will be turned into signal such as optical or electronic signal to easily measure and quantify.



Figure 4. Sensors application in daily life.

Physical sensors: Physical sensors have been used in the many fields, to name a few: ambient light sensors on the portable personal electronics could adjust brightness on the surroundings; pressure sensors on the aircrafts for the monitor the flight safety; temperature sensor for a reliable weather forecast. Physical sensors also involve in light, sound, motion, temperature, pressure, gravity, humidity, moisture, vibration, magnetic and other physical aspects. Potentiometers and force-sensing resistors are widely used including manufacturing and machinery, such as smart phones, airplanes, cars, medicine, robotics and so on.

Chemical sensors: A chemical sensor is a device that transforms chemical information into an analytically useful signal.²⁴ The chemical information contains composition of environment, presence and concentration of certain chemical species. They can have applications in different areas such as medicine (quantify, over-dosage, counterfeit medicine),²⁵⁻²⁶ home safety (explosives, poison, smoke detector),²⁷⁻²⁸ environmental pollution (sulfur dioxide, chlorofluorocarbons, heavy metals, herbicides, pesticides) and many others.²⁹⁻

32

Biological sensors: Biosensors are analytical devices for the detection of analytes combining a biological component such as enzymes, nucleic acids, protein, antibodies, microorganisms, organelles, cells and tissue, etc. The applications of biosensor cover the fields of glucose monitoring, food analysis, DNA determination, bacteria detection and metastatic cancer cell biosensors.

1.2.2 Single Sensors and Sensor Arrays

To build an effective sensor, various requirements should be fulfilled for different applications. Generally, the common requirements are high sensitivity, high accuracy and linearity, wide bandwidth, interference rejection, low power consumption and a low price. Basically, molecular recognition involves the interactions between molecules: i.e. bond formation, acid-base interactions, hydrogen-bonding, dipolar and multipolar interactions, π - π molecular complexation, Van der Waals interaction or physical adsorption. Sensors are typically responsive to certain kind of analytes, in other words for single detection (targeted molecular recognition). However under complex situation, a sensor array must not only detect but also discriminate analytes with similar characters. A sensor array is a series of sensors, after collecting and processing signals, forming a unique pattern of response.

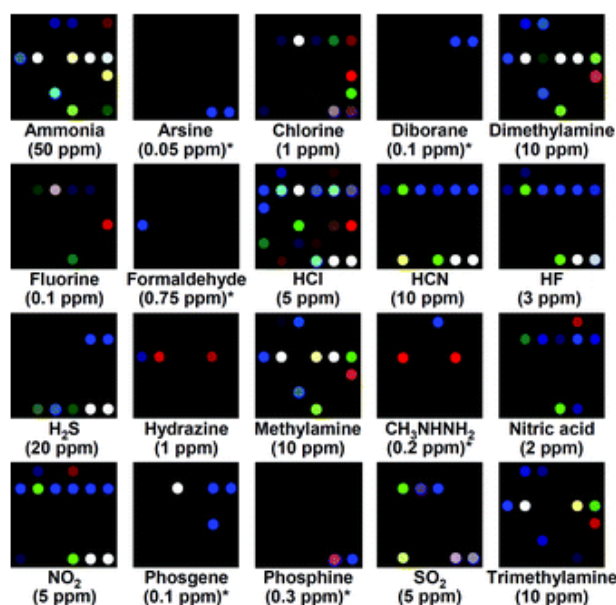


Figure 5. Color difference maps of representative TICs at their PEL concentration after 5 min of exposure at 50% relative humidity and 298 K. Adapted with permission from ref. 35 © 2010 the Royal Society of Chemistry.

The advantage of a sensor array compared to single sensor is that it can add new dimensions to the observation. Each sensor has a feedback to the analytes, the addition of sensors would produce more parameters. The sensor array based on a number of sensors can improve detecting performance and help to handle more complex situation. With a series of sensors, we can build up sensor array as chemical tongue or nose. A lot of researches about colorimetric sensor array have been reported to visualize the odour or taste.³³⁻³⁴ Figure 5 show a colorimetric sensor array for identification of toxic gases based on chemically responsive dyes.³⁵

1.2.3 Conjugated Polymers in Sensor Application

The field of chemical sensing is becoming more dependent upon novel materials. Polymers, crystals, glasses and particles have made a profound impact on modern sensory systems with a superior performance. As known, a chemosensor is composed of two functional elements, a receptor and a reporter group. However, the simple receptor-analyte detection has the disadvantage of slow dissociation kinetics resulting from reorganization and high association constants. A chemosensor with slow kinetics cannot yield a real-time response.³⁶ This shortcoming can be overcome by multiple chemosensors with a molecular wire approach. The

mechanisms of traditional single chemosensor and molecular wire effect are illustrated in Figure 6.³⁶ The sensory signal amplification in a molecular wire approach can be explained by a collective system response along the conjugated polymer wire.

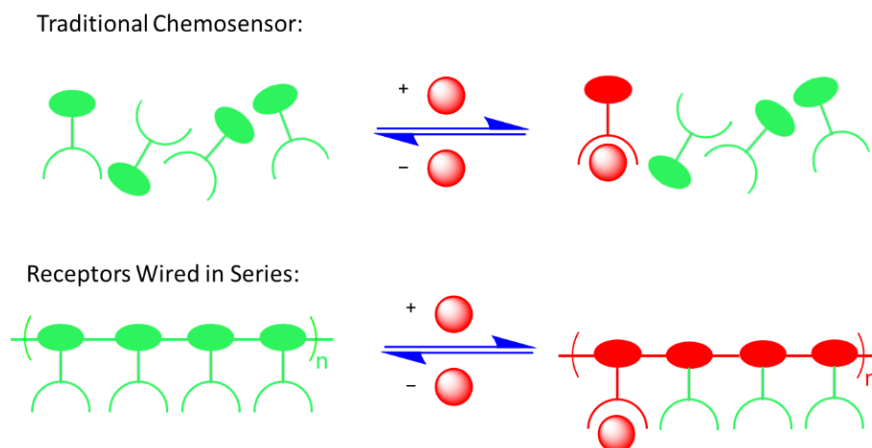


Figure 6. Traditional chemosensor and multiple chemosensor sensing mechanism. Figure reproduced with permission from ref. 36 © 1998, American Chemical Society.

The interaction between conjugated polymers and analytes can result in superquenching and produce amplified signal, thus the polymers are referred to amplifying fluorescent polymers (AFPs). As sensing materials, the excitation energy along the whole backbone of the CPs transfer to lower energy acceptor sites over long distances, resulting in the amplified fluorescence signal compared to small molecule counterparts. AFPs have been applied in many sensing fields, including detections of small ions,³⁷⁻³⁸ explosives,^{28, 39} small biomolecules,⁴⁰⁻⁴¹ proteins,⁴²⁻⁴³ DNA,⁴⁴⁻⁴⁵ and so on. Beyond these single analytes, the sensor array based on conjugated polymers are also reported to detect and discriminate complicated real samples such as beverages (white wines, red wines, whiskies, brandies, cola, tea, juices, honeys),⁴⁶⁻⁴⁹ drugs (antibiotics, non-steroidal anti-inflammatories).⁵⁰⁻⁵¹

Besides molecular wire effect, multivalency effect has also been reported by Bunz's group in 2005. The carboxylate-substituted conjugated polymer is prepared with highly negative charges. The multivalent effect happens between the polymer and lead ions, resulting in superb efficient lead detection. Therefore, multivalency effect is another approach for detection of small ions.⁵²

1.2.4 Sensor Array based on Fluorescent Conjugated Polymers

Identification and recognition of different kinds of small molecular analytes with fluorescent polymer sensors have been widely investigated, including ions, explosives, acids, amines, drugs, etc. The groups of Swager,⁵³⁻⁵⁴ Suslick,⁵⁵⁻⁵⁶ Anzenbacher⁵⁷⁻⁵⁹ and Anslyn⁶⁰⁻⁶¹ have made great contributions to this field during the past decade. The discrimination of proteins by fluorescent polymer is illustrated in Figure 7. Solutions of the fluorescent polymers were exposed to the analytes (proteins) and the fluorescence changes were recorded. After calculation, a unique quenching response pattern formed and discrimination could be visualized after processing the data by statistical analysis and modeling.⁶²

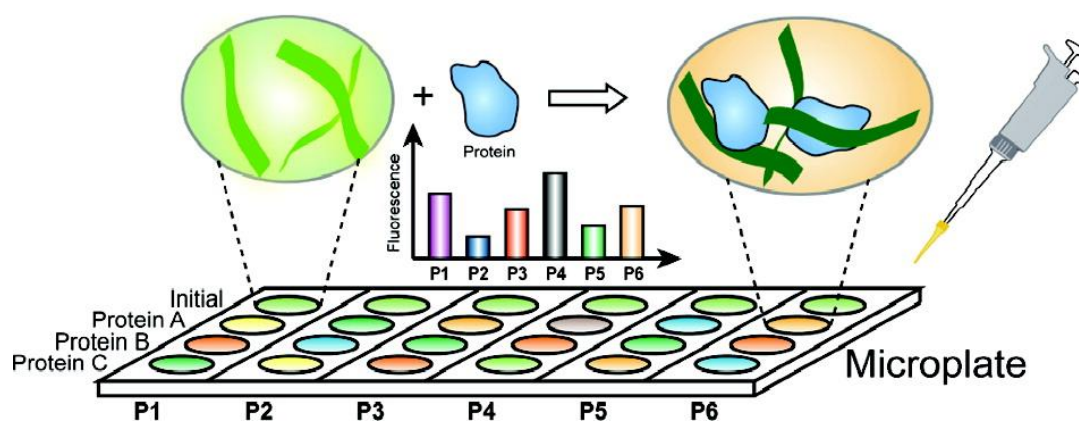


Figure 7. A sensor array to detect and identify protein analytes Adapted with permission from ref. 62 © 2007, American Chemical Society.

Sensor arrays based on chemical properties have intrinsically a high dimensional data from the indicators to the analytes.⁶⁴ Statistic methods for multidimensional data share the common goals of displaying multidimensional data effectively, evaluating data sets, and predicting the identity of unidentified samples based on a known library.⁶³ Hierarchical cluster analysis (HCA), principal component analysis (PCA), and linear discriminant analysis (LDA) are the most common approaches to deal with high dimensional data.

HCA is an agglomerative clustering technique whereby clusters are determined from the Euclidean distance between experimental data. The resultant dendrogram shows connectivity and some distance between each of the analytes. Connectivity explains relationship similarity of different species of analytes, saying ‘what samples are similar to each other?’ and distance explains magnitude, saying ‘how similar are they?’. Figure 8a shows a HCA dendrogram

from HCA of the colorimetric array responses to 100 common organic compounds.⁶⁴⁻⁶⁵ The primary limitation of HCA is that it is hardly to quantify analytes and predicting unknown samples. In most cases, it is applied as an auxiliary method for cluster observation of similar analytes.⁶⁶

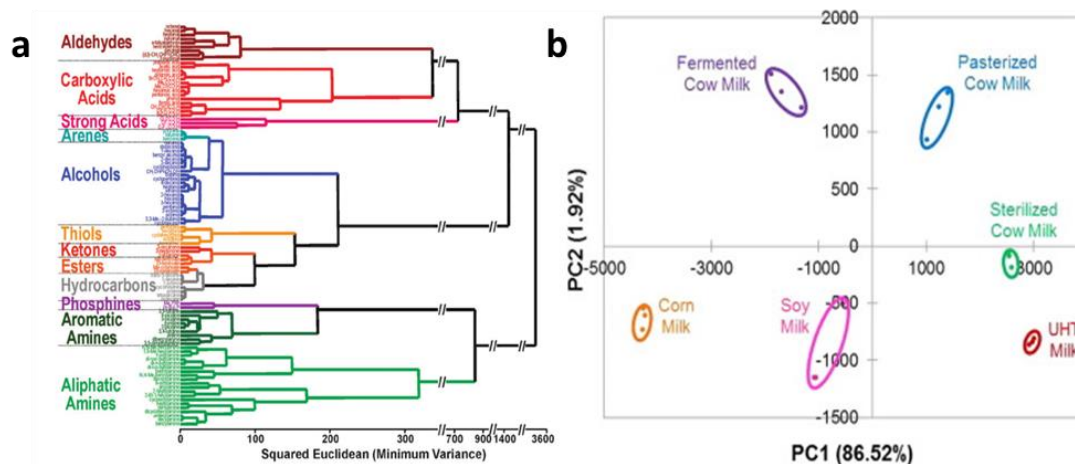


Figure 8. (a) HCA dendrogram from HCA of the colorimetric array responses to 100 common organic compounds at full vapor pressure at 300 K. Adapted with permission of ref. 63 © 2004, Elsevier. (b). PCA score plot of ΔI values in the range of 400-600 nm for 6 types of commercial milk. Adapted with permission of ref. 65 © 2016, Elsevier.

PCA is a dimensional reduction technique condensing the variance among several possibly-correlated dimensions by creating a new orthogonal set of dimensions using linear combinations of the initial dimensions. These new dimensions of data are ranked by the amount of data variance, for example, the first dimension explains the largest amount of data variance. By employing PCA, the contribution of all sensor elements can be valued and the complexed data could be easily visualized in 2D or 3D. The PCA plot of six kinds of milk can be clearly discriminated and visualized in Figure 8b.⁶⁷ PCA is an unbiased method similar to HCA. When the separation is not good enough among sample classes, PCA may not be able to predict the identity of an experimental sample precisely, thus it is more suited for evaluation of samples rather than prediction.

Linear discriminant analysis (LDA) is a dimensional reduction technique that constructs a set of orthogonal dimensions used to describe the data; LDA converts the data set with multiple sensor elements into canonical scores according to their Mahalanobis distance by calculation. Different from HCA or PCA, LDA is a biased method, it ranks components based on their

signal to noise ratio as compared among differing sample classes. Thus the dimensional components are optimized to maximize differentiability, which means LDA would have better ability to differentiate among sample classes. LDA has been applied to predict unknown samples successfully by using a "blind test". Besides, LDA shows better distinguishing ability than PCA because of the arithmetic difference between groups. Figure 9 show a LDA score plot showing separation among 22 different teas.⁶⁷

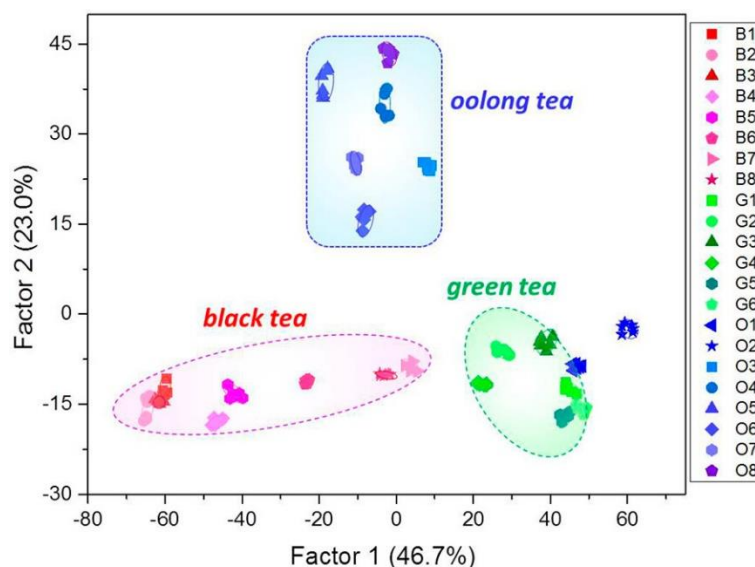


Figure 9. LDA Score Plot Showing Separation among 22 Different Teas. Adapted with permission of ref. 67 © 2018, American Chemical Society.

Sensor array have demonstrated their usefulness in conquering many sensing challenges. By using collections of receptors along with chemometric analysis, sensor arrays can be designed and refined to discriminate various structurally similar analytes or mixtures samples. The progress toward the application of sensor array methodologies is very important to solve the sensing challenges what the whole society faces.

1.3 Nitroaromatics: Detection and Discrimination

N-substituted aromatic compounds (NACs), such as nitrobenzenes, nitrophenols, aminophenols, and aromatic amines, are released into the biosphere almost exclusively from anthropogenic sources. They are widely used in the manufacturing of azo dyes, explosives, pharmaceuticals, and pesticides.⁶⁸⁻⁶⁹ It was recorded in 1978 by U.S. Environmental Protection Agency, only in the case of nitrobenzene, the production is annually in the order of 225,000 tons and it has been estimated that as much as 9,000 tons of nitrobenzene is discharged annually into natural waters.⁷⁰

NACs pollution of soil and water is highly suspected to cause neuronal and internal organ damage, as they have potentials for eliciting a variety of adverse cytotoxic, mutagenic and carcinogenic responses.⁷¹⁻⁷³ NACs are also important components for manufacturing explosives, related to potential security risks for the public.

The presence of NACs in the environment creates public health and environmental problems. Therefore, sensing of NACs in aqueous solution is an attractive and important issue. The biological effects by the NACs are dependent on their structure, the ability of the host organism to metabolize the compound and the response of the organism to the metabolites that are generated. Thereby, an effective approach which can detect and discriminate NACs with very similar properties is quite meaningful for further research of the toxicity of the NACs. Nitroaromatics, as one of the main subgroups of NACs, have drawn increasingly attention by researchers over a long history. Not only because their biological toxicity, but also because their homeland security application as explosive bombs. The toxicity of the mono-substituted benzenes was observed to increase in the following order: $\text{COOH} < \text{H} < \text{OH} < \text{NH}_2 < \text{NO}_2$.⁷¹ NO_2 -substitutions (nitroaromatic) were more toxic than other ring substituents or benzene itself. In order to assess the extent of nitroaromatic in suspected areas, it is also necessary to detect and identify them and their degradation products in groundwater and soil.

1.3.1 Nitroaromatics and Their Detection Approach

Nitroaromatic compounds are one of the most important groups of industrial chemicals. These compounds are organic molecules that consist of at least one nitro group (-NO₂) attached to an aromatic ring. The strong electron-withdrawing effect of the nitro group stems from the two combined electron-deficient oxygen atoms bonded to the relatively positive nitrogen atom. Attached to a benzene ring, the nitro group is able to delocalize-electrons of the ring. This not only provides charge to the molecule but also imparts unique properties that make the nitro group an important functional group in chemical syntheses.

Gas chromatography coupled with mass spectrometry (GC-MS), mass spectrometry, high-performance liquid chromatography, gas chromatography-electron capture detection, surface-enhanced Raman spectroscopy, cyclic voltammetry, X-ray imaging and ion mobility spectroscopy (IMS) have been used or suggested as suitable methods for the detection and quantification of the nitroaromatics (in solution and solid state).^{1, 74-78}

All the mentioned methods offer some advantages. GC-MS is a sensitive and reliable method which could detect the nitroaromatics in trace amount. IMS is also a good approach for detection and identification, as a swipe of clothing, skin, or objects will pick up particulates containing explosives residue. However, none of them is ideal due to certain features. They are expensive, complex, less sensitive, time-consuming and suffer from various drawbacks, such as portability and on-site detection. Chemical sensors are efficient method for detecting the nitroaromatics in the fields of soil pollution, water pollution and explosive detection for security check. Figure 10 shows the chemical sensors for nitroaromatics detection, including fluorescent polymers and fluorescent molecules, fluorescent MOFs, nanoparticles, quantum dots and carbon nanotubes. Optical sensing of nitroaromatics, report the change of fluorescence readout of fluorescent poly(*para*-phenyleneethynylene) (PPE)-type conjugated polymers, first introduced by Swager. This method is attractive because of its sensitivity, diversity, simplicity and some notable features, such as quick response time, portability and potential in both solution as well as solid state.⁷⁹⁻⁸¹

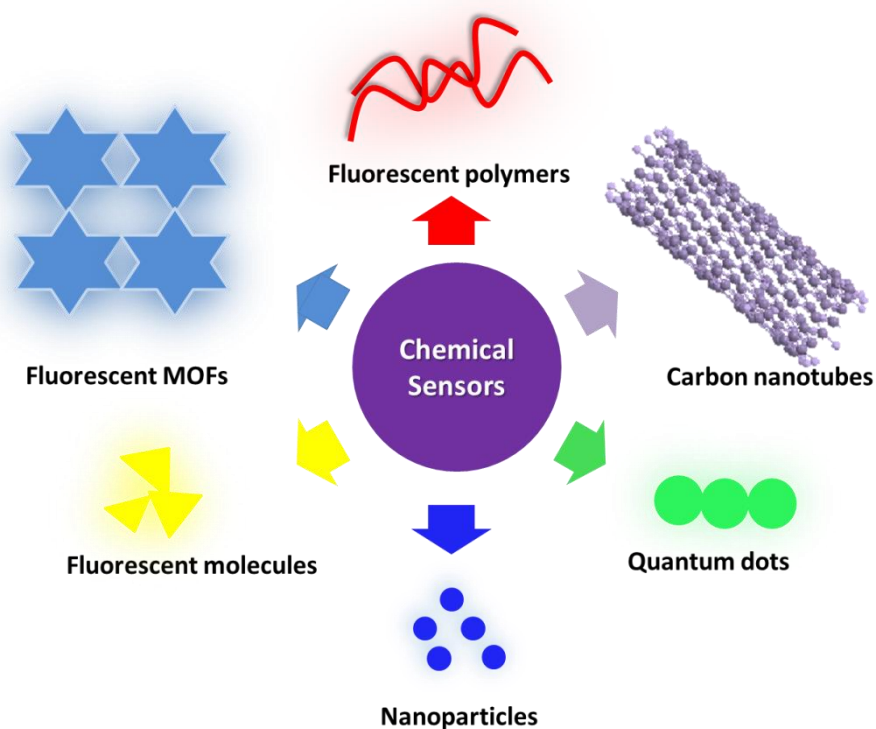


Figure 10. Chemical sensors for nitroaromatic detection.

1.3.2 Polymeric Sensors for Nitroaromatics Detection and Discrimination

The electron withdrawing capability is one property of nitroaromatics which could be exploited in detecting schemes. The substituted nitro groups lowers the energy of the empty π^* orbitals, therefore these compounds are good electron acceptors. Conjugated polymers are promising candidates for effective sensing (electron transfer) because they are electron donors.⁸² Conjugated polymers (CPs) create a myriad of opportunities to realize analyte receptor interactions. Especially, the donor ability of CPs is further enhanced in their delocalized π^* excited states. The excited state delocalization is beneficial for the effective detection of the nitroaromatics, because exciton migration increases the frequency of interaction with a bound quencher (the nitroaromatics), contributing to enhanced detection sensitivity.⁸³⁻⁸⁴ Fluorescent conjugated polymers have been applied to the detection of the nitroaromatics in solution and in the vapor phase.

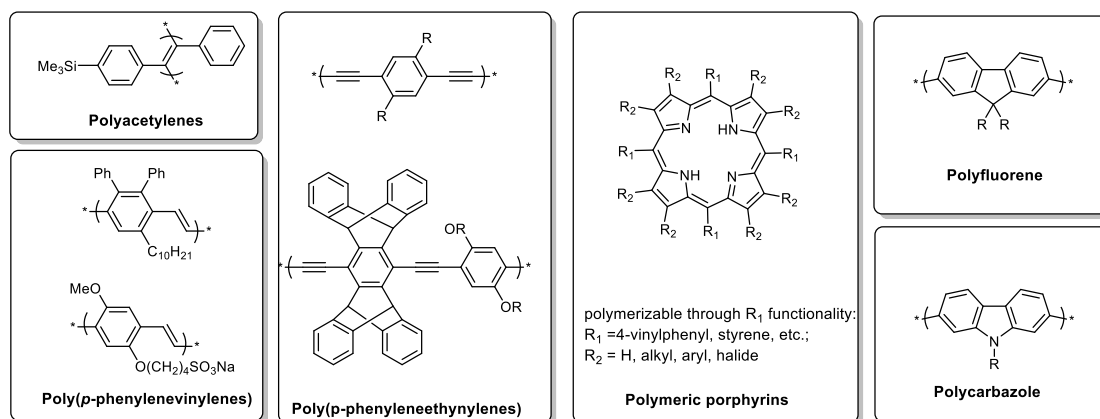


Figure 11. Basic backbone structures of the fluorescent organic polymers for nitroaromatics sensing.

Generally, fluorescent polymers are divided into organic and inorganic categories considering their basic backbone structures. As shown in Figure 11, the most reported fluorescent organic polymers are: polyacetylenes, poly(*p*-phenylenevinylenes), poly(*p*-phenyleneethynylenes), polymeric porphyrins, polyfluorene and polycarbazole. These polymers show remarkably high fluorescent quantum yields and have demonstrated great detection capability to nitroaromatics. Great efforts were devoted by the group of Swager, especially in the specific field of sensing explosives, they have reported a lot of poly(phenylene ethynylene)s employed as rapid, efficient sensor films. There are great potential for tailoring specific polymers to certain analytes owing to the diversity of the organic building blocks. Chemical and physical properties of the polymers, such as optical property, stability, hydrophilicity, could be tuned by varying constructed monomers, functional groups, crosslinking reagents, and reaction conditions.⁸⁵⁻⁸⁷ This would allow the manufacturing of a series of specific sensors for targeted analytes.

Fluorescent inorganic polymers applied for nitroaromatics sensing include polysilanes, polymetalloles, metallole-silane copolymers, etc (Figure 12). Polysilanes are stable high-fluorescent polymers with high mobility and unique electronic properties. They have been reported for the sensitive detection of NACs in THF solution and in the solid film by Fujiki and co-workers.⁸⁸ Similar to the organic polymers, the inorganic fluorescent polymers could also be tailored through different approach, such as in polysilane, the introduction of functional electron-withdrawing CF_3 groups to the Si atoms could further enhanced the sensitivity to the NACs.

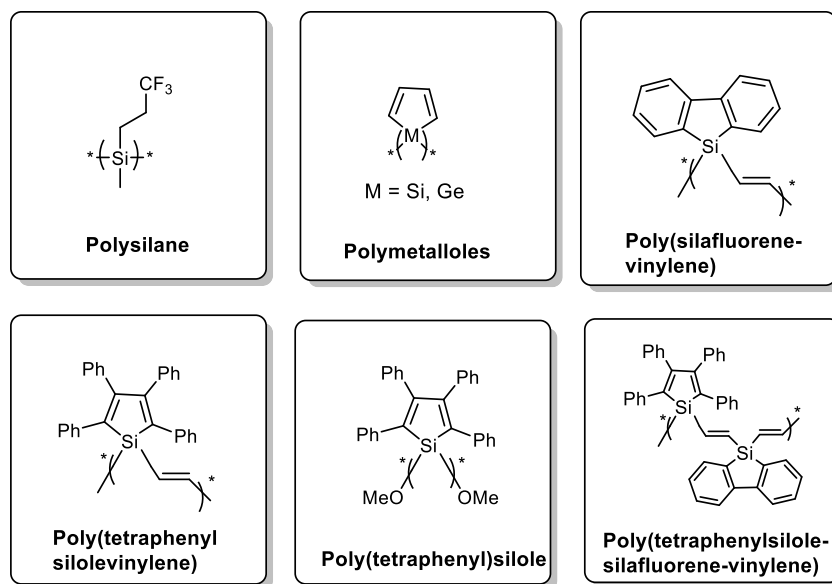


Figure 12. Basic backbone structures of the fluorescent inorganic polymers for nitroaromatics sensing.

Besides of the two main organic and inorganic polymers, the sensing of nitroaromatics could also be realized through the combination of the polymers with some other technologies. A simple device shows changes in resistance on adsorption of analyte vapors, by preparing carbon black particles coated with an organic polymer and deposited as a thin film across metallic leads.

Surface acoustic wave (SAW) detectors could also be used as chemical sensors, specifically for nitroaromatics. A SAW device consists of interdigitated electrodes on a piezoelectric substrate. By choosing the coating polymers on the electrodes, nitroaromatic sensing SAW devices can be built to detect the analytes selectively. Such devices have been prepared with carbowax polymers, siloxane polymer and cyclodextrin polymers.⁸⁹⁻⁹⁰

Polymer nanoparticles are the other kind of efficient sensor for the detection of nitroaromatics. Fluorescent inorganic nanoparticles sensors have been reported including fluorescent silicon nanoparticles and quantum dots. The adsorption of the analytes onto the nanoparticle could increase the contact chance between the polymers and the analytes, thus enhance the detection sensitivity. Polysilole and polytriazoles nanoparticles with aggregation-induced emission characteristics have been reported as nitroaromatic chemosensors.⁹¹⁻⁹²

1.4 Sensing Mechanism of Conjugated Polymers to Nitroaromatics

1.4.1 Fluorescence Quenching Mechanism

Due to the non-fluorescent properties of nitroaromatics, the optical detection is an indirect method to use fluorescent sensory materials that undergo fluorescence changes upon interactions with explosives. Therefore, a change of fluorescence intensity (quenching or enhancement), wavelength, anisotropy or lifetime related to the concentration and exposure time of explosives has the potential to sense nitroaromatics. Fluorescence intensity is the most common parameter. Fluorescence intensity quenching refers to the process of decreases the fluorescence intensity of fluorescent conjugated polymers. Fluorescence quenching is often achieved through several mechanisms such as Förster resonance energy transfer (FRET), Dexter electron transfer (DET), intramolecular charge transfer (ICT), twisted intramolecular charge transfer (TICT), metal-ligand charge transfer (MLCT), etc.⁹³ The mechanism of FRET, DET and TICT are depicted in Figure 13.⁹⁴

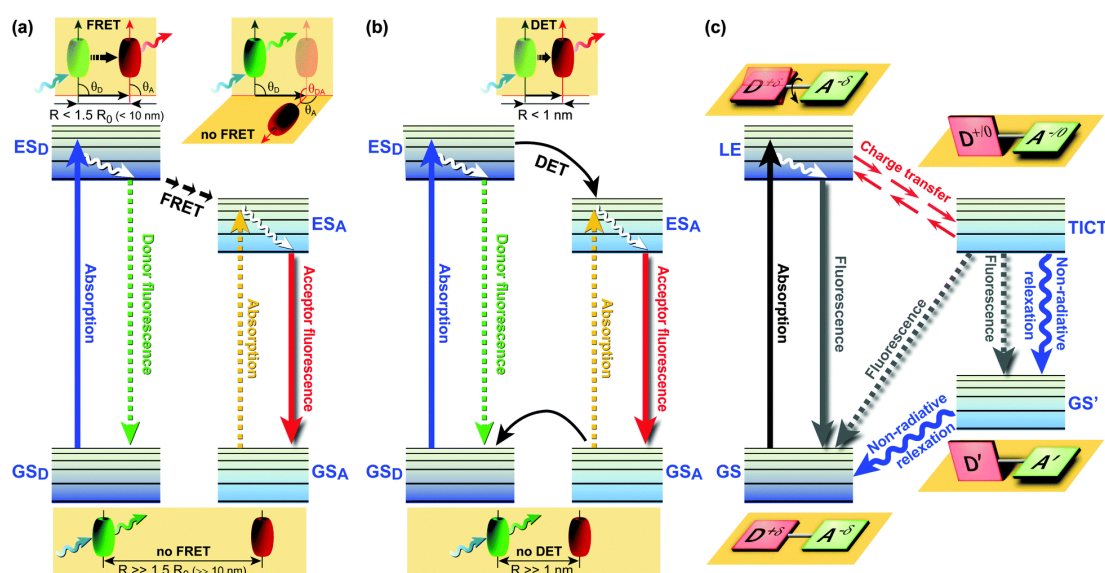


Figure 13. Jablonski diagrams of various energy/electron donor-acceptor (D-A) systems. (a) Förster Resonance Energy Transfer. (b) Dexter Energy Transfer; (c) Twisted Intramolecular Charge Transfer dynamics. (GS = ground state; GS D = ground state donor; GS A = ground state acceptor; ES D = excited singlet state donor; ES A = excited singlet state acceptor; LE = locally excited state; R = effective D-A distance.) Reproduced with permission from ref. 93 © 2016 the Royal Society of Chemistry.

FRET (Förster Resonance Energy Transfer) involves non-radiative energy transfer from the excited state donor fluorophore to the acceptor molecule via Coulomb interaction.⁹⁵ FRET relies on the distance between donor and acceptor (D-A) proximity, requires spectral overlap between the donor's emission and acceptor's absorption spectra, and depends on the relative orientation of the donor emission and acceptor absorption dipole moments.⁹⁶⁻⁹⁷

Dexter energy transfer (DET) is an exchange process where an excited electron is transferred from the donor molecule to the acceptor molecule via a non-radiative path. The excited electron is transferred to the acceptor at, and the acceptor then transfers an electron back to the donor. It has been utilized to create a variety of fluorescent sensors, especially for nitroaromatic sensing as their electron-deficiency.⁹⁸ The highest occupied molecular orbital (HOMO) of the electron donors lies higher in energy than electron acceptors, after excitation and before emission, the electron transfer to the acceptor's HOMO, thereby resulting in fluorescence quenching.⁹⁹

Intramolecular charge transfer (ICT): the transfer of charge from an electron-rich donor moiety to an electron-poor acceptor part located in different molecules is known as intermolecular charge-transfer (ICT) process. Application of ICT in the nitroaromatics detection is relatively less to FRET and DET.¹⁰⁰ Through rational design of ICT fluorescent molecules, an effective approach for the nitroaromatics sensors could be developed.

1.4.2 Fluorescence Quenching Theory

Fluorescence quenching usually requires molecular contact between the fluorophore and the quencher. This contact can be resulted from diffusive encounter, which is dynamic quenching, or resulted from complex formation, which is static quenching.

Dynamic quenching results from collisions between the excited fluorophores and quenchers, The resulting decrease in fluorescence emission intensity or lifetime is related directly to the concentration of analytes. Elements such as temperature, which can affect the chances of collision, will surely influence the quenching performance. There are typically no changes in fluorophore absorption spectra as collisional quenching only affects the excited state of the fluorophore. Static quenching is a process of complex formation, which does not rely on

diffusion or molecular collisions. Static quenching frequently results in the absorption spectrum alteration due to the formation of a new complex. The lifetime of the system would not change with the concentration of the analytes.

1.5 Objective

Fluorescent conjugated polymers are good candidates as sensing materials for nitroaromatics detecting. In this research, novel conjugated polymers will be designed and synthesized to improve the sensibility and selectivity of the polymeric sensors. The new structures are developments based on the molecular wire effect of conventional **PPEs**. Those polymers should have a better detecting and discriminating ability for nitroaromatics.

Furthermore, application of the novel sensors into aqueous phase is another thoughtful topic. To realize the detection of discrimination of nitroaromatics in nature surrounding (soil or groundwater), the fluorescent polymers are expected to retain good fluorescent performance in water, at the same time possess excellent recognizing ability to nitroaromatics.

**Chapter 2. Truxene-Based Conjugated Polymers and
Fluorescent Micelles Detect Nitroaromatics**

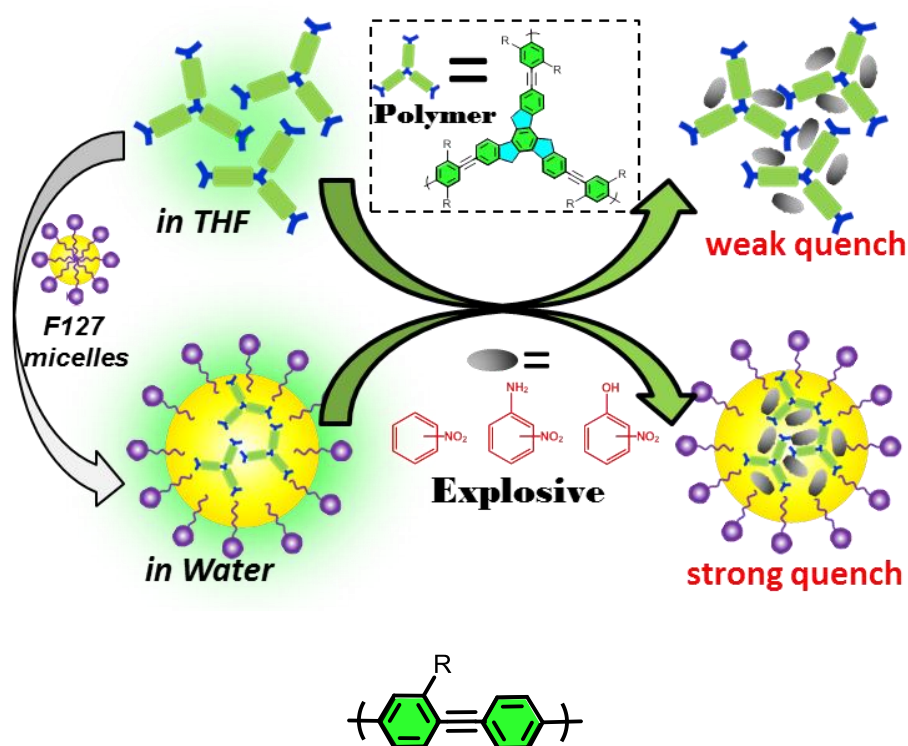


Figure 14. Systematic illustration of **HCPs** and **PPEs** and their micelles quenched by the explosives. Reproduced with permission of ref. 101 © 2017, American Chemical Society.

In this Chapter, two hyperbranched conjugated polymers (**HCPs**) with truxene units and two analogous poly(*para*-phenylene-ethynylene)s (**PPEs**) are prepared. These polymers are quenched by electron-deficient nitroaromatic and display different fluorescence quenching responses.¹⁰¹ The quenching efficiencies of the polymers to the analytes depend on the spectral overlap between the absorbance of the analytes and the emission of the polymers. Specific optical fingerprints form, based on the unique response patterns of the polymers towards the analytes. The presented polymers form a sensor array which distinguishes nine nitroaromatic analytes with 100% accuracy. **F-127**, an amphiphilic polymer with oligoglycol side chains, carries the hydrophobic HCPs and self-assembles into micelles in water. The highly fluorescent HCP micelles detect nitroaromatic analytes more efficient (100 % accuracy) in water than organic solvents.

2.1 Truxene-based Polymers

Polyfluorenes are a unique class of conjugated polymers that their fluorescence can be tuned through the entire visible range; the systematic illustration of polyfluorenes is shown in Figure 15.¹⁰² Truxene (10,15-dihydro-5H-diindeno[1,2-a;1',2'-c]fluorene) is a planar heptacyclic polyarene which can be considered as three annulated fluorene moieties.¹⁰³

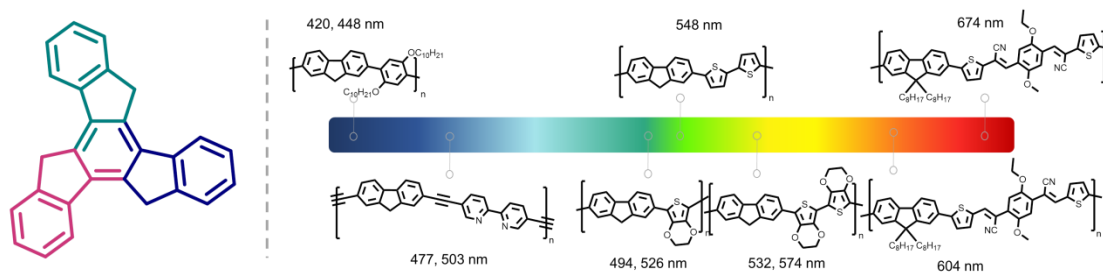


Figure 15. Systematic illustration of truxene and optical tunability of fluorene derivatives.

The star-shaped truxene, with its unique trigonal topology is an attractive building block for constructing electron-rich, extended π -conjugated polymers. The full potential of truxene-based substance is not only limited to some highly attractive research fields such as organic electronics (organic diodes, solar cells, and organic transistors), but also in emerging fields such as organic lasers, fluorescent probes and liquid crystals/ gels.^{102, 104} Figure 16 shows one organic electronic application example (**Trux-OMeTAD**) of a hole transport layer for perovskite truxene-based solar cells with PCE of 19%.¹⁰⁴ The truxene core consist of attached hexyl side chains and is capped with terminal aryl amines.

We concentrate on the truxene core when synthesizing polymers because its physical properties can easily be chemically tailored. Especially, truxene-based polymers have rarely been reported as chemosensors.¹⁰² Thus, we designed two fluorescent polymers, investigated their fluorescent performance and further utilized them in detection and discrimination of nitroaromatics. Comparing the performance we prepared two analogous poly(*p*-phenylene-ethynylene)s (**PPE**) s are also synthesized as comparison to demonstrate the difference between truxene and benzene moieties on the sensing effect to explosives.

2.2 Hyperbranched Truxene Polymers and Poly(*para*-phenylene-ethynylene)s

In this section, two hyperbranched conjugated polymers (**HCPs**) with truxene units and two poly (*p*-phenylene-ethynylene)s (**PPEs**) are prepared. Characterizations of the molecular and optical properties of the polymers are also exhibited.

2.2.1 Synthesis of Monomers, HCPs and PPEs

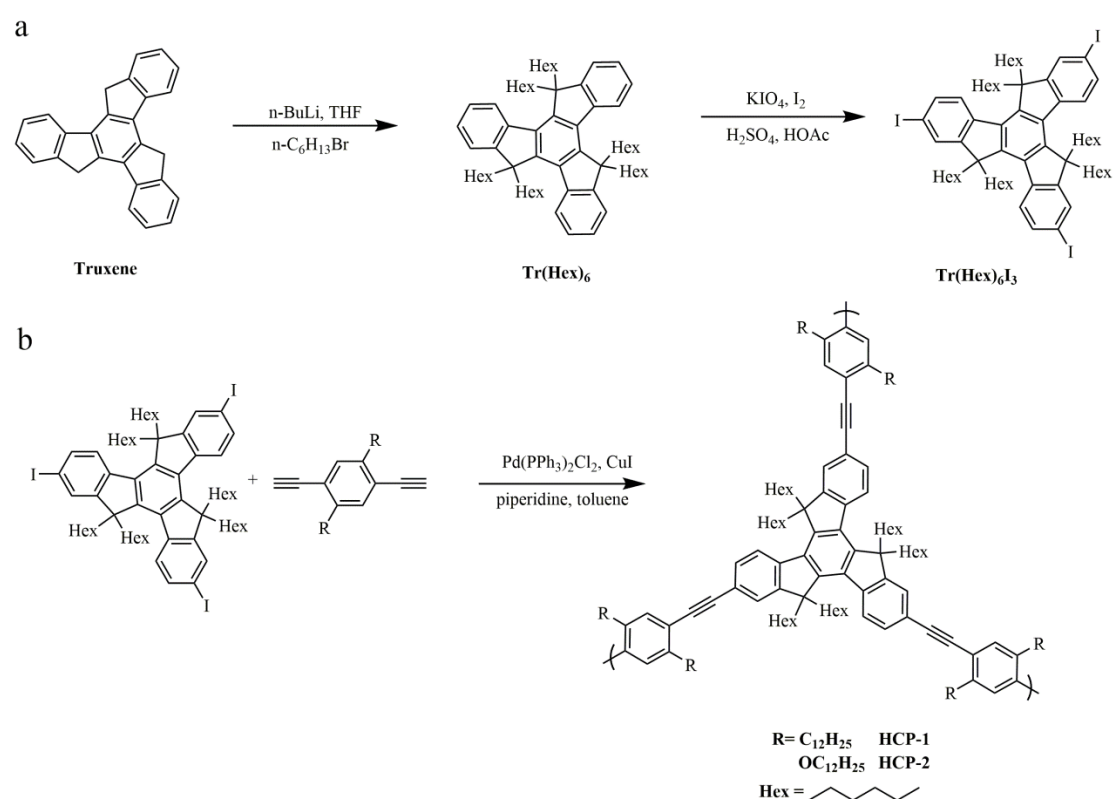


Figure 17. Synthetic route to Tr(Hex)₆I₃ (a) and HCPs (b).

Monomer Tr(Hex)₆I₃ was prepared by the synthetic route in Figure 17a.¹⁰⁶ Two conjugated polymers (**HCP-1** and **HCP-2**) were synthesized through Sonogashira coupling reaction. The polymers are built up with truxene monomer Tr(Hex)₆I₃ and comonomer phenyleneethynylene moieties, carrying dodecyl and dodecyloxy chains (Figure 17b).¹⁰⁷ For comparison, two analogous poly(*para*-phenyleneethynylene)s (**PPEs**, **PPE-1** and **PPE-2**) with identical phenyleneethynylene backbones were synthesized with the same procedure. The final structures of the four polymers are shown in Figure 18.

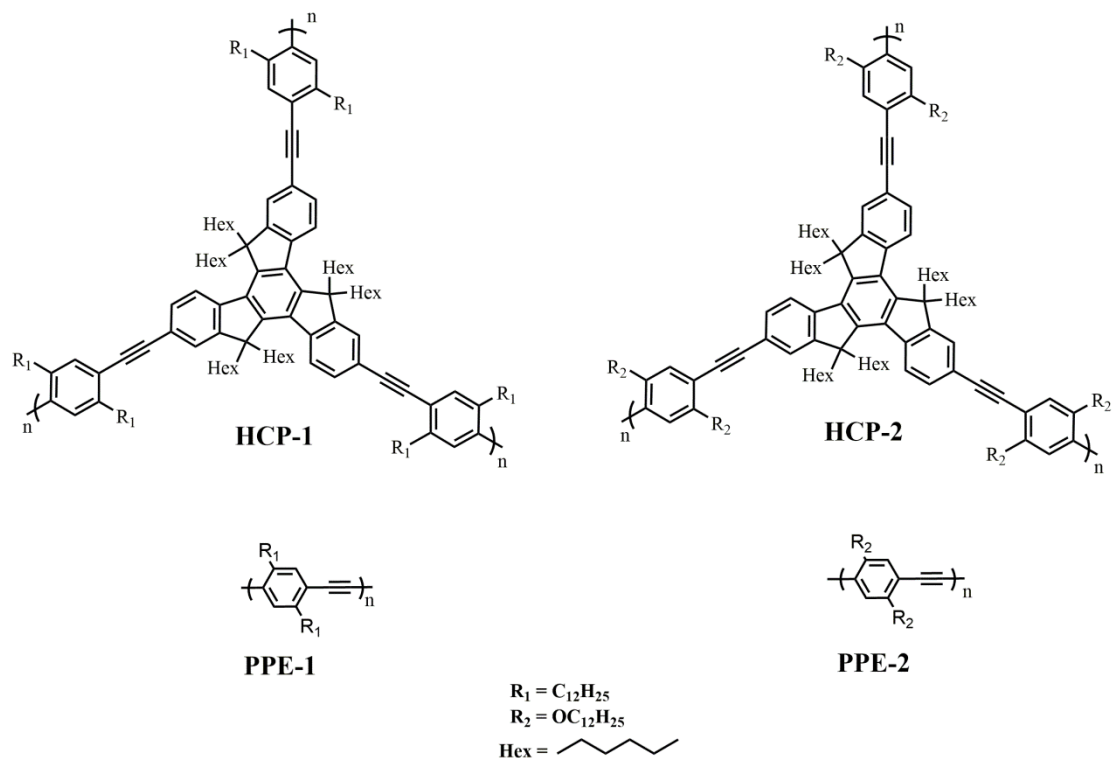


Figure 18. Structures of **HCP-1**, **HCP-2**, **PPE-1** and **PPE-2**. Reproduced with permission of ref. 101 © 2017, American Chemical Society.

2.2.2 Molecular and Photophysical Properties of the Polymers

Molecular and photophysical properties of the four polymers are listed in Table 1. The number-average molecular weights (M_n) and PDIs (\mathcal{D}) of these polymers ranges between $1.2\text{--}4.8 \times 10^4$ g/mol and 1.5–3.1. The molecular weights of the **HCPs** are lower than those of the **PPEs**. The big spatial structure of **Tr(Hex)₆I₃** may sterically hinder the polymerization process resulting in a lower degree of polymerization. A higher degree of polymerization could not be obtained as the longer backbones lead to insoluble polymers. The PDI range is quite normal for polycondensed polymers.

The photophysical properties of the polymers in THF are shown in Figure 19 and Table 1. In the fluorescence spectra, **HCPs** (402 nm, 428 nm) absorb and emit at shorter wavelengths than **PPEs** (424 nm, 471 nm). The maximum emission peaks of polymers with dodecyl chains (**HCP-1** and **PPE-1**) display a blue shift compared with polymers containing dodecyloxy chains (**HCP-2** and **PPE-2**). The fluorescence quantum yields (Φ_F) for **HCP-1**, **HCP-2**,

Table 1. Photophysical properties and GPC data for **HCP-1**, **HCP-2**, **PPE-1** and **PPE-2**

polymer	$\lambda_{\max, \text{abs}}$ [nm] ^a	$\lambda_{\max, \text{em}}$ [nm] ^a	Φ_F [%] ^a	M_n [g/mol] ^b	M_w/M_n ^b
HCP-1	320	402	56.1	11821	1.5
HCP-2	320	428	64.5	11878	1.9
PPE-1	406	424	80.2	149920	3.1
PPE-2	445	471	79.8	47966	1.7

^aDetermined in THF. ^bDetermined by GPC in THF.

PPE-1 and **PPE-2** are 56%, 65%, 80% and 80% respectively in THF. **PPE-1** and **PPE-2** display a higher fluorescence quantum yield than **HCP-1** and **HCP-2**. The polymers based on benzene moieties demonstrate stronger fluorescent ability compared with those based on truxene core in this work. The attractive polymer properties are used in the following applications to differentiate different analytes in molecular sensor technology.

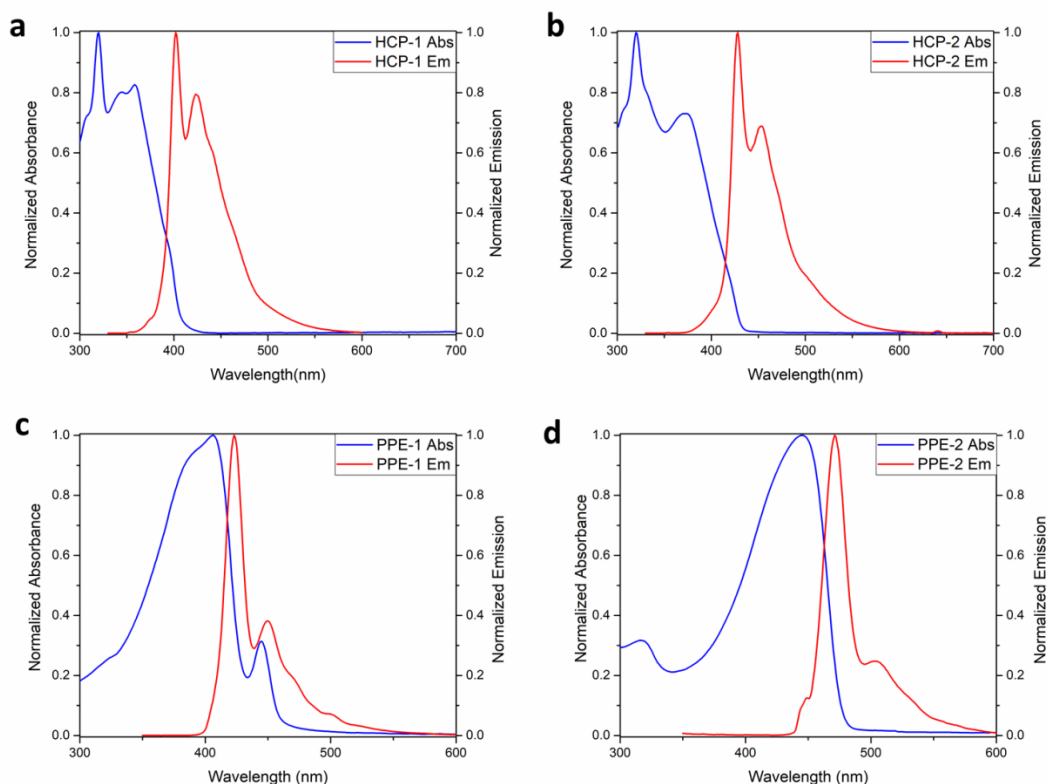


Figure 19. Normalized absorption and emission spectra of **HCP-1**(a), **HCP-2**(b), **PPE-1**(c) and **PPE-2**(d) in THF. Reproduced with permission of ref. 101 © 2017, American Chemical Society.

2.3 Detection and Discrimination in Organic and Water Milieus

Nitroaromatics pollution in soil and water are suspected to cause health issues such as damage to internal organs and neurological damage. Therefore, suitable fluorescent conjugated polymers with high sensitivity and selectivity are still in demand particularly if they are applied in aqueous condition.

2.3.1 Detection and Discrimination of Nitroaromatics in Organic Solvents

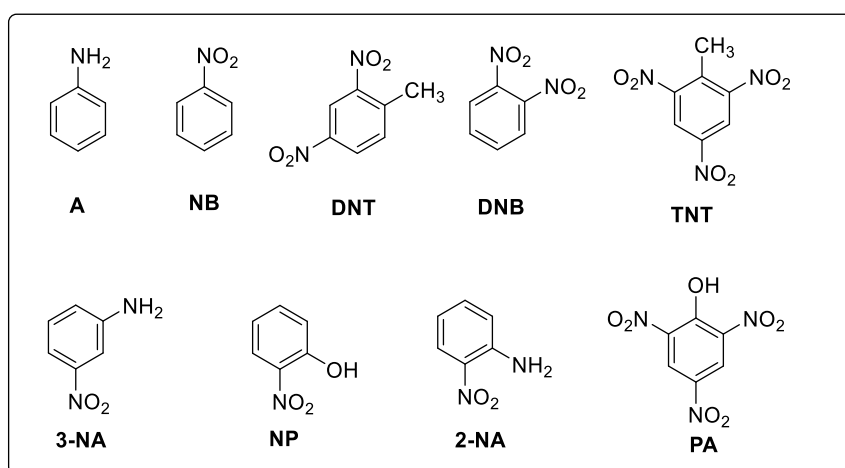


Figure 20. Structures of nine tested nitro analytes.

The four polymers detect explosives via fluorescent quenching. Nine analytes (Figure 19) were investigated, including eight nitroaromatics: picric acid (**PA**), nitrobenzene (**NB**), dinitrobenzene (**DNB**), dinitrotoluenes (**DNT**), trinitrotoluenes (**TNT**), nitrophenol (**NP**), 2-nitroaniline (**2-NA**), 3-nitroaniline (**3-NA**) and aniline (**A**) as a comparison. The fluorescence intensity of polymers is gradually quenched after adding the analyte (nitroaromatics) into the solution. Fluorescent intensity changes were recorded. To quantify the quenching efficiencies of the polymers to the analytes, we calculated the Stern-Volmer constants (K_{sv}) according to the standard Stern-Volmer equation (1); however, the linear behavior was poor. Thus for better fitting, a modified Stern-Volmer equation (2) was adopted to calculate the quenching efficiencies.¹⁰⁸⁻¹⁰⁹ In these two equations, K_{sv} is the Stern-Volmer constant, I_o is the initial

fluorescence intensity of the fluorophore (HCPs and PPEs), I_{final} is the final fluorescence intensity of the fluorophore, $[F]$ is concentration of the fluorophore and $[Q]$ is the total concentration of the added quencher Q . The non-linear nature of the Stern-Volmer plots suggests a combination of static and dynamic quenching or an energy transfer process between the polymers and analytes.

$$\frac{I_0}{I_{\text{final}}} = 1 + K_{sv}[Q]$$

Equation 1: Regular Stern-Volmer equation

$$I_q = I_0 + \frac{I_{\text{final}} - I_0}{2} \times \left\{ 1 + \frac{[Q]}{[F]} + \frac{1}{K_{sv}[F]} - \left[\left(1 + \frac{[Q]}{[F]} + \frac{1}{K_{sv}[F]} \right)^2 - 4 \frac{[Q]}{[F]} \right]^{1/2} \right\}$$

Equation 2: Modified Stern-Volmer equation

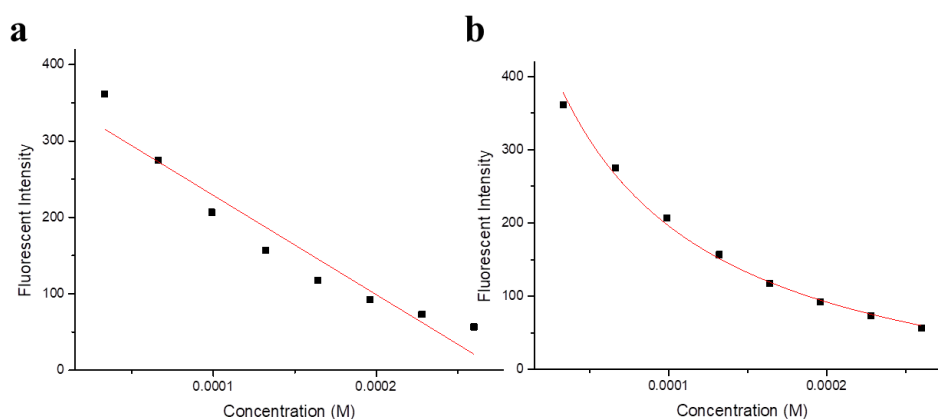


Figure 21. K_{sv} plot **HCP-1** to **PA** fitted by equation 1 (a) and equation 2(b).

The fitting plots of **HCP-1** to **PA** are shown in Figure 21. It is clear that the fitting plot according to modified Stern-Volmer equation 2 is much better than the regular Stern-Volmer equation 1. Therefore, equation 2 was adopted to calculate the quenching efficiencies of the polymers to these nitroaromatics.

The fluorescence quenching efficiencies and the K_{sv} values to the analytes are mainly in the order of **2-NA** > **PA** > **NP** > **TNT** > **DNB** > **DNT** > **3-NA** > **NB** > **A** (Figure 22, Table 2). When comparing **2-NA**, **NB** and **A**, neither aniline (**A**) nor nitrobenzene (**NB**) showed strong quenching effects. However, **2-NA** (with amino and nitro at the same time) results in the highest fluorescence quenching to our polymers. When it comes to the polymers, the four polymers also give a trend of quenching constants: **HCP-1** has the highest quenching

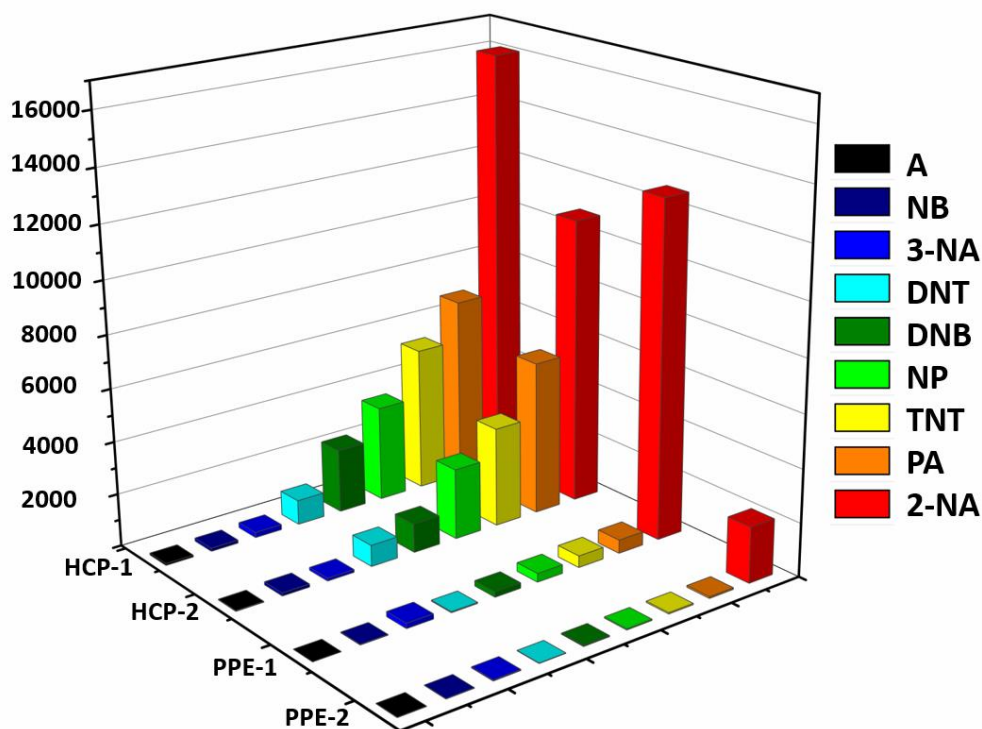


Figure 22. Fluorescent quenching efficiencies of **HCP-1**, **HCP-2**, **PPE-1** and **PPE-2** for different analytes in THF. The z-axis denotes the Stern-Volmer constant K_{sv} . Reproduced with permission of ref. 101 © 2017, American Chemical Society.

efficiency, followed by **HCP-2**, **PPE-1** and **PPE-2** (**HCP-1** > **HCP-2** > **PPE-1** > **PPE-2**). Although **PPE-1** is more sensitive towards **2-NA** than **HCP-2**, HCPs are better sensors in most cases. The quenching experiments are also carried out in different solvents (THF, CHCl_3 and toluene). K_{sv} values of **HCP-1** for the detection of analytes (**DNT**, **NP**, **PA** and **2-NA**) are investigated in these good solvents. The values are quite close in the three solvents (Figure 23). The K_{sv} values are independent from the solvents, indicating the quenching process is not affected by the solvents we used here.

Table 2. K_{sv} values of the polymers to different analytes

Analytes	HCP-1	HCP-2	PPE-1	PPE-2
A	69	25	5	11
NB	118	114	23	17
3-NA	197	105	194	37
DNT	931	805	38	15
DNB	2412	1092	203	36
NP	3607	2667	326	44
PA	6939	5811	507	62
2-NA	16084	10827	12695	2099

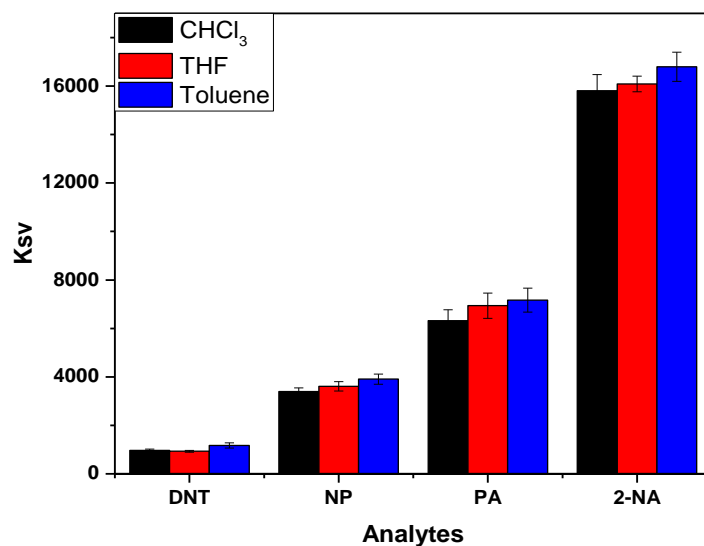
**Figure 23.** Fluorescence quenching efficiencies of HCP-1 to DNT, NP, PA and 2-NA in different solvents (CHCl₃, THF and toluene).

Figure 24 shows the normalized absorbance spectra of the analytes and the emission spectra of the polymers (spectra range: 300-600 nm). The quenching constants (K_{sv}) are mainly consistent with the spectral overlap area, suggesting a Förster resonance energy transfer (FRET) process.¹ As we know, FRET relies on the distance between donor and acceptor (D-A) proximity, which requires spectral overlap of donor emission and acceptor absorption spectra. Thus, the greater of the spectral overlap area imply a bigger chance for the quenching process. The greatest spectral overlap are between 2-NA and HCP-1, which explains the high K_{sv} .

value.¹¹⁰ **HCP-1** with the bluest emissive spectrum, has the greatest spectral overlap with all of the analytes, revealing the best sensing efficiencies to them. **PPE-2** has the least overlap with the analytes, resulting in the worst sensor. The spectra of **HCP-2** and **PPE-1** are quite close. **PPE-1** has a larger overlap (402 nm -600 nm) than **HCP-2** to **2-NA**. However, to other analytes, the overlap theory does not fit well, as the analytes have shorter absorption wavelengths than **2-NA**. To **A**, **NB**, **DNT**, **TNT** and **DNB**, the overlap of their absorbances are negligible with the emission spectra of polymers. In these cases, excited stated electron transfer (between the electron-withdrawing nitroaromatic and the electron-donating polymers) may play a more important role during quenching process.¹¹¹

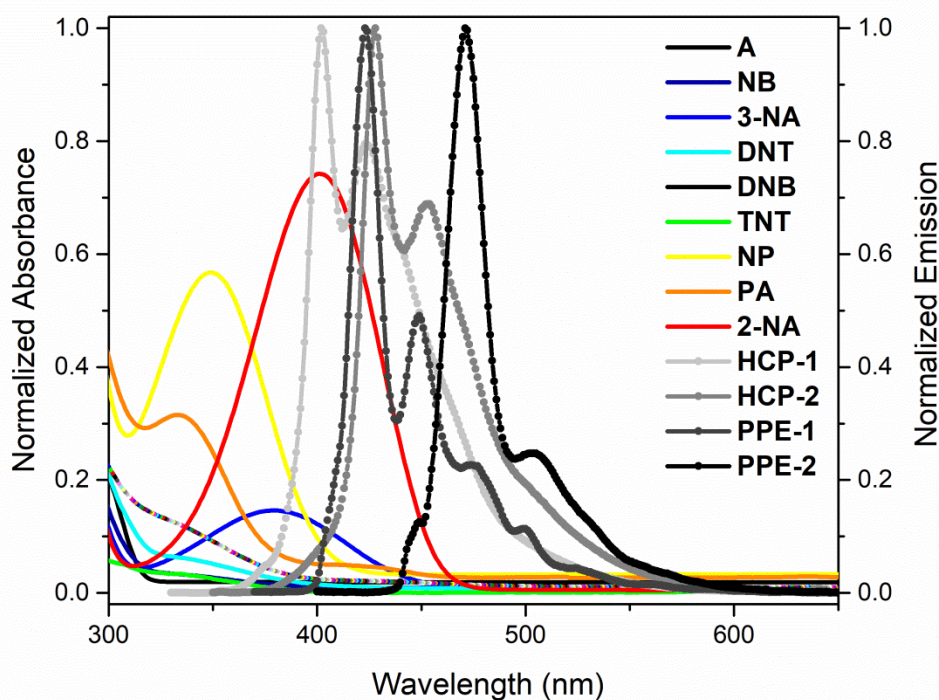


Figure 24. Spectra overlap between normalized absorbance spectra of nitro analytes (colorful lines) and emission spectra of polymers (black and grey lines with dots). Reproduced with permission of ref. 101 © 2017, American Chemical Society.

The excited electron from the polymer transfers to the LUMO orbitals of the analytes upon excitation, thus quenching the fluorescence intensity. The lower the HOMO-LUMO gap between the analytes and the fluorophore, the better quenching effect to the fluorescence could be obtained. The energy level of the analytes were calculated at B3LYP/6-311++G**

level of theory. The values of energy level are given in Table 3. The fluorescence quenching abilities of the analytes are mainly in accordance with their low LUMO energies. The LUMO value of **3-NA**, **NP** and **2-NA** are inconsistent with their performances, suggesting the electron transfer mechanism is not the dominant interaction during the quenching process, where energy transfer may play the key role.

Table 3. Calculated Energy Level of the Analytes at B3LYP/6-311++G** Level of Theory.^a

analytes	A	2-NA	3-NA	NB	NP	DNT	DNB	TNT	PA
LUMO[eV]	-0.37	-2.67	-2.75	-2.92	-3.19	-3.40	-3.45	-3.91	-4.32
HOMO[eV]	-5.78	-6.48	-6.52	-7.95	-7.22	-8.44	-8.35	-8.84	-8.62

^aAnalytes are ordered according to their calculated LUMO level.

Instead of a single response of a specific polymer to one analyte, these four polymers make up sensor arrays, recognizing and discriminating the nitro-analytes.^{62,112-113} The nine analytes were tested with all four polymers simultaneously to explore their common response patterns. The fluorescent polymers (0.03 μM in THF) were quenched by the analytes (0.3 mM in MeOH) six times to calculate the mean response patterns. The fluorescence intensity changes were recorded before and after adding the analytes. Figure 25 shows the quenching results of the polymers when the analytes were added.

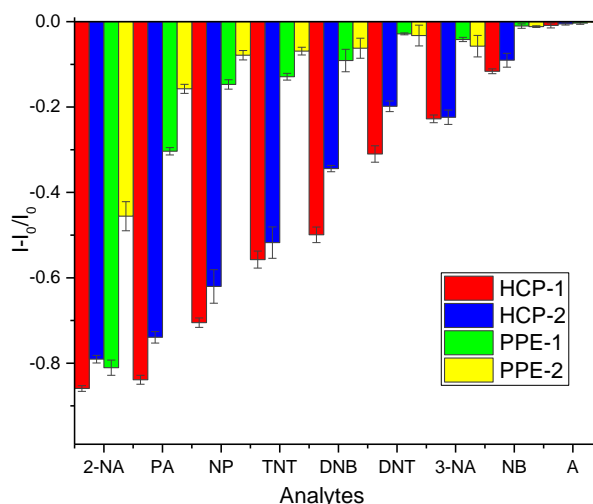


Figure 25. Fluorescence response pattern ($(I-I_0)/I_0$) obtained by **HCPs** and **PPEs** (0.03 μM) treated with analytes (0.3 mM). Reproduced with permission of ref. 101 © 2017, American Chemical Society.

The whole quenching data were analyzed by linear discriminant analysis (LDA), and four canonical factors were generated (62%, 28%, 6% and 4%). The two larger canonical factors give a 2-D discrimination plot with nine distinct clusters, well resolved without overlap (Figure 26). Especially, good quencher **2-NA** and **PA** are well separated from the others. The tested analytes are easily discriminated by the four-element sensor array in THF. For further study, all the analytes were tested randomly under the same condition for four times. Identification of the unknown samples was carried out by the LDA training matrix based on our polymer sensor array. The response of polymers to each unknown sample was compared with the classification data. 100% accuracy can be obtained by this polymer sensor array under 95% confidence interval, which means the sensor array could recognize the unknown samples.

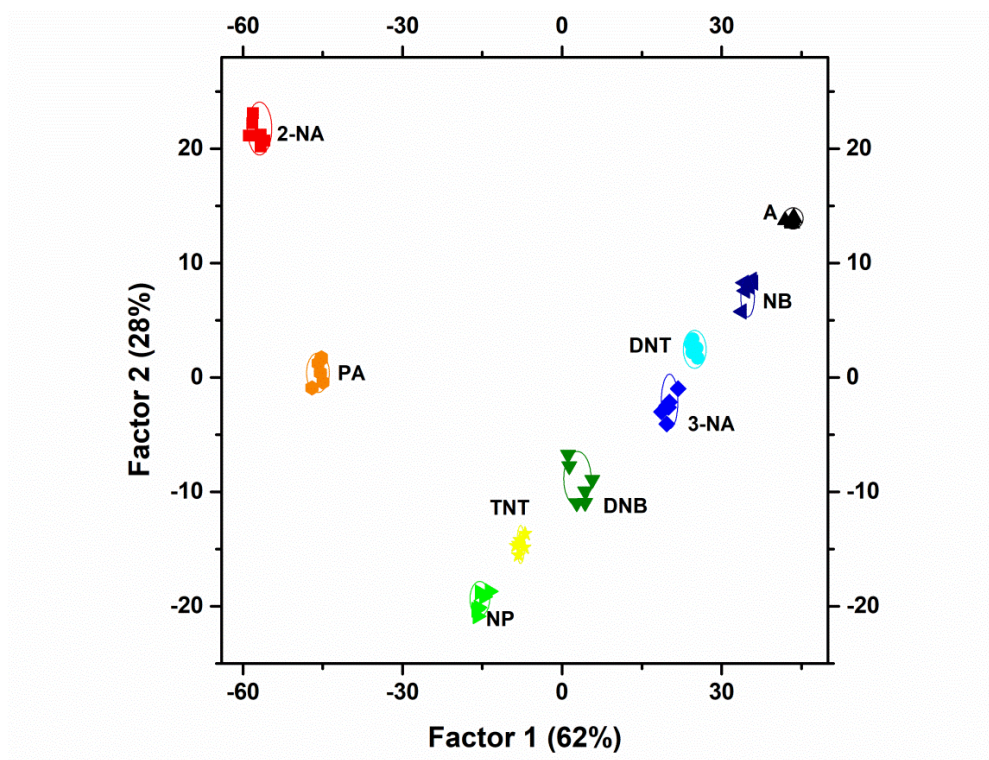


Figure 26. 2-D canonical score plot of discriminant scores with 95% confidence ellipses for all obtained data points against different analytes. Reproduced with permission of ref. 101 © 2017, American Chemical Society.

Detection of the nitroaromatic in water is attractive concerning to the water pollution and its biological effect. Nitroaromatics pollution of soil and water is suspected to cause neuronal and internal organ damage.⁷¹ Thus to utilize the fluorescent polymers in aqueous phase is a

problem to be solved. However, suitable fluorescent conjugated polymers with high sensitivity and selectivity are still in demand, particularly if they are applied in aqueous condition. The tested polymers are poorly dissolved in water. Taking care of this issue, a micellar approach is investigated in the following research.

2.3.2 Detection and Discrimination Nitroaromatics in Water by Fluorescent Micelles

As indicated above, amphiphilic polymers could encapsulate the hydrophobic molecules (fluorescent polymers) into its cores and form amphiphilic micelles, which could disperse in a hydrophilic aqueous phase.¹¹⁴ Poly(oxyethylene)-block-poly(oxypropylene)-block-poly(oxyethylene) (Pluronic **F-127**), is a typical non-toxic and low cost amphiphilic polymer, which self-assembles into nano-micelles in water. Therefore, **F-127** is applied as a carrier for HCPs and PPEs as fluorescent sensing cores to form the amphiphilic micelles (the formation of the micelles is illustrated in Figure 27).

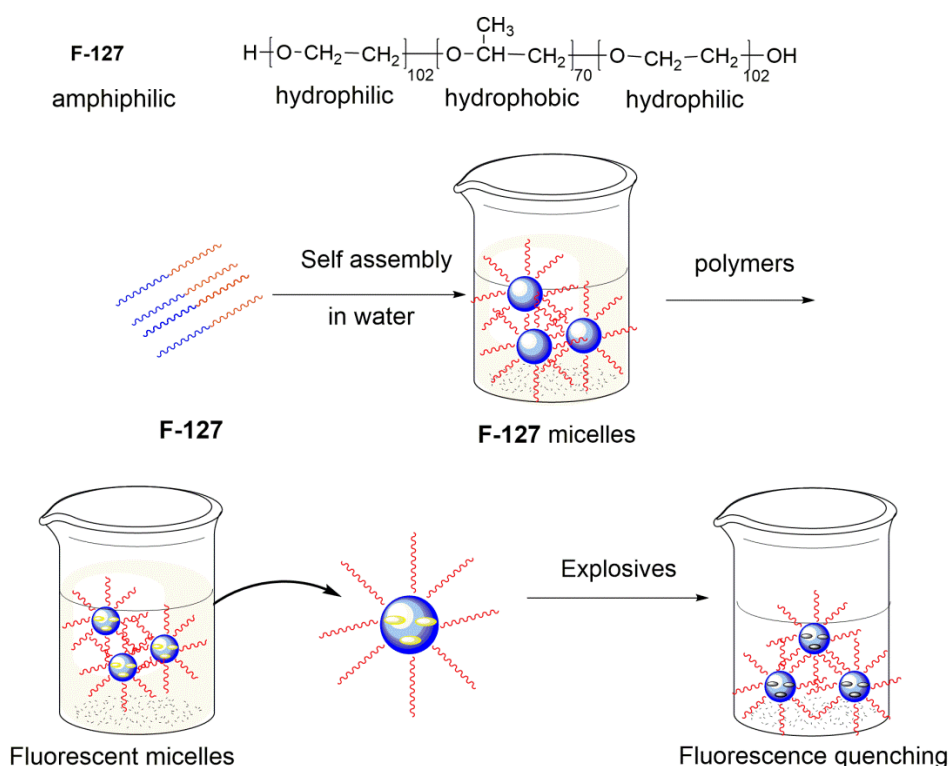


Figure 27. Formation of **F-127** micelles, addition of polymers into the micelles to form fluorescent micelles and their schematic quenching process in water. Reproduced with permission of ref. 101 © 2017, American Chemical Society.

The resulting micelles detect and discriminate nitroaromatics in water. The polymers dissolved in THF were dropped into the micellar solution of **F-127** in water.¹¹⁵ Then the mixtures were treated in an ultrasonic bath for 1 h, THF was removed by vacuum distillation, resulting in the final micellar preparations (**HCP-1-M**, **HCP-2-M**, **PPE-1-M** and **PPE-2-M**) with **F-127** at a concentration of 10 mg/L and the **HCPs** and **PPEs** at 0.5 μM .

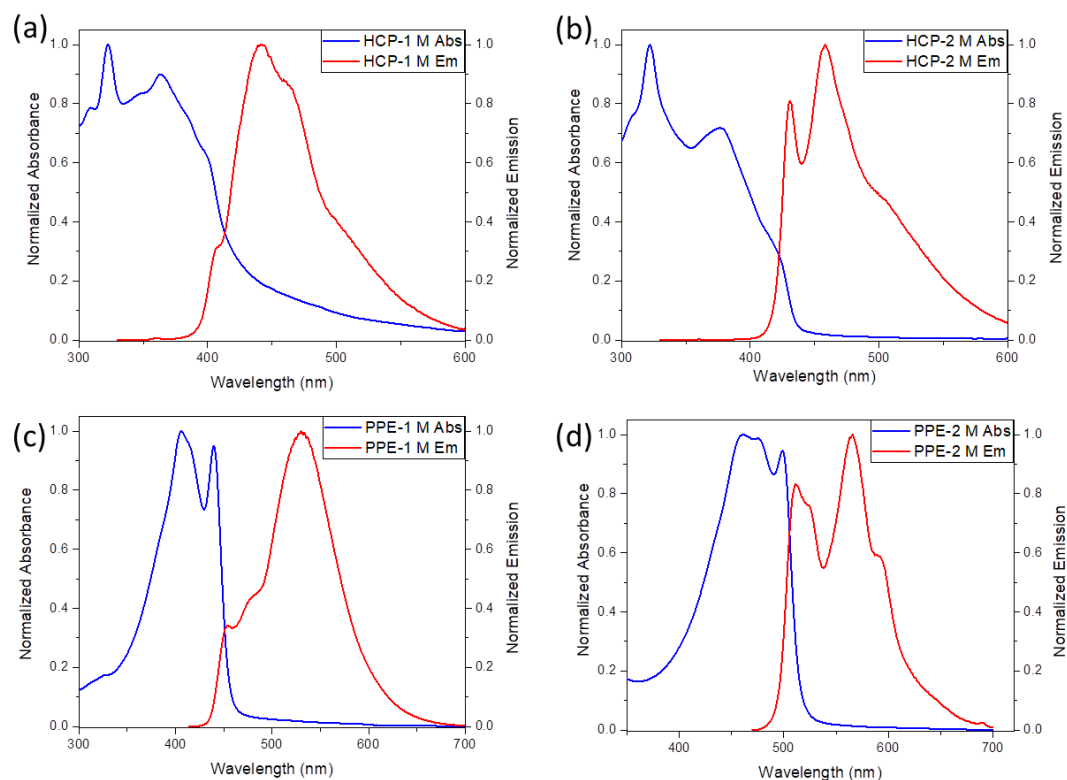


Figure 28. Normalized absorption and fluorescence spectra of (a) **HCP-1-M**, (b) **HCP-2-M**, (c) **PPE-1-M** and (d) **PPE-2-M**. Reproduced with permission of ref. 101 © 2017, American Chemical Society.

The photophysical properties of HCP micelles (**HCPs-M**) and PPE micelles (**PPEs-M**) are shown in Figure 28 and summarized in Table 4. The maximum emission peaks of the fluorescent micelles are all red shifted compared to that of the original polymers, suggesting the formation of aggregates and / or planarization of the backbones. Emission spectra of micelles are broader than that of the pure polymers. The fluorescence quantum yields (Φ_F) for **HCP-1-M**, **HCP-2-M**, **PPE-1-M** and **PPE-2-M** are 12%, 17%, 19% and 20% respectively in water, which are lower than their Φ_F in THF. This phenomenon is due to the aggregation-caused quenching.

Table 4. Photophysical properties of the **HCPs-M** and **PPEs-M**.

micelles	UV-Vis $\lambda_{\text{max}}/\text{nm}$	PL λ/nm	Stokes shift/nm	Quantum Yield
HCP-1 M	322	442	120	12.2 %
HCP-2 M	322	458	138	17.1 %
PPE-1 M	406	530	124	19.4 %
PPE-2 M	460	565	105	20.3 %

Field Emission Scanning Electron Microscopy (FESEM) visualized the morphology of the fluorescent micelles. The images of **F-127**, **HCP-1** and **HCP-1-M** in water were shown in Figure 29. For **F-127** micelles in water (Figure 29a), only small round particles were observed. Without amphiphilic surfactant **F-127**, polymer **HCP-1** (prepared using the same procedure for **HCP-1-M**) gathered together and formed into fibers (Figure 29b). Interestingly, after the formation of the fluorescent micelles, **HCP-1-M** (Figure 29c) showed larger average particle size compared to the **F-127** alone. The explanation of the phenomenon is the hydrophobic polymers trapped in the core of the **F-127** and formed into amphiphilic micelles. **F-127** prompted the polymers aggregate into the fluorescent micelles and dispersed properly in water.

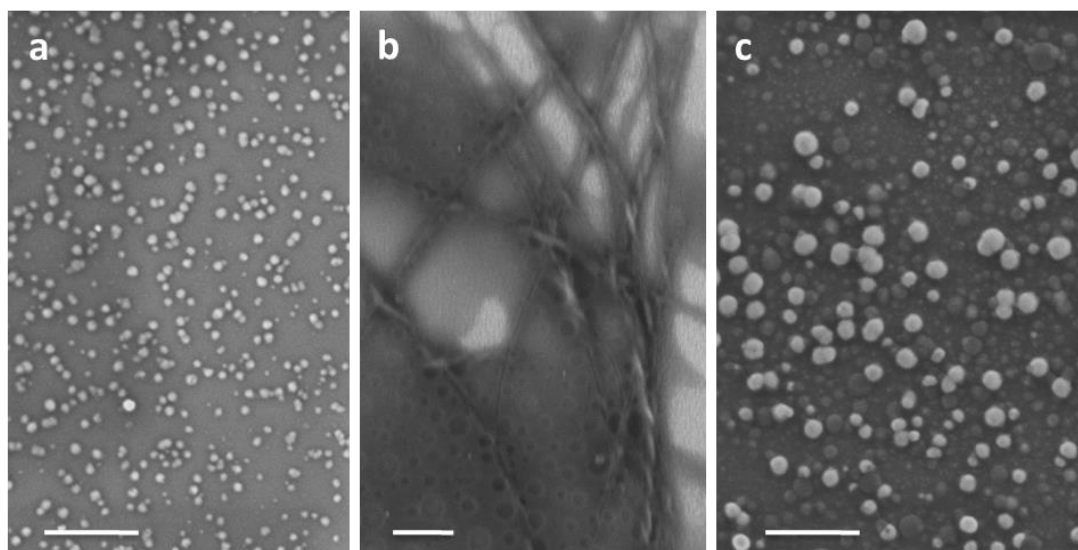


Figure 29. SEM images of (a) **F127**, (b) **HCP-1** and (c) **HCP-1-M** in water, scale bars shown 500nm. Reproduced with permission of ref. 101 © 2017, American Chemical Society.

The images of the other three polymers alone in aqueous suspensions (a, c, e) and micelle suspensions of polymers in **F-127** (b, d, f) are shown in Figure 30. Similar to **HCP-1**, these polymers are formed fibers in water, but the micelles all displayed round particles in aqueous suspensions.

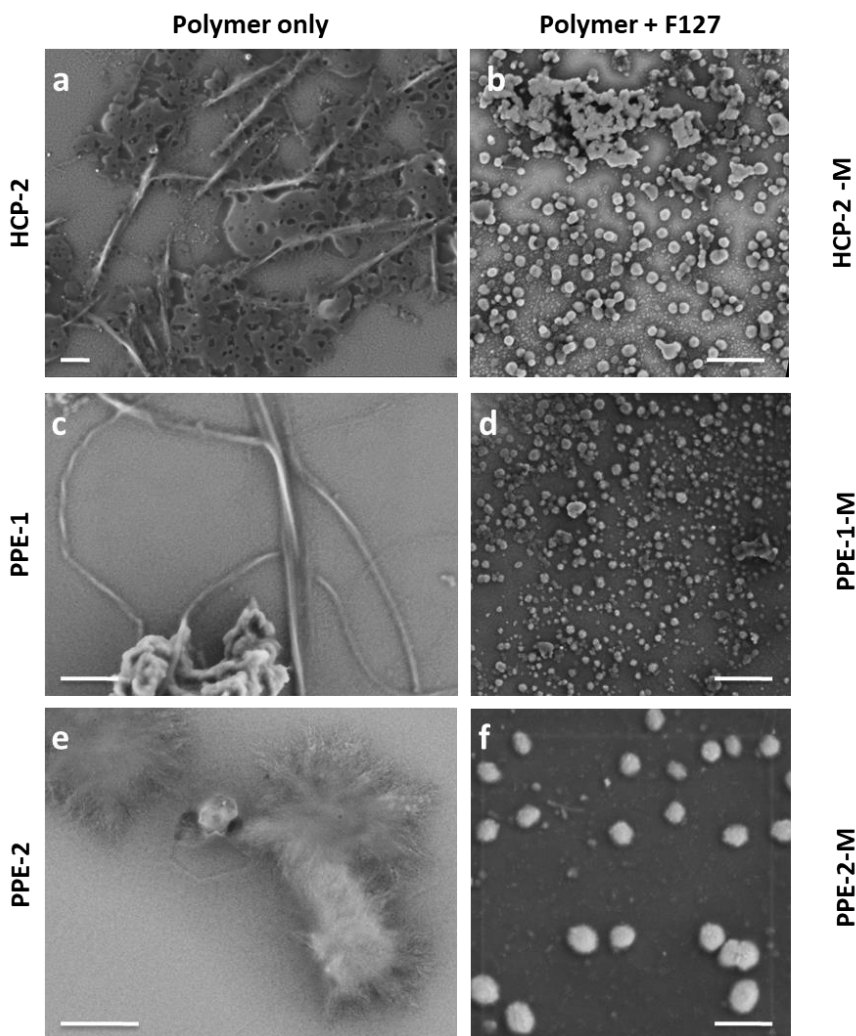


Figure 30. Comparison of aqueous suspensions of polymers alone (a, c, e) with micelle suspensions of polymers in **F-127** (b, d, f), scale bars 500 nm.

The formed micelles show excellent sensing performance to the nitroaromatic analytes, as compared to those in organic solvents such as THF. The K_{sv} values of the **HCPs-M** and **PPEs-M** are shown in Figure 31 and summarized in Table 5. The fluorescence quenching efficiencies of the fluorescent micelles for nitro-analytes are in the same order as their original polymers: **2-NA** > **PA** > **NP** > **TNT** > **DNB** > **DNT** > **3-NA** > **NB** > **A**. The micelles of HCPs show better quenching efficiencies to the analytes than the micelles of PPEs,

consistent with the performances of their polymers. The K_{sv} of the fluorescent micelles **HCPs-M** are doubled (Figure 32) in comparison to the values of the **HCPs**.

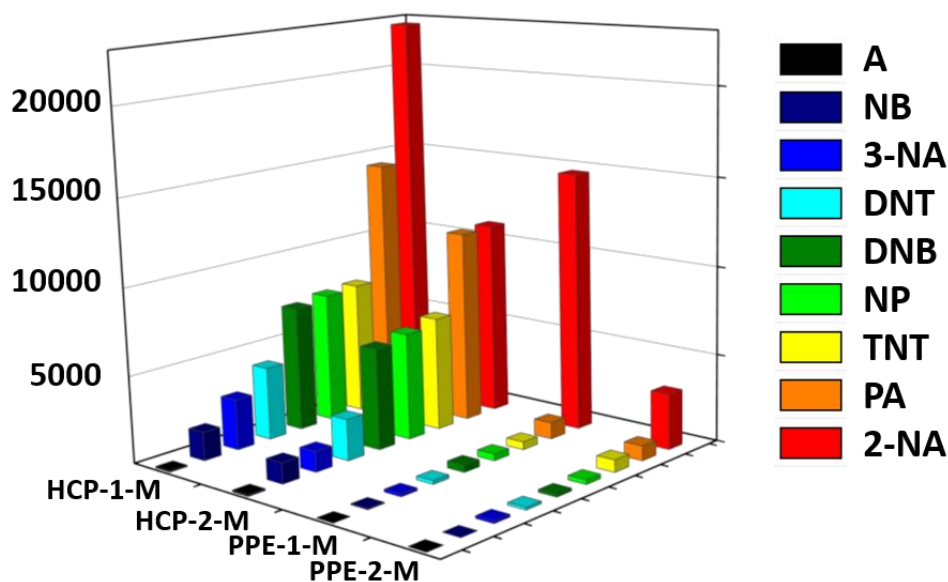


Figure 31. Fluorescence quenching efficiencies of HCPs-M and PPEs-M for different analytes. The z-axis denotes the Stern-Volmer constant K_{sv} . Reproduced with permission of ref. 101 © 2017, American Chemical Society.

Table 5. K_{sv} values of the fluorescent micelles to different analytes.

Analytes	HCP-1-M	HCP-2-M	PPE-1-M	PPE-2-M
A	85	99	1	1
NB	1649	1197	63	8
3-NA	2927	1187	162	147
DNT	4216	2374	211	145
DNB	7208	5831	405	161
TNT	7495	6157	394	260
NP	7624	6548	447	707
PA	14468	11076	948	851
2-NA	22720	11145	14837	3180

The limits of detection (LOD) of HCPs and their micelles for the analytes were estimated and listed in Table 6. The LOD of HCP-1-M to 2-NA in water is as low as 18 ppm, which is one

third of the LOD of HCP-1 for 2-NA in THF. It turns out the HCP micelles are more sensitive towards nitroaromatics than the HCPs in THF. The construction of fluorescent micelles is an effective method to realize the aqueous phase detection of nitroaromatic by the fluorescent conjugated polymers. **F-127** carries HCPs as sensing cores into water where nitroaromatic species can be detected.

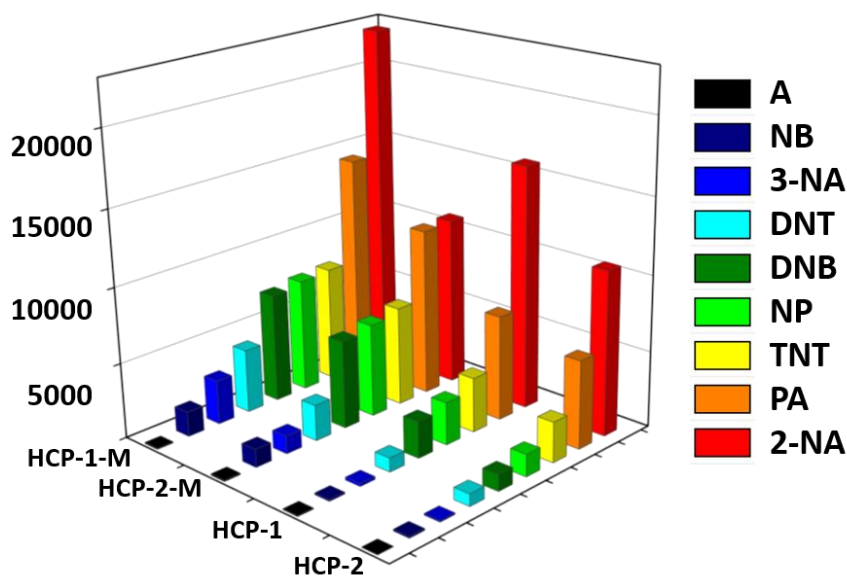


Figure 32. Fluorescence quenching efficiencies of **HCP-1**, **HCP-2**, **HCP-1-M** and **HCP-2-M** for different analytes. The z-axis denotes the Stern-Volmer constant K_{sv} . Reproduced with permission of ref. 101 © 2017, American Chemical Society.

Table 6. Limits of detection (LOD) for HCPs-M and HCPs towards the nitroaromatics.

analytes	HCP-1-M [mol/L]	HCP-2-M [mol/L]	HCP-1 [mol/L]	HCP-2 [mol/L]
A	4.7×10^{-5}	1.0×10^{-4}	1.2×10^{-4}	5.5×10^{-4}
NB	2.4×10^{-6}	8.3×10^{-6}	6.8×10^{-5}	1.2×10^{-4}
3-NA	1.4×10^{-6}	8.4×10^{-6}	4.1×10^{-5}	1.3×10^{-4}
DNT	9.5×10^{-7}	4.2×10^{-6}	8.6×10^{-6}	1.7×10^{-5}
DNB	5.5×10^{-7}	1.7×10^{-6}	3.3×10^{-6}	1.3×10^{-5}
TNT	5.3×10^{-7}	1.6×10^{-6}	2.8×10^{-6}	9.4×10^{-6}
NP	5.2×10^{-7}	1.5×10^{-6}	2.2×10^{-6}	5.1×10^{-6}
PA	2.8×10^{-7}	9.0×10^{-7}	1.2×10^{-6}	2.4×10^{-6}

2-NA	1.8×10^{-7}	9.0×10^{-7}	5.0×10^{-7}	1.3×10^{-6}
------	----------------------	----------------------	----------------------	----------------------

The polymers are in a more aggregated state in the micelles than in THF. Therefore, they may aggregate together to form 2D or 3D patterned structures under a confinement effect.¹¹⁶ The inner space of micelles provides an environment, not only the fluorescent polymers are closer to each other, the trapped polymers are also more close to the neighboring analytes. Thus, long-range exciton migration may happen between the analytes and the polymers, and stronger electrostatic interactions are expected between the analytes and micelles in aqueous phase. This enhanced interaction in the relatively confined space could further facilitate the electron/ energy transfer process, resulting in the amplified quenching effect of the fluorescent micelles subsequently.¹¹⁷

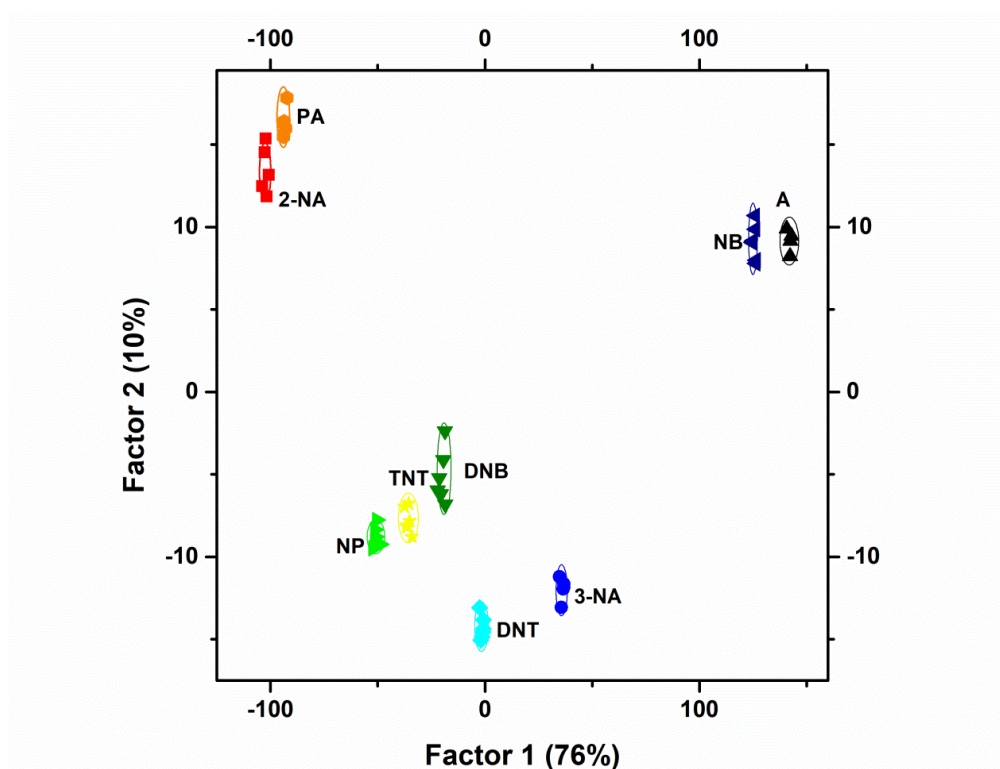


Figure 33. 2-D canonical score plot of discriminant scores with 95% confidence ellipses for all obtained data points of the fluorescent micelles against different analytes. Reproduced with permission of ref. 101 © 2017, American Chemical Society.

Linear discriminant analysis (LDA) was carried out with the quenching results obtained of the fluorescent micelles ($0.5 \mu\text{M}$) quenched by the analytes (0.3 mM). The fluorescence intensity changes were recorded and analyzed by LDA; four canonical factors were generated as 76%,

10%, 8% and 6%. The two larger canonical factors build a 2-D discrimination plot with nine distinct clusters. As illustrated in Figure 33, the nine clusters are well separated without any overlap. The unknown samples were identified with 100% accuracy based on this sensor array of fluorescent micelles. This suggests that nitroaromatics can be detected and discriminated in water, which in principle should also allow analyzation of the nitroarenes origin from explosives or as industrial pollution.

2.4 Conclusion

In summary, two truxene-based polymers (**HCP-1** and **HCP-2**) were synthesized and their sensory responses were compared to those of their analogous poly(*p*-phenyleneethynylene)s (**PPE-1** and **PPE-2**) with alkyl and alkyloxy chains. Star-shaped **HCPs** with a truxene moiety reveal better sensing performance to the nitroaromatics compared to linear **PPEs**: a) the presence of the electron rich truxene unit and b) the hyperbranched character lead to higher sensing efficiencies in explosive detecting even though the observed K_{sv} are only in a medium range. The alkyl and alkyloxy side chains make a difference in the sensing performance of the polymers. Polymers with alkyl side chains (**HCP-1** and **PPE-1**) demonstrate a better performance to the nitroaromatics than those with alkyloxy side chains (**HCP-2** and **PPE-2**). The quenching efficiency of polymers to the nitroaromatics correlates with a) the overlap area of the absorption spectra of analytes and the emission spectra of polymers, suggesting strong Förster energy transfer in the quenching process; b) electron transfer between the electron-deficient nitroaromatic and the electron-rich polymers based on the calculated energy level. The sensor array built on the four polymers could successfully discriminate the nine analytes and identify them with 100% accuracy.

Fluorescent micelles formation was carried out by covering the polymers with amphiphilic **F-127** micelles. These fluorescent micelles realize the effective detection and discrimination of nitroaromatics in water. This approach could increase the sensitivity towards nitroaromatics in water than the **HCPs** in THF, which is more effectively and friendly to the environment.

**Chapter 3. A Tetraphenylethene-Based Polymer Array:
Detect and Discriminate Nitroaromatics**

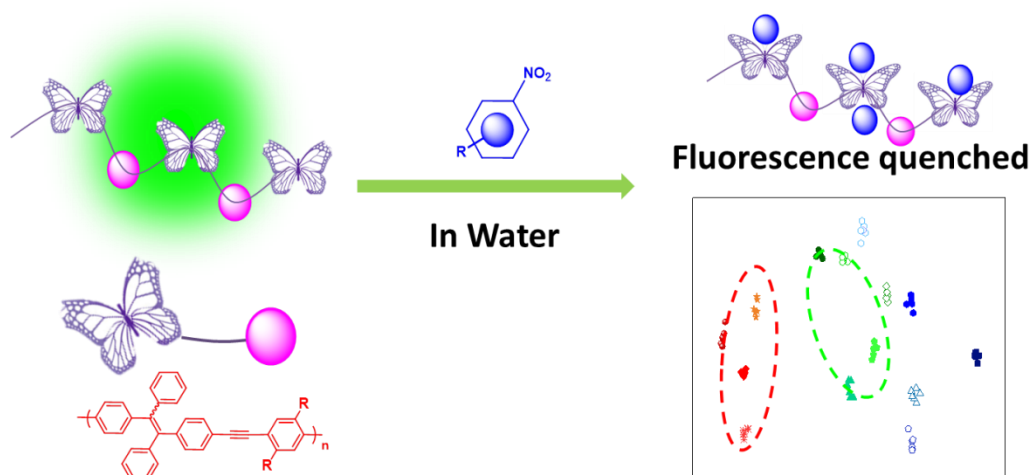


Figure 34. Systematic illustration of TPE-based polymers for detection and discrimination of nitroaromatics.

In this chapter, a new sensor array for nitroaromatics detection based on four polymers-containing tetraphenylethene struts (**TPEPs**) is investigated.¹¹⁸ The **TPEPs** build up a sensor array for detecting fourteen nitroaromatics. Their optical properties in different solvents have been investigated. All polymers show aggregation induced emission (AIE) in water. The sensor array displays unique fluorescence quenching responses to the analytes. The **TPEPs** demonstrate good sensitivity and discriminatory power to the detected nitroaromatics. The quenching efficiencies are highly related to the spectral overlap areas (absorbance of the analyte and the emission of the fluorescent polymer), and also the electron deficiency of the analytes. The four-element sensor array has great discrimination power. Even five pairs of regio-isomers, with very similar physical and chemical properties, were easily discriminated.

3.1 Aggregation-Induced Emission and the TPE Moiety

In most cases, the photophysical parameters of the organic fluorophores are measured in highly dilute solution, where the fluorescent molecules are approximately isolated. However, the fluorophores usually show different emission behaviors in dilute and aggregated state. For instant, fluorescence is quenched in high concentrations state, the main cause of the concentration quenching process is associated with the formation of aggregates. The concentration quenching effect is referred to as “aggregation-caused quenching” (ACQ). An example of *N,N*-dicyclohexyl-1,7-dibromo-3,4,9,10-perylenetetracarboxylic diimide (DDPD) is recommended here (Figure 35).¹¹⁹ DDPD is highly fluorescent in the good solvent THF. The emission is weakened by adding the poor solvent water. The molecules are aggregated together owing to the immiscibility of the mixture of THF and water. When the water content is increased to >60 vol%, the solvating power of the mixed solvents becomes very poor that most of the DDPD molecules get aggregated. The emission is almost fully quenched as a result of the aggregation.

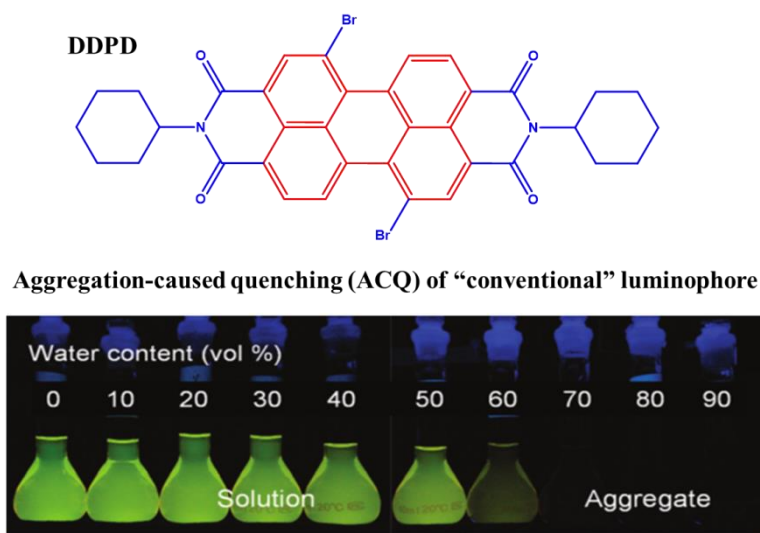


Figure 35. Fluorescence photographs of solutions/suspensions of DDPD (10 mM) in THF/water mixtures with different water contents. Reproduced with permission of ref. 119 © 2011, The Royal Society of Chemistry.

The reason for the ACQ effect of conventional fluorophores is typically caused by the planar aromatic rings. The aggregates of the planar aromatic rings may arouse strong π - π stacking

interactions, which prompts the formation of detrimental species as excimers and lead to the ACQ effect. The ACQ effect is quite harmful for practical applications.

In 2001, Tang's group reported an uncommon fluorescent system, which is precisely opposite to the blamed ACQ effect.¹²⁰ The emission of a series of siloles was induced by aggregate formation, namely "aggregation-induced emission" (AIE). AIE fluorophores are non-fluorescent in dilute solution, but exhibit high fluorescence when aggregated. Hexaphenylsilole (**HPS**) is an example of the AIE effect (Figure 36). In a dilute state, the phenyl rotors in the HPS molecule undergo dynamic intramolecular rotations, leading to non-radiatively annihilation of its excited state. As a result, the molecule is non-luminescent. While in the aggregated state, the HPS molecules cannot go through a π - π stacking process due to its propeller shape, the intramolecular rotations of its phenyl rotors are restricted owing to the physical constraint. This restriction of intramolecular rotations (RIR) blocks the non-radiative pathway and opens up the radiative channel. As a result, the HPS molecules come emissive in the aggregated state. The AIE process offers a platform to look into light emissions from fluorescent aggregates and expand the practical application of organic fluorophores.

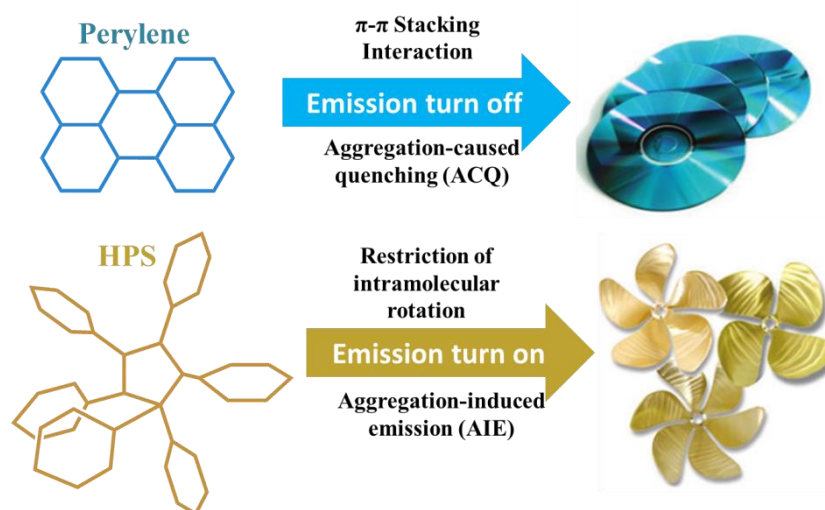


Figure 36. Schematic diagram of aggregation-caused quenching of planar luminophoric molecules (a) and aggregation-induced emission of non-planar luminogenic molecules (b). Reproduced with permission of ref. 119 © 2011, The Royal Society of Chemistry.

Tetraphenylethene (TPE) is a well-known moiety for constructing AIE fluorophores.¹²¹⁻¹²² AIE was noticed for TPE-based polymers. They emit weakly in good solvents but strongly in poor solvents or in films. The AIE effect is dependent upon polarity, viscosity, electrostatic and hydrophobic interactions, steric hindrance, coordination or reactivity. These elements can all be exploited in sensing schemes.⁹³ AIE sensors have been designed for ions, explosives and biomolecules to name a few.¹²³⁻¹²⁴ Figure 37 shows an example of fluorogenic Zn(II) and chromogenic Fe(II) sensors based on terpyridine-substituted TPE, **TPE2TPy**.¹²⁵ TPE's AIE performance, easy synthesis and its modular functionalization make it attractive targets for building optical sensor materials. TPE-based polymeric sensor arrays with high sensitivity and discrimination function are rarely reported so far. Thus, we have prepared four TPE-based polymers (**TPEPs**) constituting a sensor array comprising four elements.

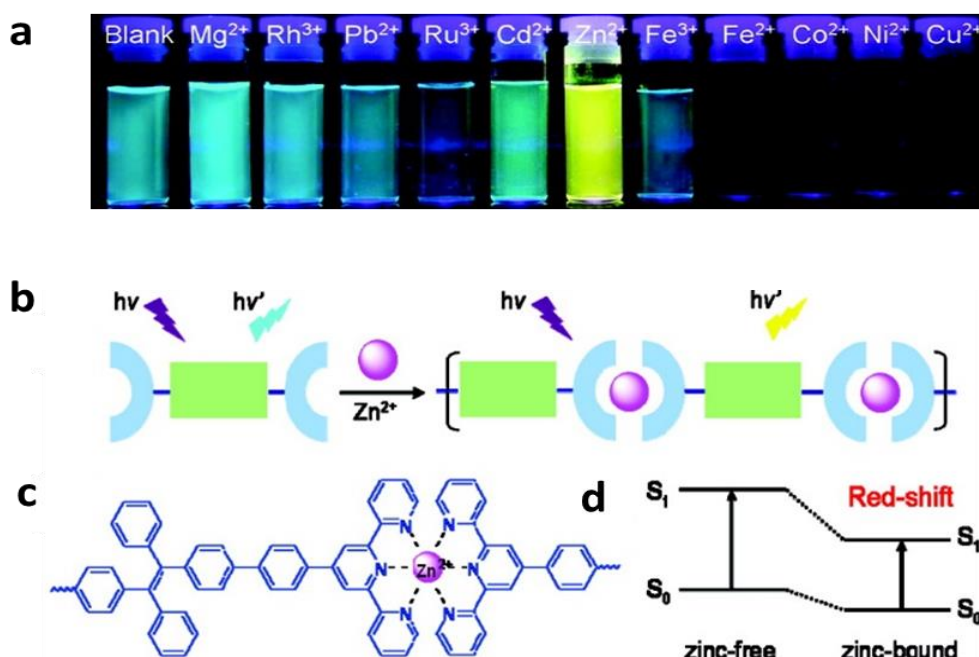


Figure 37 (a) Photograph of the aqueous solutions of **TPE2TPy**/cation mixtures taken under UV illumination. (b) Possible stoichiometry of zinc-**TPE2TPy** complex. (c) Structure of zinc-bound **TPE2TPy**. (d) Proposed mechanism for the spectral red-shift of **TPE2TPy** upon binding to Zn²⁺. Reproduced with permission of ref. 125 © 2011, American Chemical Society.

nm) and **TPEP-3** (140 nm), while **TPEP-4** shows the broadest Stokes shift (158 nm). The differences of the Stokes shift for **TPEP-1** to **TPEP-3** are attributed to a side chain effect, as the polymers have a similar degree of polymerization and a similar PDI.

Table 7. Photophysical Properties and GPC Data for **TPEPs**.

Polymer	$\lambda_{\max, \text{abs}}$ [nm] ^a	$\lambda_{\max, \text{em}}$ [nm] ^a	$\Phi_{F \text{ sol}}$ [%] ^a	$\Phi_{F \text{ agg}}$ [%] ^b	M_n [g/mol] ^c	M_w/M_n ^c	τ_{sol} [ns] ^a	τ_{agg} [ns] ^b
TPEP-1	385	515	4.0	26	17000	1.5	0.08	1.26
TPEP-2	376	522	1.3	35	12000	1.8	0.08	1.24
TPEP-3	377	517	2.4	18	17000	1.8	0.07	0.62
TPEP-4	362	520	1.6	16	5000	1.3	0.05	0.68

^a Determined in THF. ^b Determined in THF/H₂O (5:95). ^c Determined by GPC in THF.

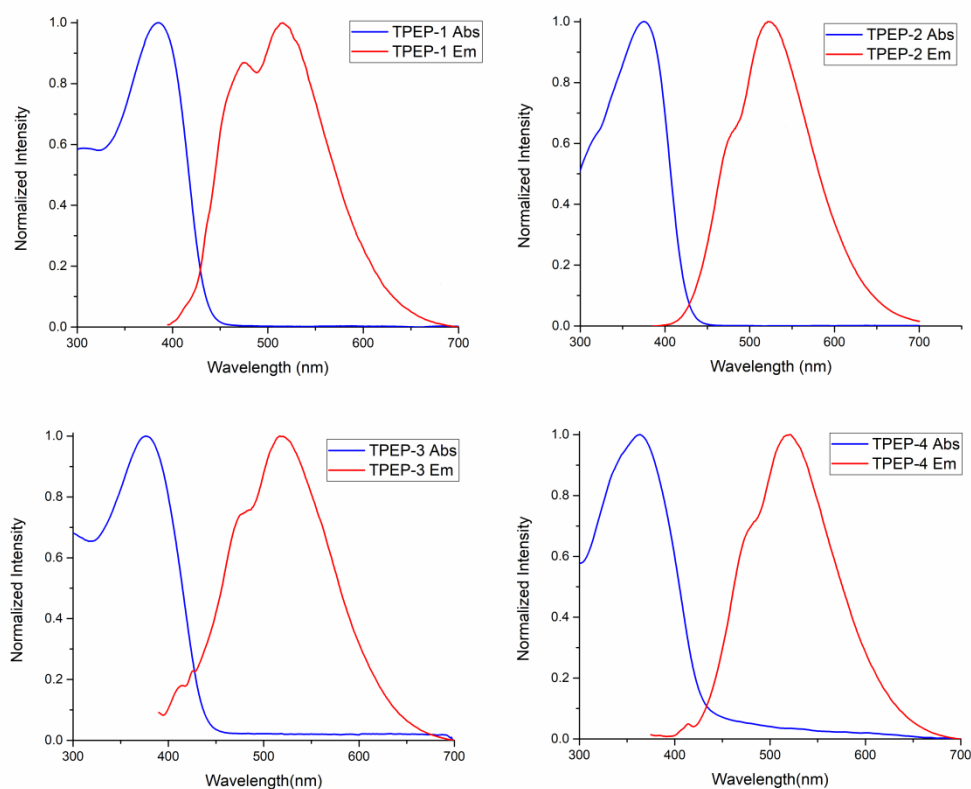


Figure 39. Absorption and emission spectra of **TPEPs** in THF. Reproduced with permission of ref. 118 © 2018, American Chemical Society.

The emission spectra of the polymers are measured in different solvents (CHCl_3 , THF, hexane, methanol, water and mixtures of water/THF) to investigate their AIE effect. Normalized absorption and emission spectra of **TPEPs** are solvent-independent, which means the shape and maximum peaks stay the same in those solvents, but the emission intensity depends on the solvents. **TPEP-2** (excited at 376 nm) is almost non-emissive in good solvent THF and CHCl_3 (Figure 40a). In poor solvents such as water and MeOH, the emission intensity increases sharply. The AIE characteristics of **TPEP-2** were further evaluated by incremental water fractions in $\text{H}_2\text{O}/\text{THF}$ mixtures (see Figure 40b). The emission intensity increases with increasing the water fractions. At a water content over 70%, a rapid increase of fluorescence intensity is observed.

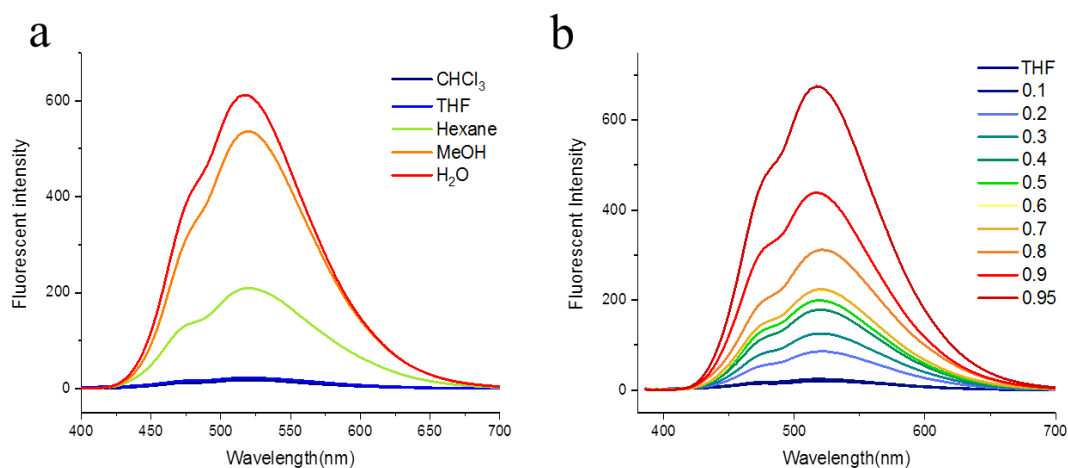


Figure 40. (a) Emission spectra of **TPEP-2** in different solvents. (b) Emission spectra of **TPEP-2** in different ratios of $\text{H}_2\text{O}/\text{THF}$ (excited at 376 nm). Reproduced with permission of ref. 118 © 2018, American Chemical Society.

The quantum yields of **TPEPs** in THF are 4.0%, 1.3%, 2.4% and 1.6%, respectively (see Table 7). In a $\text{H}_2\text{O}/\text{THF}$ mixture (95/5) the quantum yields increase to 26%, 35%, 18%, and 16%, which are 6.5 to 27 times higher than their emission intensities in pure THF (see Table 7). The quantum yields of **TPEPs** in different states of aggregation (a: in THF; b: in $\text{H}_2\text{O}/\text{THF}$ mixture (95/5); c: in film) are listed in Table 8. All of the TPE-based polymers demonstrate aggregation enhanced emission (AEE) effects. However, the difference of the AEE effect from the polymers seems not quite clear. The different side chains demonstrate a significant influence on the **TPEPs'** AIE performances. **TPEP-1**, with the hydrophilic OSw

sidechain, shows a low quantum yield increase (only 6.5 times in H₂O/THF mixture (95/5)) compared to THF. **TPEP-2**, with the most hydrophobic hexyl sidechain, has the strongest AIE performance increase (27 times). Therefore, the hydrophobic chains are more favorable than the hydrophilic in building strong AIE structures. The hydrophilic groups could help the polymers distribute better than the hydrophobic ones in water, leading to a low degree of aggregation. The low aggregation results in weak fluorescence of the polymers.

Table 8. The quantum yields of **TPEPs** under different conditions.

Polymers	$\Phi_{F_{sol}}^a$ (%)	$\Phi_{F_{agg}}^b$ (%)	$\Phi_{F_{film}}^c$ (%)
TPEP-1	4.0	26	26
TPEP-2	1.3	35	32
TPEP-3	2.4	18	16
TPEP-4	1.6	16	15

^a Determined in THF. ^b Determined in H₂O/THF (95/5). ^c Determined in film.

The morphologies of **TPEPs** in aggregated state are explored through SEM, carried out with a Zeiss Ultra55. This work was done by Prof. Schröder's Group, University of Heidelberg. A 1 mL droplet of each suspension (**TPEPs** 1 μ M in a H₂O/THF mixture (95/5)) was placed on a piece of plasma-cleaned silicon wafer and air dried. Samples were imaged in a FESEM (Ultra, Carl Zeiss Microscopy). The images in are shown in Figure 41. **TPEP-1** with the hydrophilic OSw sidechain is quite different from the other three, presenting relatively homogeneous aggregated state. **TPEP-2**, **TPEP-3** and **TPEP-4**, are heterogeneous with different dimensions of spheres. The morphology of the polymers is mainly determined by the side chains. **TPEP-1** with the hydrophilic OSw side chain is homogeneous when aggregated from aqueous solution. The other ones with hydrophobic chains (Hexly and OHexyl) are heterogeneous aggregated in aqueous solution.

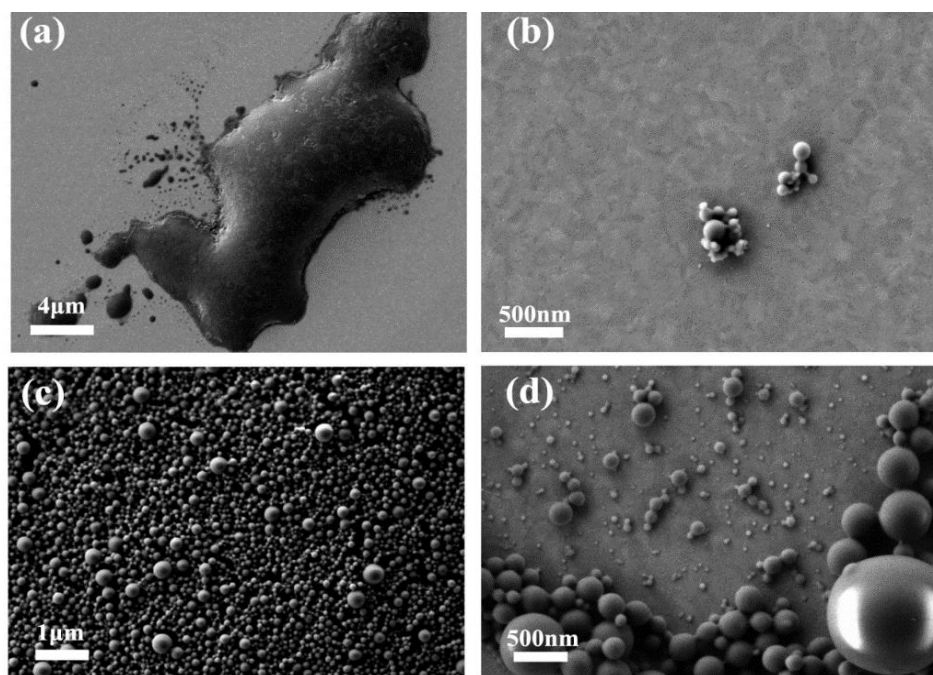


Figure 41. SEM images of (a) **TPEP-1**, (b) **TPEP-2**, (c) **TPEP-3** and (d) **TPEP-4**. Reproduced with permission of ref. 118 © 2018, American Chemical Society.

Those **TPEPs** suspensions are tested as sensors for different nitroaromatic analytes and formed into sensor array which can detect and discriminate the analytes.

3.3 Detection of Nitroaromatics by the TPEPs

In practical applications, both selectivity and sensitivity are critical to successfully detect and discriminate analytes. Here a detector approach for nitroaromatics is evaluated. A good sensor should not only spot the nitroaromatics very sensitively and quickly, but also precisely tell the difference between two distinct analytes. Discrimination of strong electron acceptors (such as picric acid) from weak ones (such as nitrobenzene) is fairly easy. However, it is more challenging to discriminate different isomeric nitroaromatics.

Isomer classification is challenging for chemical identification, and analytical techniques such as GC-MS often struggle to discriminate isomers, so this is an acute question. Regio-isomers have the same molecular formula and same functional groups, but the substituents locate at different positions on a parent framework. The discrimination of positional isomers is difficult because they display similar physical and chemical properties. For nitroaromatics, regio-isomers are common, as secondary substituents can be placed *ortho*, *meta* or *para* to one or more NO₂ group(s). Thus efficient sensitive and selective sensors are highly desired, especially for the discrimination of isomers.

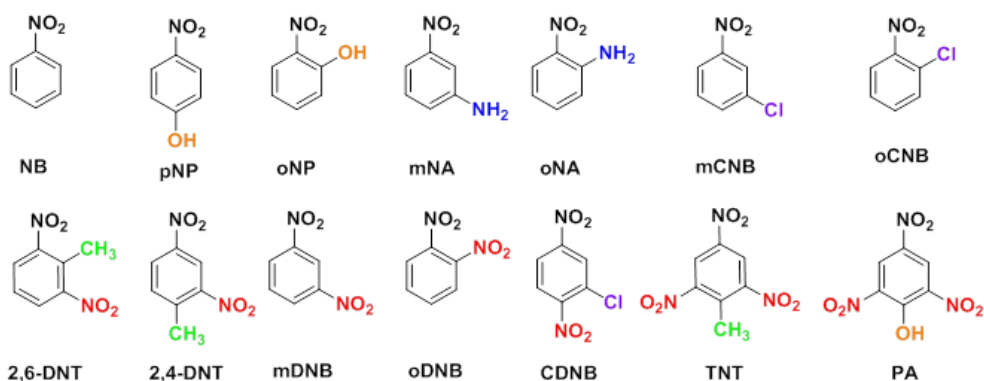


Figure 42. Structures of the different tested nitroaromatics. Reproduced with permission of ref. 118 © 2018, American Chemical Society.

The **TPEPs 1-4** are exploited for the detection and discrimination of 14 nitroaromatics, including 5 pairs of structural isomers: nitrobenzene (**NB**), 4-nitrophenol (**pNP**), 2-nitrophenol (**oNP**), 3-nitroaniline (**mNA**), 2-nitroaniline (**oNA**), 3-chloro-2-nitrobenzene (**mCNB**), 1-chloro-2-nitrobenzene (**oCNB**), 2,4-dinitrotoluene (**2,4-DNT**), 2,6-dinitrotoluene

(**2,6-DNT**), 1,3-dinitrobenzene (**mDNB**), 1,2-dinitrobenzene (**oDNB**), 1-chloro-2,4-nitrobenzene (**CDNB**), trinitrotoluene (**TNT**) and picric acid (**PA**). The structures are shown in Figure 40, and the different substitutes are marked in different colors.

The fluorescence intensity of the **TPEPs** solutions decreases when adding the analytes. The K_{sv} constants were determined with all of the analytes in aqueous solution ($H_2O/THF=95/5$).¹²⁶ The fourteen nitroaromatics show distinct quenching abilities for the polymers (Figure 43, summarized in Table 9). **NB** is the weakest quencher, while **CDNB**, **TNT** and **PA** are good quenchers. These good quenching ability are related to their highly electron deficiencies. The four **TPEPs** present different optical properties (absorption and emission spectra), electrical properties (energy level) and physical properties (especially in aggregation state). Thus, every **TPEP** has a unique quenching response to the fourteen analytes (see Figure 43).

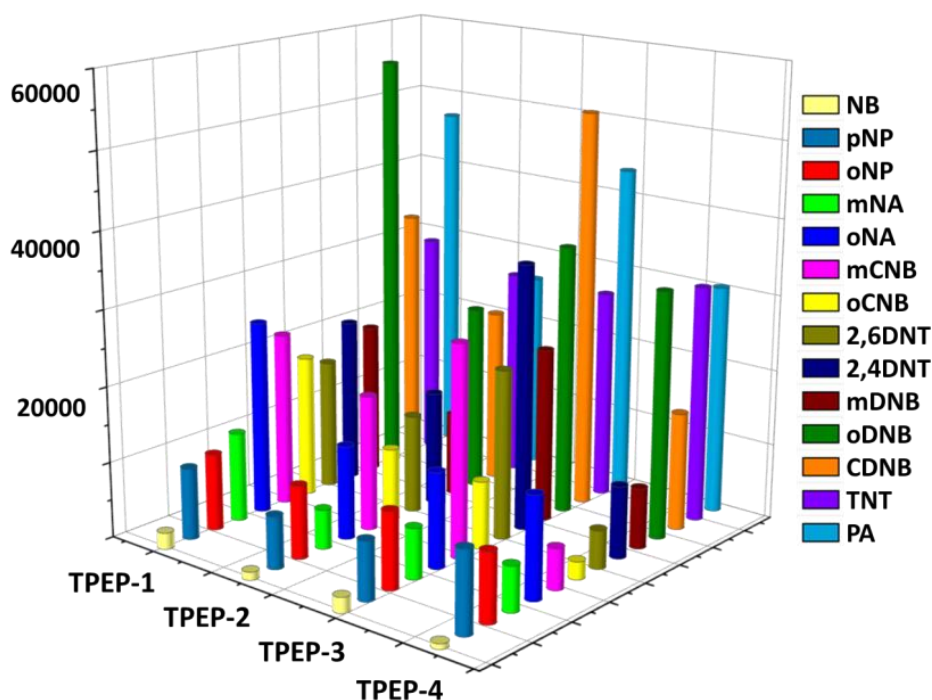


Figure 43. The K_{sv} constants of **TPEPs** to the analytes. Reproduced with permission of ref. 118 © 2018, American Chemical Society.

TPEP-1 and **TPEP-3** display a higher quenching efficiency for most of the analytes than **TPEP-2** and **TPEP-4**, attributed to their electron rich character and also their improved

emission spectral overlap with the absorption spectra of the analytes. This is highly related to their K_{sv} values (see Table 9).

Table 9. The K_{sv} constants of **TPEPs** to the analytes.

Analyte	TPEP-1	TPEP-2	TPEP-3	TPEP-4
NB	2180	1073	2057	720
pNP	9495	6932	7750	10762
oNP	10138	9622	10148	9067
mNA	11812	5216	6700	5951
oNA	25587	12405	12582	13442
mCNB	23003	17902	27925	5426
oCNB	18851	9668	8944	2363
2,6-DNT	17238	13006	22413	5066
2,4-DNT	21776	15039	35130	9506
mDNB	20128	11023	22995	7993
oDNB	55986	24594	35624	32595
CDNB	34029	23075	52361	15588
TNT	29869	27560	27643	31263
PA	47016	26168	43469	30340

The emission spectra of the polymers (Figure 44) are mainly dominated by the TPE backbone. However, **TPEP-1** and **TPEP-3** have a blue-shifted shoulder peak which might be due to planarization of the polymers. The shoulder peak increases the spectral overlap with absorption spectra of some analytes (such as **oNA** and **PA**), and therefore increases the interaction between nitroaromatic and polymer.¹¹⁰

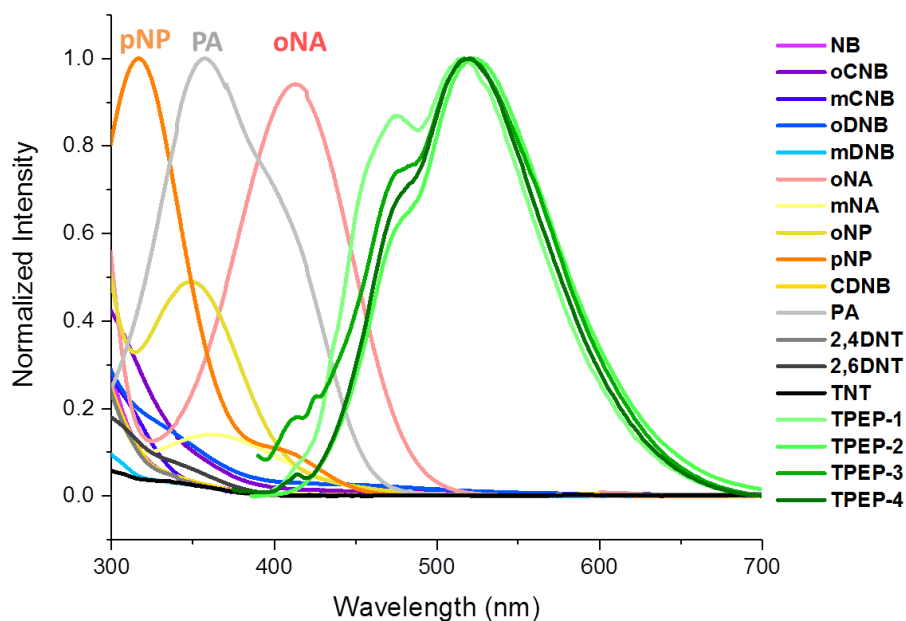


Figure 44. The normalized absorption spectra of analytes and emission spectra of the **TPEPs** in water. Reproduced with permission of ref. 118 © 2018, American Chemical Society.

The polymers are powerful sensors towards the analytes as the K_{sv} are in excess of 10^4 M^{-1} , especially for **oDNB**, **CDNB**, **TNT** and **PA**. The limits of detection (LOD) of TPEPs for the analytes are estimated and listed in Table 10. The LOD of the nitroaromatics are below ppm level, demonstrating the polymers' excellent detecting ability as nitroaromatics sensors.

Table 10. Limits of detection (LOD) for **TPEPs** towards analytes

Analytes	TPEP-1(μM)	TPEP-2(μM)	TPEP-3(μM)	TPEP-4(μM)
NB	5.18	3.26	6.03	29.1
pNP	1.19	5.05	1.6	1.94
oNP	1.11	3.64	1.22	2.31
mNA	0.96	6.71	1.85	3.52
oNA	0.44	2.82	0.98	1.56
mCNB	0.49	1.96	0.44	3.86
oCNB	0.60	3.62	1.39	8.86
2,6-DNT	0.66	2.69	0.55	4.13

2,4-DNT	0.52	2.33	0.35	2.2
mDNB	0.56	3.18	0.54	2.62
oDNB	0.20	1.42	0.35	0.64
CDNB	0.32	1.52	0.24	1.34
TNT	0.38	1.27	0.45	0.67
PA	0.24	1.34	0.29	0.69

The performance of **TPEPs** exceeds that of the earlier evaluated polymers **HCPs**¹⁰¹ and **PPEs**¹²⁷ in Chapter 2, which also can detect the nitroaromatics in water. **PA**, is taken as an example to compare the performance of the three series of polymers (see Table 11). Compared to the water-soluble PPEs, TPE-based polymers show an order of magnitude higher K_{sv} for PA, and concomitantly low LODs (one to two order of magnitude lower than for the **PPEs**. The **HCPs** are more similar in sensing performance, but they do need additional surfactant (**F-127**) to work properly for nitroaromatics sensing. These sensors exploit surfactochromic behavior for the detection. **TPEPs** directly detect nitroarenes in aqueous solution employing the AIE effect, therefore, these structures are excellent choice for nitroaromatics sensing in water.

Table 11. The K_{sv} and LOD values of **TPEPs** compared to **HCPs**¹⁰¹ and **PPEs**¹²⁶ for Picric Acid.

TPEPs	TPEP-1	TPEP-2	TPEP-3	TPEP-4
K_{sv}	$4.7 \cdot 10^4$	$2.6 \cdot 10^4$	$4.3 \cdot 10^4$	$3.0 \cdot 10^4$
LOD(M)	$2.4 \cdot 10^{-7}$	$1.3 \cdot 10^{-6}$	$2.8 \cdot 10^{-6}$	$6.9 \cdot 10^{-7}$
HCPs ¹⁰¹	HCP-1-M	HCP-2-M	HCP-1	HCP-2
K_{sv}	$1.4 \cdot 10^4$	$1.1 \cdot 10^4$	$6.9 \cdot 10^3$	$5.8 \cdot 10^3$
LOD(M)	$2.8 \cdot 10^{-7}$	$9.0 \cdot 10^{-7}$	$1.2 \cdot 10^{-6}$	$2.4 \cdot 10^{-6}$
PPEs ¹²⁶	P1	P2	P3	P4
K_{sv}	$1.8 \cdot 10^3$	$1.8 \cdot 10^3$	$7.4 \cdot 10^2$	$1.2 \cdot 10^2$
LOD(M)	$1.1 \cdot 10^{-5}$	$1.4 \cdot 10^{-5}$	$1.0 \cdot 10^{-5}$	$4.0 \cdot 10^{-5}$

The detection of the nitroaromatics is composed of FRET and DET mechanism from the polymers to the analytes, modulated by hydrophobic interactions.⁶¹ Analytes with lower LUMO energy display better quenching performance due to strong DET. The energy level of the fourteen analytes were calculated via B3LYP/6-311++G** level of theory (Table 12). The analytes with lower LUMO level values should have a better quenching potential to the electron rich polymers because of their severely electron deficiency. **PA**, **TNT** and **CDNB** are the analytes with the lowest LUMO level, and at the same time the best quencher to the polymers. At the same time, the analytes listed in the first row of Table 12 are relative weak quencher to all the fluorescent polymers.

Table 12. Calculated LUMO level of the analytes at B3LYP/6-311++G** Level of Theory^a

Analytes	pNP	oCNB	oNA	mNA	mCNB	NB	oNP
LUMO (eV)	-2.42	-2.64	-2.67	-2.75	-2.90	-2.92	-3.19
Analytes	2,4-DNT	mDNB	2,6-DNT	oDNB	CDNB	TNT	PA
LUMO (eV)	-3.25	-3.31	-3.40	-3.45	-3.67	-3.92	-4.20

^a Analytes are ordered according to their increasing, calculated LUMO level.

Cyclic voltammetry measurement was performed to investigate the electrochemical properties of the polymers, shown in Figure 45. On the basis of the onset potential and according to the equation 3, the highest occupied molecular orbital (HOMO) energy level can be estimated. The lowest unoccupied molecular orbital (LUMO) energy level can be calculated from equation 4:

$$E_{HOMO} = -(E_{onset(ox),FOC} + 4.8) eV$$

Equation 3: HOMO energy level calculation.

$$E_{LUMO} = (E_{HOMO} + E_g^{opt}) eV, \text{ where } E_g^{opt} = 1240[nm * eV]/\lambda_{onset} [nm]$$

Equation 4. LUMO energy level calculation.

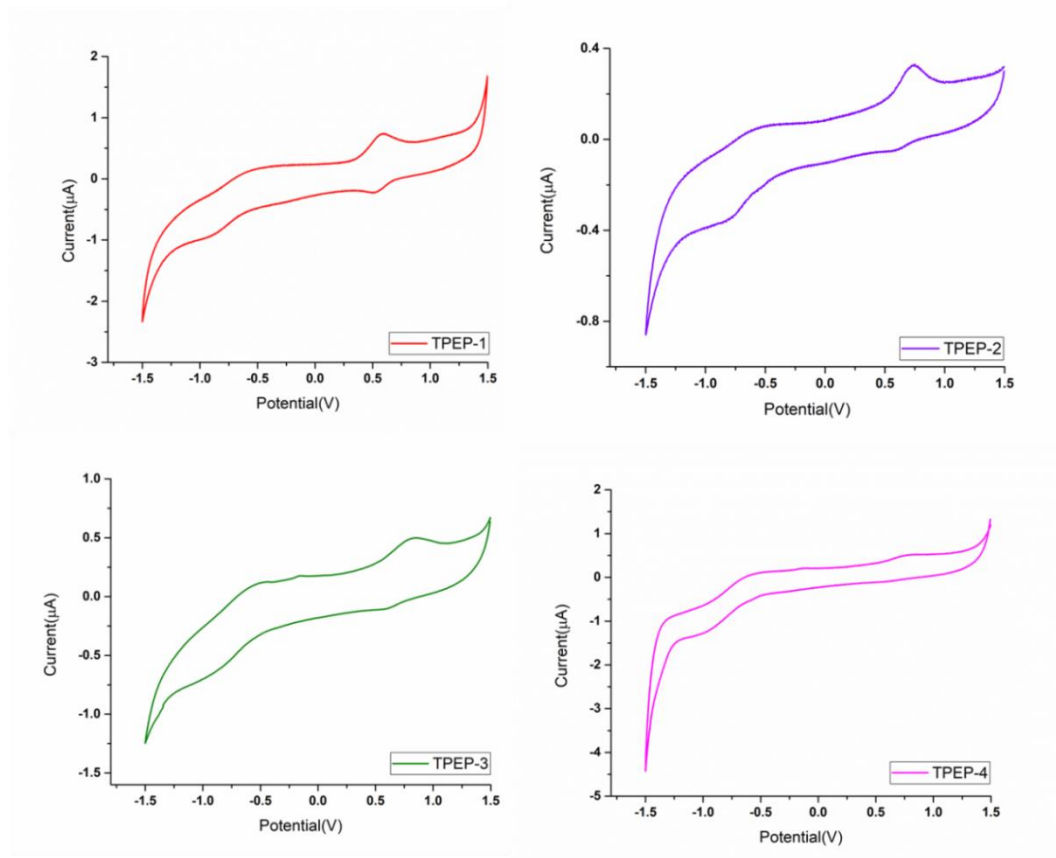


Figure 45. Cyclic voltammograms of the **TPEPs**.

The full electrochemical properties of the **TPEPs** are listed in Table 13. The HOMO levels of the **TPEPs** are measured as -4.76, -4.90, -4.93 and -4.83 eV. The LUMO are -1.83, -2.00, -2.12 and -1.99 eV, respectively.

Table 13. Electrochemical Properties of the **TPEPs**

Polymer	λ_{onset}	$E_{\text{gopt}}(\text{eV})$	$E_{\text{on}}^{\text{ox}}(\text{V})$	HOMO(eV)	LUMO(eV)
TPEP-1	423	2.93	0.56	-4.76	-1.83
TPEP-2	428	2.90	0.79	-4.90	-2.00
TPEP-3	441	2.81	0.73	-4.93	-2.12
TPEP-4	436	2.84	0.63	-4.83	-1.99

The energy gap between the **TPEPs** and the analytes is a driving force for the quenching process. The high LUMO values of the **TPEPs** surely contribute to the sensitive detection of nitroaromatics. The discrimination power of the sensor array is evaluated in the following subchapter.

3.4 Discrimination of Nitroaromatics by TPEPs

Four **TPEPs** form a sensor array that discriminates all of the 14 analytes. Solutions of the TPE polymers (1 μM in water) were exposed to the nitroaromatics (0.1 mM in methanol) in six replicates. The fluorescence changes were measured and calculated. The average fluorescence changes form a distinct response pattern (Figure 46).

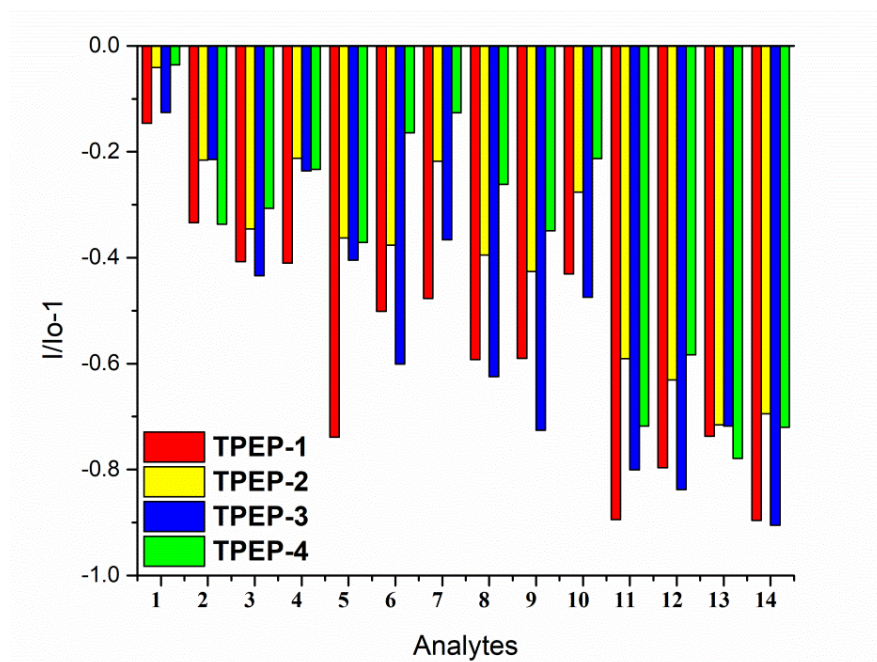


Figure 46. Fluorescent response pattern (I/I_0-1) of the TPE-based sensor array (1 μM in water) to the analytes (1-14 are **NB**, **pNP**, **oNP**, **mNA**, **oNA**, **mCNB**, **oCNB**, **2,6-DNT**, **2,4-DNT**, **mDNB**, **oDNB**, **CDNB**, **TNT** and **PA** (0.1 mM in methanol)). Reproduced with permission of ref. 118 © 2018, American Chemical Society.

Discrimination is visualized after processing the data by linear discriminant analysis (LDA), converting the training matrix (4 polymers * 14 analytes * 6 replicates) into canonical scores according to their Mahalanobis distance. After LDA, the data generate four canonical factors (66%, 18%, 11%, 5%). All of the analytes are separated as fourteen distinct clusters on the 2-D score plot map, based on the two larger canonical factors with 100% accuracy (see Figure 47). The location of the clusters on the score map is affected by the LUMO value of the analytes. The analytes with the lower LUMO level (**oDNB**, **CDNB**, **TNT** and **PA**) are located on the left side of the 2-D map (red circle). And the four analytes (**oNP**, **2,4-DNT**, **mDNB**, **2,6-DNT**) with medium LUMO level (-3.00 to -3.40 eV) are located in the middle of the map

(green circle). The five pairs of regioisomers are marked with same shape, with solid or hollow symbols to distinguish them. It turns out that the sensor array can effectively discriminate the regioisomers. Therefore, the four-element sensor detects and discriminates 14 different nitroaromatics without any problem. The sensitivity of the **TPEPs** is better than other systems **HCPs** and **PPEs**.

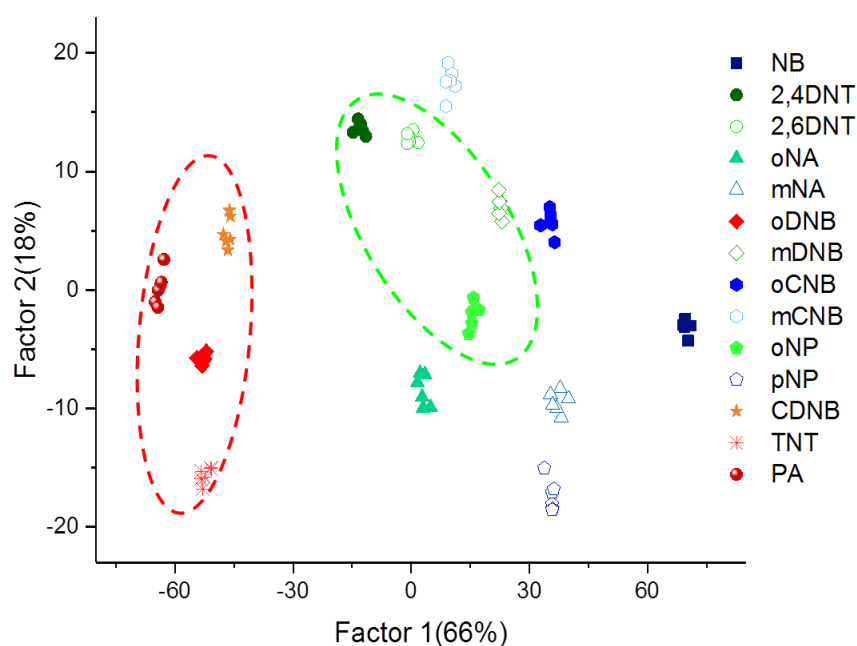


Figure 47. 2-D canonical score plot of discriminant scores with 95% confidence ellipses for all obtained data points against different analytes. Reproduced with permission of ref. 118 © 2018, American Chemical Society.

Monitoring the lifetime changes is the conventional effective method for identifying the quenching mechanism. The fluorescence lifetimes of the quenching system will be shortened if the system undergoes a dynamic quenching process. For the static quenching, the life time will be unaffected by the addition of the analytes.¹²⁸ **PA** is selected as the representative quencher owing to its superior quenching power. The lifetimes of **TPEPs** were recorded without **PA** and with different concentrations of **PA**. The lifetime changes of **TPEPs** to **PA** are shown in Figure 48. Only small, irregular changes of lifetimes were noticed, suggesting that the lifetime is irrelevant to the presence of the analytes. This means the static quenching is the dominant mechanism during the fluorescent quenching process.

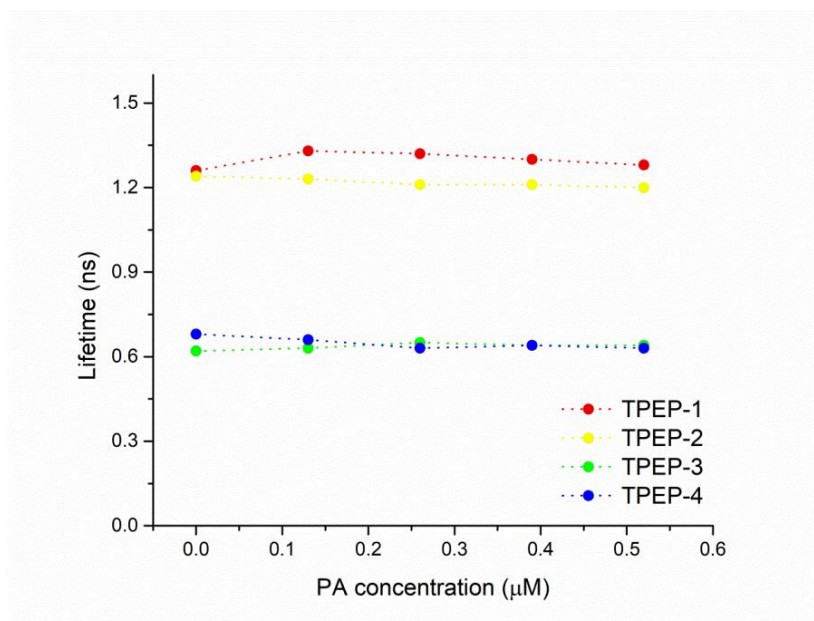


Figure 48. The lifetime of the TPEPs under different concentration of PA.

3.5 Conclusion

In this chapter, four AIE polymers based in tetraphenylethylene cores (**TPEPs**) are synthesized. The **TPEPs** display rapid emission increase under poor solvents compared with good solvents, which is an advanced AIE effect. The hydrophobic chains are favorable than the hydrophilic in building strong AIE structures. The hydrophilic groups could help the polymers separate better than the hydrophobic groups in water, leading to a low degree of aggregation and resulting in lower intensities.

A sensor array formed with **TPEPs** detects and discriminates nitroaromatics through fluorescence quenching in an aqueous phase. The **TPEPs** display very good sensitivities to the nitroaromatics and the detecting performance beyond the reported **PPEs** and **HCPs** series in Chapter 2. Fourteen analytes were effectively detected and discriminated by this simple four-element sensor array, including five pairs of regio-isomers. The dominant quenching mechanism is static in nature, as the fluorescent lifetimes of TPE polymers are not affected by the concentration of analytes. Over all, the **TPEPs** open up an interesting research field for sensory materials. The TPE moiety successfully overcome the ACQ effect and display an interesting and useful AIE effect, which can exploit the fluorescence of the conjugated polymers in aqueous phase or solid state. The TPE core can be massively engineered to display further electronic properties that should allow the sensing of either electron deficient but also electron rich analytes that plague the environment. Questions of discrimination but also of LOD are of great interest and should be tackled with this hypothesis free sensor arrays.

**Chapter 4. Functional TPE Polymers: Aggregation-
Enhanced Emission, pH Response, Solvatochromic and
Nitroaromatics Sensing**

In this Chapter, four functional tetraphenylethylene-based polymers (**F-TPEPs**) containing amino and/or nitro groups were designed and synthesized.¹²⁹ Amino-substituted **P1-P3** exhibit pH response through protonation of the amino groups. **P1** and **P2** display amino groups on the TPE unit, display similar trends and show aggregation-induced emission (AIE). Protonation leads to blue shifted emission in **P1** and **P2**. **P3** featuring amino groups on the end of its side chains shows fluorescence intensity changes as response to different pH values, but without shift of the emission color. Nitro-substituted **P4**, with a donor-acceptor structure, shows no response to pH changes, but reacts to different solvents and is AIE-active. AIE, ICT and FRET define the fluorescence-based performance of the polymers in sensor applications. Strong AIE is responsible for the emission in the aggregate state. **P1-P3** detect nitroaromatics, while the acceptor-substituted **P4** is much less effective. The presence of amino groups enhances the sensing performance of TPE polymers for nitroaromatics.

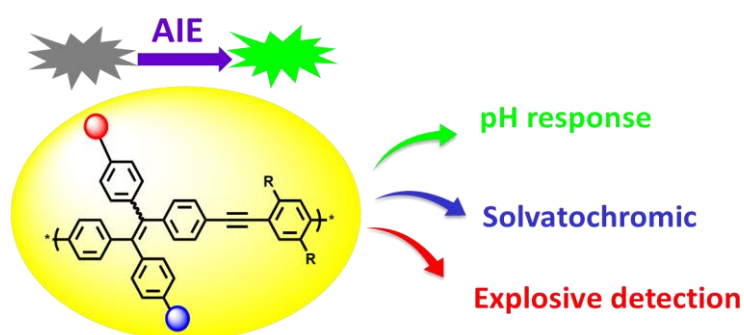


Figure 49. Systematic illustration of functional TPE polymers with aggregation-induced emission, pH response and explosive detection.

4.1 Functionalization on TPE moiety

TPE-based derivatives are broadly investigated owing to aggregation-induced emission (AIE) or aggregation-enhanced emission (AEE) properties. Researches about how to functionalize the TPE moiety with different substitutes or combine them with building block, are quite attractive.

For example, aromatic groups such as divinyl-anthracene¹³⁰ and triphenylamine-anthrylenevinylene¹³¹ were introduced onto the TPE motif to enable tunable mechanofluorochromic properties. Those functionalized fluorophores display great potential as smart materials in fields of pressure sensors, rewritable media and security ink.¹³²⁻¹³⁴ The zinc ion complex dye based on the ligand dye containing TPE and terpyridine moieties has been reported as the first mechanofluorochromic AIE complex to date.¹³⁰ When decorating it with tetraphenylethene units on pyrene, an advanced bright emitter could be obtained. The emitter, with its quantum yield is as high as 70% of the solid state, is quite stable thermally and morphologically and its light-emitting diode reveals excellent performance, with an external quantum efficiency of 4.95% and high current efficiency of 12.3 cd A⁻¹.¹³⁵ An AIE dye was also synthesized by the incorporation of a benzothiazolium unit into TPE moiety through vinyl functionality. The resulting luminogen exhibits cryschochromism. The emission in solid state could be tuned reversibly from yellow to red by grinding-fuming and grinding-heating processes due to the morphological change. The functionalized luminogen could be applied as a fluorescent visualizer for tumor cell targeting and imaging.¹³⁶ A zwitterionic-copolymer poly(MPC-co-FPEMA) was synthesized via RAFT polymerization and further converted to PMPC-hyd-TPE after conjugation of TPE via acid-cleavable hydrazone bonds. The resulting PMPC-hyd-TPE self-assembles into spherical zwitterionic micelles. The multifunctional micelles reveal non-fouling surface and show great potentials in AIE-active imaging and pH-responsive drug delivery.¹³⁷

The functionalization based on the TPE moiety opens up a spacious road for multi-factor response fluorophores. The diversity of functionalization based on the TPE core creates a lot of possibility for the interesting photo-behavior of new fluorescent materials.

4.2 Synthesis and Characterization of Functional Polymers

TPE-based polymers with their AIE characterization should be useful as potent fluorescent sensing materials in water. For fluorescence-based sensing, the emission characteristic of the fluorophores must be modulated upon binding to analytes. Benzene rings with several electron-withdrawing nitro-groups cause fluorescence quenching by effective charge-transfer or FRET to the electron-rich polymeric fluorophores. Nitroaromatics are classic electron withdrawing substance. Thus, polymers functionalized with electron donating groups will surely improve the reaction between the polymers and nitroaromatics. One efficient approach is to improve the sensing performance by decorating the polymers with electron donating sidechains. Under this consideration, the amine group appeared to be the best targeted functional group to TPE moiety, and should enhance the sensitivity of TPE-based polymers to nitroaromatics.¹³⁸⁻¹³⁹

Here, we designed and synthesized four polymers (**F-TPEPs**) based on TPE modules. Four F-TPEPs are referred to as **P1**, **P2**, **P3** and **P4**. Two of them are based on diethylamino-TPE (**DEA-TPE**), coupled to a phenylene-ethynylene moiety, incorporated into the polymers. The phenylene-ethynylene moieties contain different side chains as co-monomers (**P1** and **P2**, Figure 50). In **P3**, a bare TPE monomer is cross-linked with phenylene-ethynylene units containing amino side chains. The amino groups appear at same position on **P1** and **P2**, differently on **P3**. **P4** is constructed from a dinitro-substituted TPE and phenyleneethynylene moiety.

We synthesized three TPE monomers through McMurry coupling with diethylamino (for **P1** and **P2**), nitro (for **P4**) and no residue (for **P3**) as functional groups, respectively. The three monomers are mixture of cis-trans isomers, as the isomers could not be separated. The polymers were then obtained through Sonogashira coupling of the diiodo-TPEs and diethynylbenzene monomers and yields for P1-P4 are 63%, 68%, 39% and 63%, respectively. **P1-P3** are donor-polymers as they bear amino groups, while P4 is a donor-acceptor polymer with electron withdrawing nitro groups.

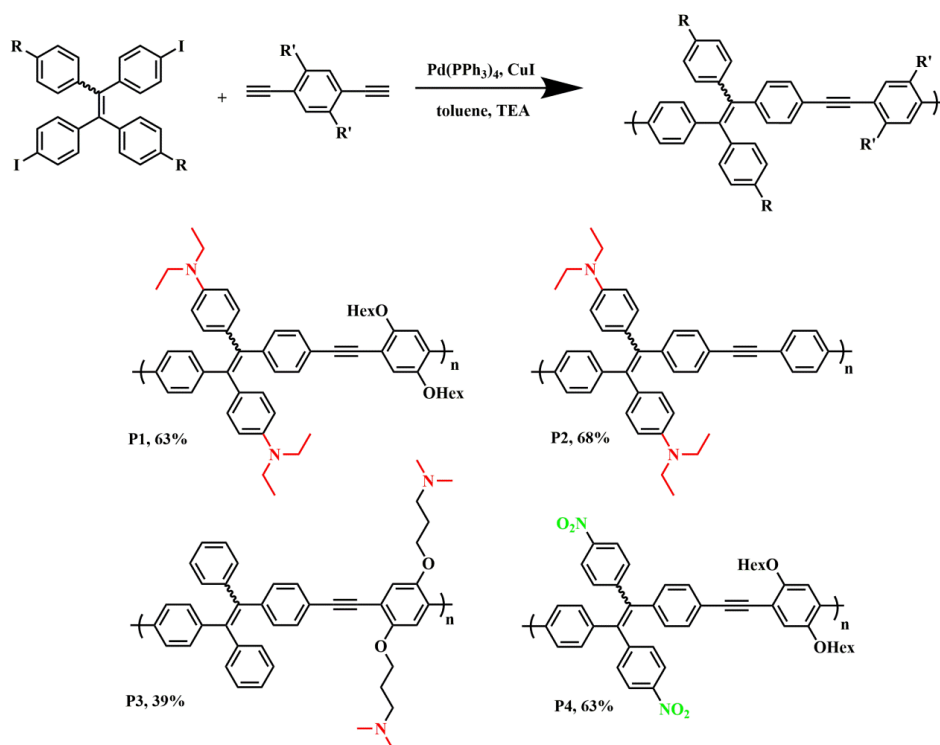


Figure 50. Synthetic route to the polymers and structures of the **F-TPEPs** (yields are shown under the structures).

The number-average molecular weights (M_n) of the polymers **P1-P4** are estimated by gel permeation chromatography (GPC) as 12400, 9100, 6300, and 7900 g/mol, respectively. The polydispersity (\mathcal{D}) is 1.1 for **P1** and 1.5 for **P2**, **P3** and **P4**. The low \mathcal{D} is due to the working-up process, as the insoluble high molecular weight parts were removed by filtration and the low molecular weight parts were removed by precipitation from methanol and from hexanes, leading to the observed low yields and relatively narrow polydispersity. The detailed information about the polymers is shown in Table 14.

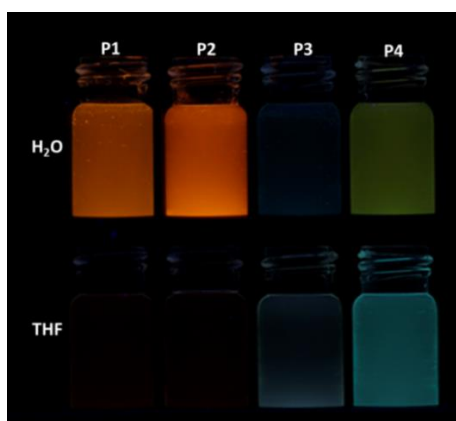


Figure 51. Photograph of the **F-TPEPs** in H_2O and THF ($c = 2 \mu\text{g/mL}$) under a 365 nm UV lamp.

The photograph of **P1-P4** ($c = 2 \mu\text{g/mL}$) in H_2O and THF under a 365 nm UV lamp is shown in Figure 51, clearly the polymers show stronger fluorescent in H_2O compared in THF. **P1** and **P2** show orange color, **P3** is one with the weakest fluorescence, **P4** display a weak yellow in H_2O but a blue color in THF.

The emission of polymers are quite weak in THF when they are totally dissolved, however the fluorescent increases when they aggregate in water. Therefore, the absorption and emission spectra of the polymers were measured in $\text{H}_2\text{O}/\text{THF}$ (95/5). The normalized spectra of the **F-TPEPs** are shown in Figure 52. The maximum emission peak is 598, 590, 513 and 552 nm for the **F-TPEPs**, respectively (Table 14). The emissions of **P1** and **P2** are red shifted compared to that of **P3** with TPE and **P4** with the nitro-TPE moiety. **P3** with dimethylamine chains attached to the phenyl rings shows the most blue-shifted emission spectrum. **P1** and **P2** exhibit the most red-shifted emission spectra.

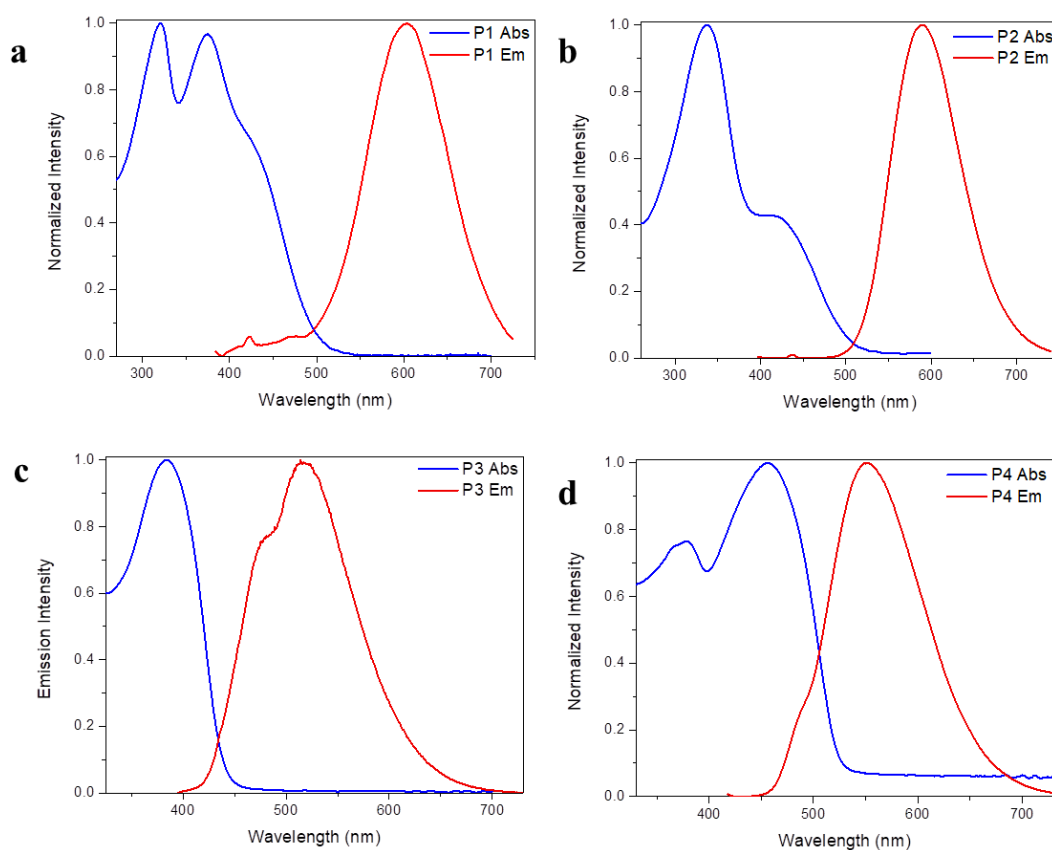


Figure 52. Normalized absorption and emission spectra of **P1(a)**, **P2(b)**, **P3(c)**, **P4(d)** in $\text{H}_2\text{O}/\text{THF}$ (95/5).

The quantum yields of the **F-TPEPs** are 1.8%, 0.8%, 1.6%, and 4.8% in the good solvent THF. In a mixture of H₂O/THF (95/5), the quantum yields are much higher (23%, 32%, 6% and 7%), which are evidently AIE effects of the polymers (see Table 14). However, the different degrees of the AIE effect for different polymers are still unclear.

Table 14. Photophysical properties and molecular weights for **F-TPEPs**.

Polymer	$\lambda_{\max, \text{abs}}[\text{nm}]^{\text{a}}$	$\lambda_{\max, \text{em}}[\text{nm}]^{\text{a}}$	M_n [g/mol] ^b	\mathcal{D}^{b}	Φ_F $_{\text{agg}}[\%]^{\text{a}}$	Φ_F $_{\text{sol}}[\%]^{\text{c}}$	τ $_{\text{agg}}[\text{ns}]^{\text{a}}$	τ $_{\text{sol}}[\text{ns}]^{\text{c}}$
P1	374	598	12400	1.1	23	1.8	1.20	0.08
P2	338	590	9100	1.5	32	0.8	2.20	0.07
P3	383	513	6300	1.5	6	1.6	0.95	0.11
P4	456	552	7900	1.5	7	4.8	0.82	0.37

^a Determined in H₂O/THF (95/5). ^b Determined by GPC in THF. ^c Determined in THF.

Emissive life times in H₂O/THF (95/5) as a poor solvent are measured as 1.2, 2.2, 0.95 and 0.82 ns for **P1** to **P4**, which are highly increased compared to the lifetimes of 0.08, 0.07, 0.11 and 0.37 ns in THF. We observe that the nitro-containing **P4** is fluorescent both in solution and to a lesser extent in the aggregation state. This phenomenon is quite unusual: nitro-containing conjugated polymers are usually fully quenched as normally, due to intramolecular excited state charge transfer etc. Yet there are some aromatics substituted with nitro groups out, particularly nitrobenzoxadiazoles and nitrated benzofurazans.¹⁴⁰⁻¹⁴²

We were interested if **P1-P4** would form nanoscale matter when brought into a non-solvent condition. Morphology of the **F-TPEPs** was carried out by SEM (Figure 53). SEM experiments were carried out by Dr. Wacker from Prof. Schröder's Group, University of Heidelberg. The samples were prepared as suspension of polymers in H₂O/THF (95/5). A 1ml droplet of each suspension was placed on a piece of plasma-cleaned silicon wafer and air dried. Samples were imaged in a FESEM (Ultra, Carl Zeiss Microscopy) at 1.5kV using SE and InLens detectors for secondary electrons. All polymers form into nanospheres with irregular sizes that range from around 10 nm - 500 nm. **P1** and **P2**, however, seem to produce much larger nanospheres than **P3** and **P4**.

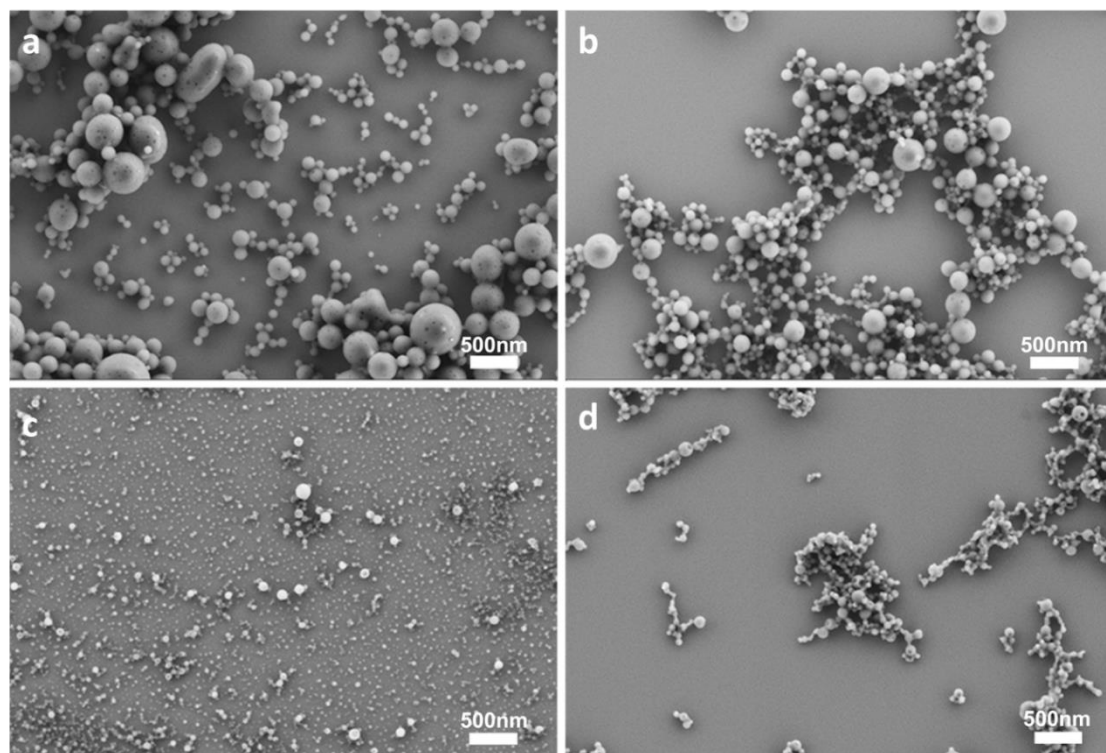


Figure 53. SEM images of **P1**(a), **P2**(b), **P3**(c) and **P4**(d). Adapted with permission of ref. 129 © 2018, Wiley VCH.

4.3 AIE effect of P1-P4 and Solvatochromism of P4

AIE materials show strong emission in the aggregated state, i.e., in poor solvents or films. **P1-P4** emit stronger in the non-solvent water. The emission spectra of **P1-P3** (5 μM) in different solvents and different fractions of $\text{H}_2\text{O}/\text{THF}$ are shown in Figure 54.

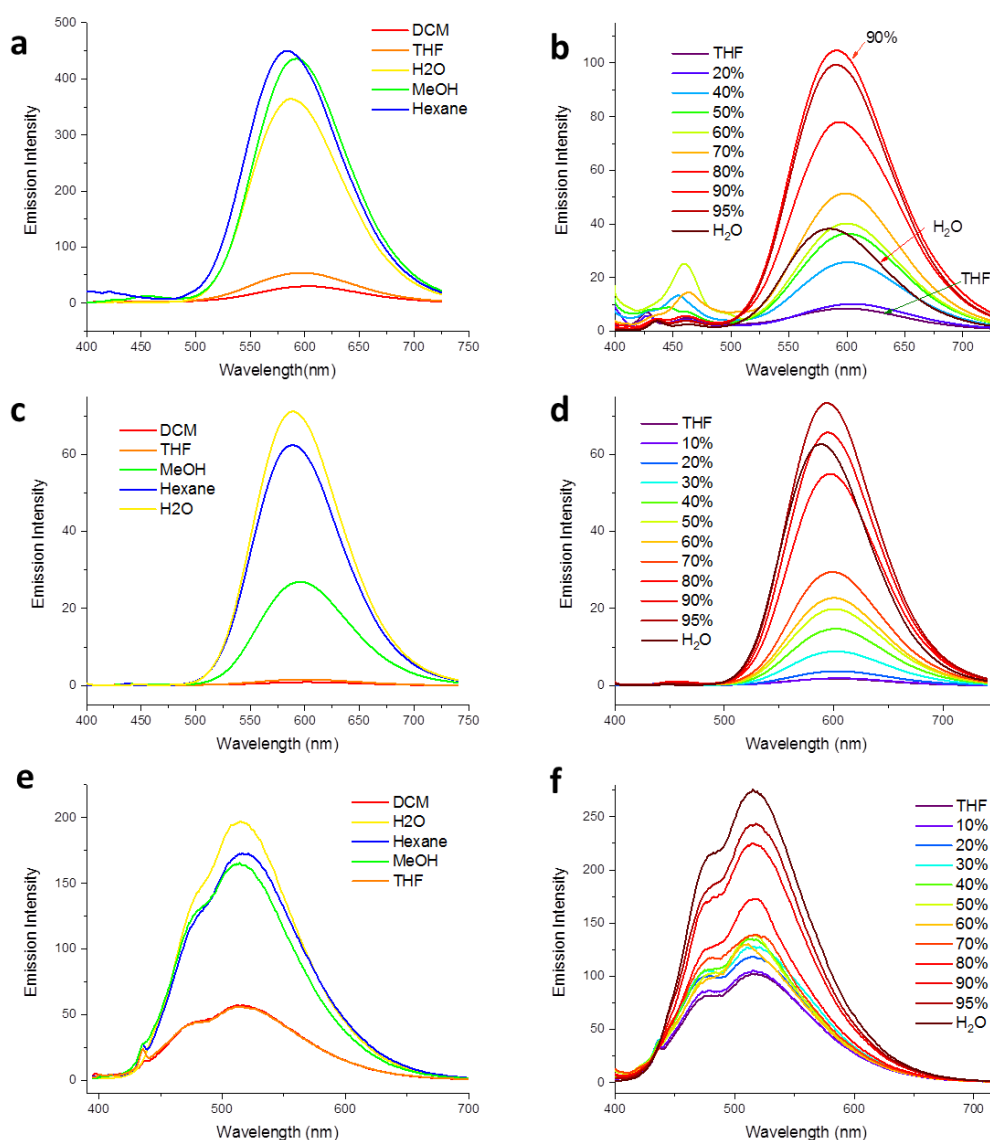


Figure 54. The emission spectra of **P1** (a, b), **P2** (c, d) and **P3** (e, f) (5 μM) in different solvents and fractions of $\text{H}_2\text{O}/\text{THF}$. Reproduced with permission of ref. 129 © 2018, Wiley VCH.

P1-P3 show strong AIE effect. They are weak emissive under good solvents, but highly demonstrate high emission in poor solvent, such as MeOH and H_2O . This phenomenon also appears when the water fraction changes in the mixture of THF/ H_2O . It is obvious that only

the emission intensity changes but with slight peak shifts (<5 nm) in different solvents. **P4** reveals a distinctly different emission behavior from **P1-P3**. **P4**, with nitro-groups, not only changes the emission intensity, but also displays a significant wavelength shift in different solvents (Figure 55).

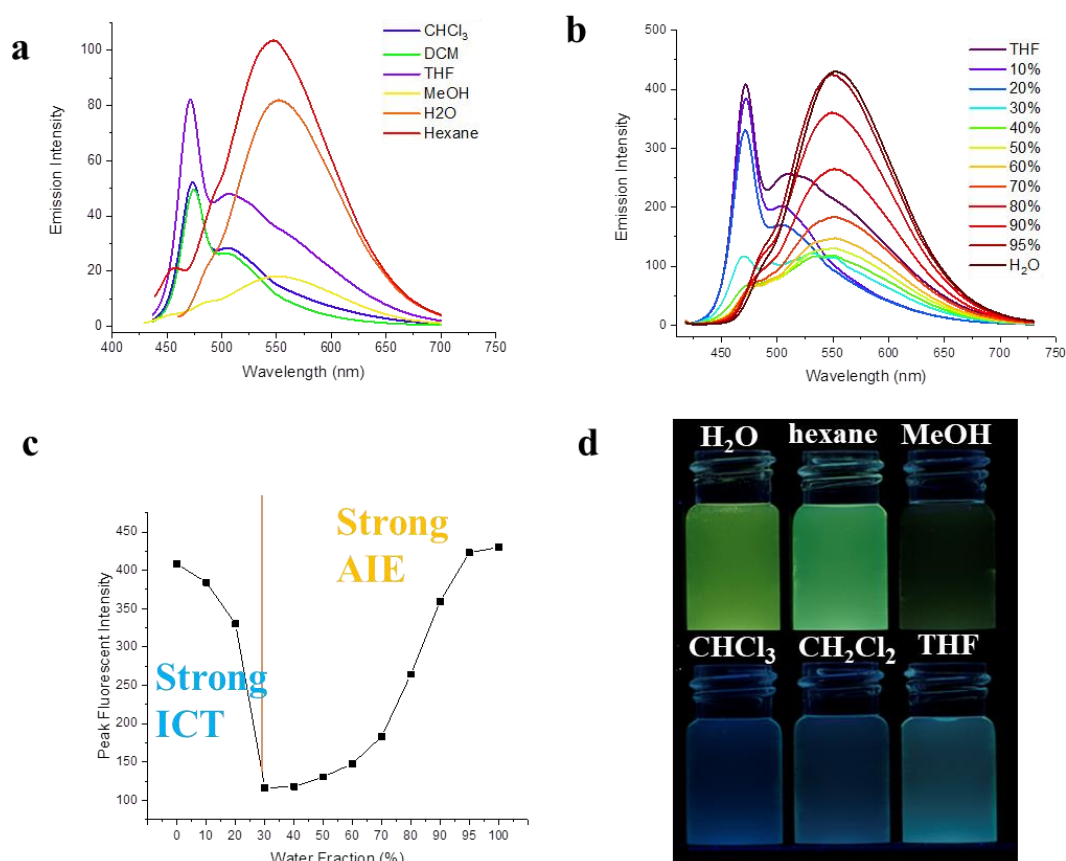


Figure 55. (a) Emission spectra of **P4** (5 μM) in different solvents, (b) different fraction of $\text{H}_2\text{O}/\text{THF}$, (c) peak emission intensity change under different water fractions and (d) a photograph of **P4** in different solvents under a 365 nm UV lamp. Reproduced with permission of ref. 129 © 2018, Wiley VCH.

P4 (5 μM) emits blue with a maximum peak at 471 nm in good solvents like CHCl_3 , DCM and THF. But in poor solvents (H_2O , hexane and MeOH), the peak shifts to 552 nm showing a yellow color (Figure 55a and d). The quantum yield of **P4** in different solvents is 4.8% in THF, 2.5% in DCM, 1.7% in CHCl_3 , 1.6% in MeOH, 8.1% in Hexane and 7.2% in H_2O . A similar feature has been reported by Tang's group for a dyad from TQ-BPN (*N,N*-diphenyl-naphthalen-1-amine (donor units) and thiadiazolo[3,4-*g*]quinoxaline (acceptor units)).

Their donor-acceptor system incorporates TPE, and also shows intensity-enhanced and red-shifted emission in the aggregated state.¹⁴³

We use a model to investigate the electronic structure of **P4** (Figure 56). The lowest unoccupied molecular orbital (LUMO) of the model is dominated by the orbitals from the nitrophenyl parts. The HOMO is mainly located on the non-nitro-carrying stilbene part. We assume intramolecular charge transfer (ICT) between the nitro-TPE and the phenyleneethynylene units in **P4** contributes to the emission in solution.¹⁴⁴⁻¹⁴⁶

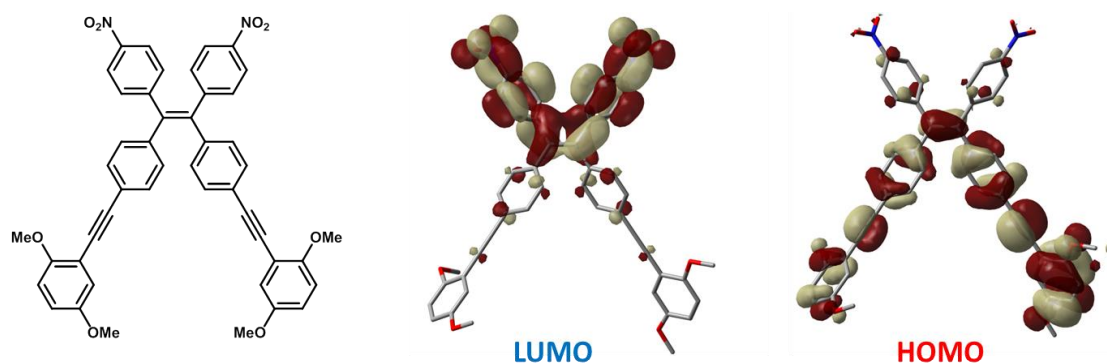


Figure 56 Structure of **P4** skeleton and molecular orbital distribution of HOMO and LUMO energy levels of it calculated using DFT/B3LYP/6-311G. Reproduced with permission of ref. 129 © 2018, Wiley VCH.

The same phenomenon also happens in the mixture of H₂O/THF. The emission intensities and peak locations change simultaneously with the fraction of H₂O/THF (Figure 55b). For the water fractions under 40%, the peaks locate at 471 nm and the intensity decreases with the raising water content. The peak appears at 552 nm when there is more than 40% water. The changing peak emission intensity in relation to the water fraction is shown in Figure 55c. At low water fractions, ICT rules the emission. However, in water AIE was believed to determine the emission of **P4**. Figure 55d shows the photograph of **P4** in different solvents under a hand-held black light with illumination at 365 nm. The color changes notably from yellow (in H₂O) to blue (in THF).

4.4 pH Response of P1-P3

The protonation of the amino groups prompt pH responses of **P1-P3**. The fluorescence of the polymers was measured in different pH buffers. **P1-P3** are pH-responsive, testament to their amino substituents. **P4** is pH-insensitive, as it only contains nitro groups. The pH-dependent emission spectra and peak intensities of **P1**, **P2** and **P3** are shown in Figure 57. **P1** and **P2**

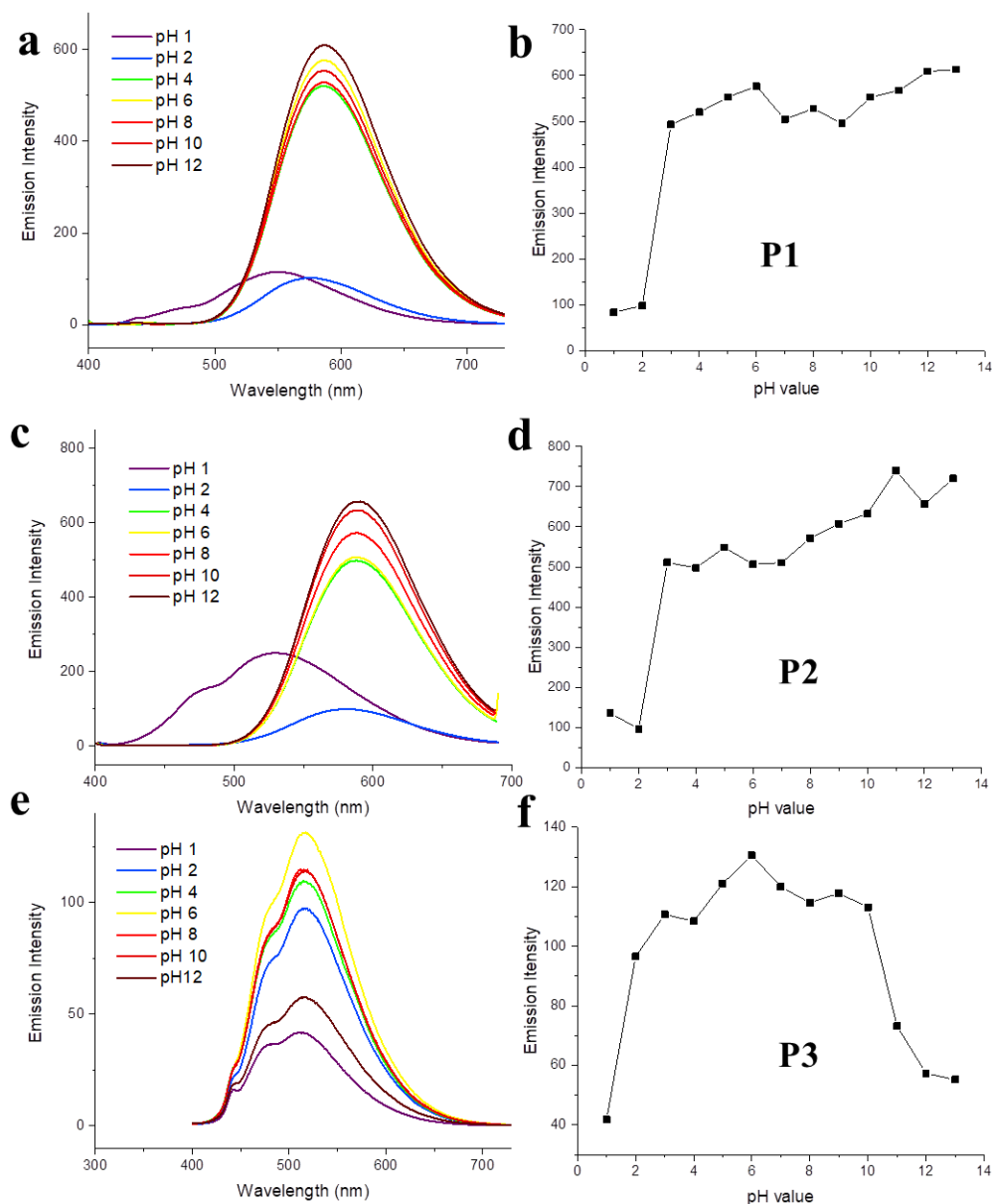


Figure 57. The emission spectra of **P1** (a), **P2** (c), **P3** (e) and peak emission intensity change of **P1** (b), **P2** (d), **P3** (f) in different pH buffers. Reproduced with permission of ref. 129 © 2018, Wiley VCH.

show similar response trends. The maximum emission of **P1** and **P2** are blue-shifted at pH = 1 (**P1**: 550 nm from 598 nm, **P2**: 530 nm from 590 nm). **P1** and **P2** readily dissolve at pH 1 and do not show AIE but regular weak fluorescence. Rising pH value would lead to deprotonation, thus no more molecularly dissolved polymers strands but aggregates instead, which are responsible for the fluorescence turn on. The emission intensity of **P1** and **P2** increases sharply from pH 2 to pH 3, then only slightly with increasing pH, but without any change in emission wavelength. **P3** shows the highest emission intensity at pH 6 without any wavelength change in different pH buffers. As expected, the directly linked amino groups on TPE in **P1** and **P2** affect the optical properties of the polymers more fierce than on the side chains like **P3**.

4.5 Detection of Nitroaromatics based on P1-P4

The introduction of the electron-donating amino group is expected to enhance the interaction between the fluorescent polymers and electron-deficient explosives. We expect an increase in the sensitivity when comparing **P1** and **P2** to **P3** and **P4**. The fluorescence of **P1-P4** is quenched by adding nitroaromatics into their water suspensions. The nitroaromatics in this study are **pNP**, **oNP**, **mNA**, **oNA**, **mCNB**, **oCNB**, **NB**, **DNT**, **DNB**, **CDNB**, **TNT** and **PA**, the structures are shown in Figure 58. The analytes contain at least one nitro group, plus substituents, such as amino, chloro, hydroxyl and methyl groups.

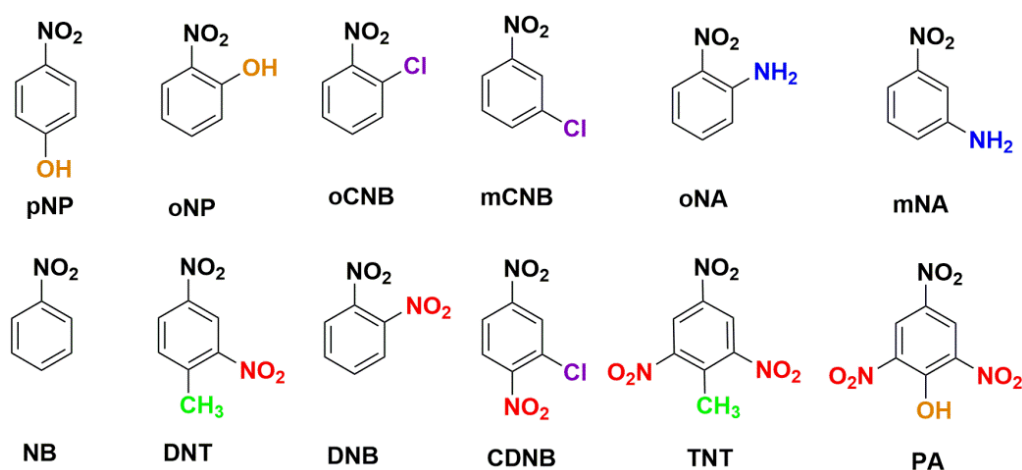


Figure 58. Structures of the analytes.

The Stern-Volmer constant K_{sv} is measured by gradually adding analytes into the polymer suspensions in water (final concentration of the polymers is 2 μ M). A modified Stern-Volmer equation quantifies quenching efficiencies of **P1-P4**. The K_{sv} values are shown in Figure 59 and listed in Table 15. **P1**, **P2** and **P3** display a better quenching efficiency to all the analytes than **P4**. Because of the strong electrostatic interaction exist between the electron-donating amino groups in these polymers with the electron-withdrawing nitro groups in the analytes. **P4** with nitro group, in return, shows weaker fluorescence quenching. **P3** has the highest K_{sv} values in general. In particularly, **P3** shows extremely high sensitivity to **PA** and **TNT**.

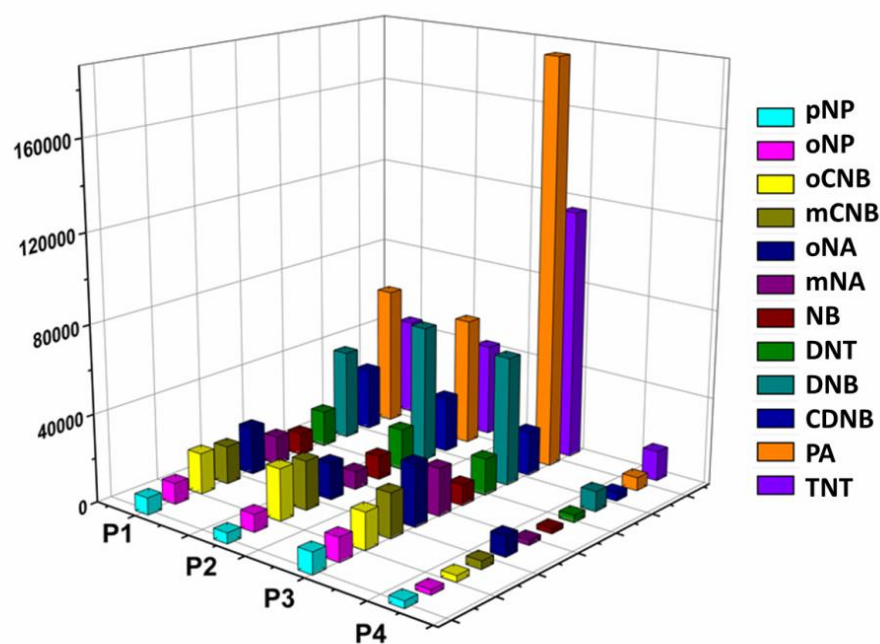


Figure 59. Fluorescence quenching efficiencies of the **F-TPEPs** (the z-axis is the Stern-Volmer constant K_{sv}). Reproduced with permission of ref. 129 © 2018, Wiley VCH.

Table 15. The K_{sv} of the polymers for different analytes.

Analytes	P1	P2	P3	P4
pNP	7789	4914	9893	3255
oNP	9586	8069	11019	2306
oCNB	18595	23580	16851	2878
mCNB	17293	22374	20309	3694
oNA	21803	16812	28403	9281
mNA	12948	8231	21693	2237
NB	10188	10781	9479	2237
DNT	16351	18843	16711	3276
DNB	41165	62719	58714	9171
CDNB	28674	25564	20309	3694
PA	63786	58630	187000	6043
TNT	44935	42571	115000	13607

DNB, **CDNB**, **TNT** and **PA** are good quenchers for the fluorescent polymers because of the high electron deficiency compared to that of the other analytes. For the polymers, **P4** with the nitro-withdrawing groups, the response is weakest to the analytes, while **P1-P3** have superior detecting performance thanks to their functional amino groups. The sensing power of the novel functional sensors the **F-TPEPs** stands out from the sensors, **HCPs** and **PPEs** in Chapter 2 and **TPEPs** in Chapter 3. The comparison of the sensitivity of different sensor systems with respect to quenching is shown in Figure 60. The polymers turn out to be more effectively than our previous sensors for sensing the nitroaromatics. For picric acid, the lowest limit of detection of is as low as 0.1 μM according to **P3**.

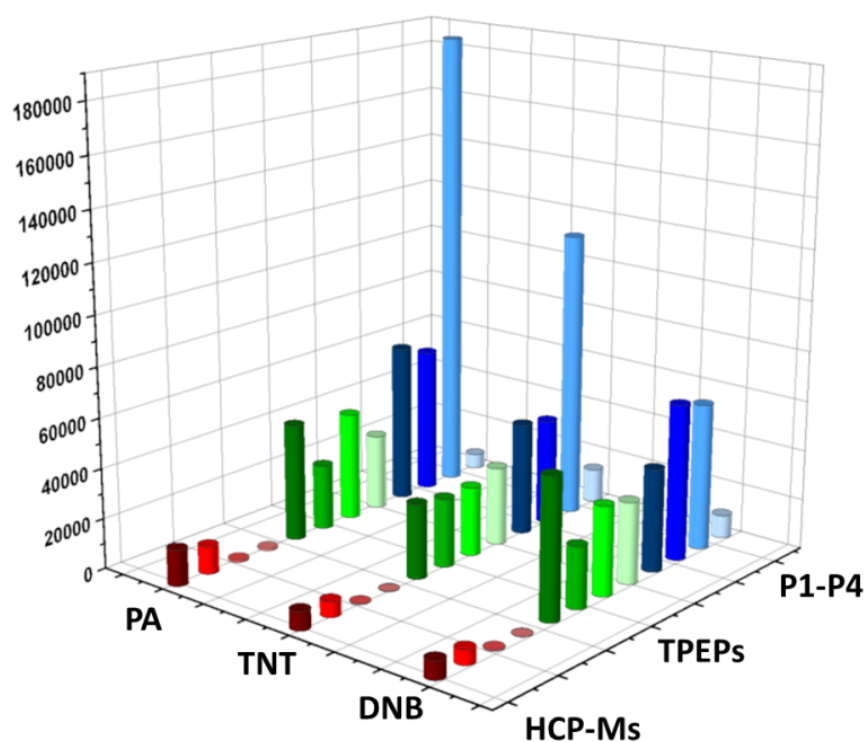


Figure 60. Comparison of the sensitivity of different sensor systems with respect to quenching (the z-axis is the Stern-Volmer constant K_{sv}). Reproduced with permission of ref. 129 © 2018, Wiley VCH.

The quenching efficiency of analytes to the **F-TPEPs** can be explained via the electrostatic interaction between the analytes and polymers. The interaction between amino groups and electron-deficient nitroaromatics should facilitate binding and the electron and/or energy transfer process. To investigate the possibility of electron transfer process in the quenching mechanism, LUMO and HOMO levels of the polymers were calculated by using model

compounds, constructed from the basic building blocks of the **F-TPEPs**. Structures of the model compounds are shown in Figure 61 and the molecular orbitals calculated by DFT/B3LYP/6-311G are shown in Figure 62.

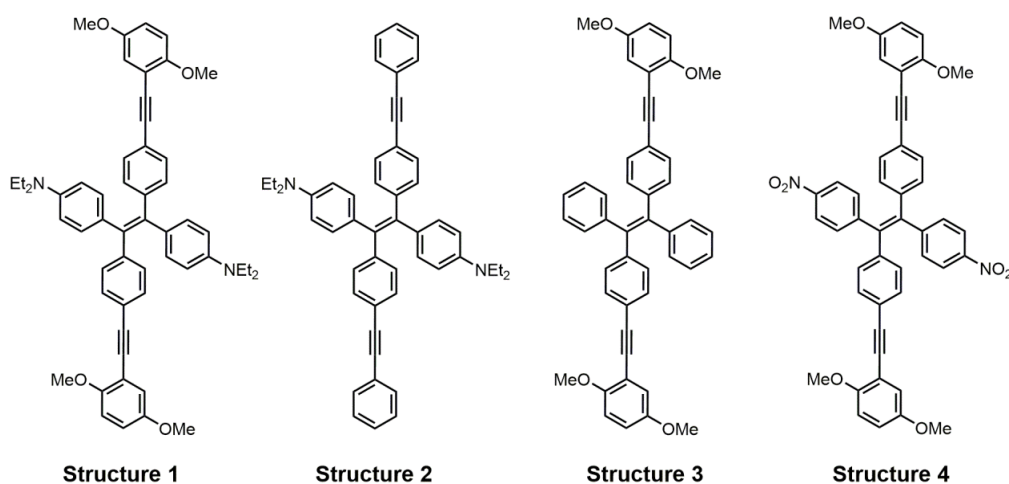


Figure 61. Structures of the model compound of the four polymers.

The LUMO values of **P1-P4** are calculated to be -1.92, -1.93, -2.03, and -3.29 eV, respectively (see Table 16). Excited state electron transfer from LUMO of **P1**, **P2** and **P3** (-1.92~ -2.03) to the LUMO of analytes (-2.42~ -4.20 eV) should be possible, resulting in effective fluorescent quenching. **P4** (-3.29 eV) on the other hand, has very low chance to achieve the electron transfer, thus resulting in very weak sensory response to the analytes.

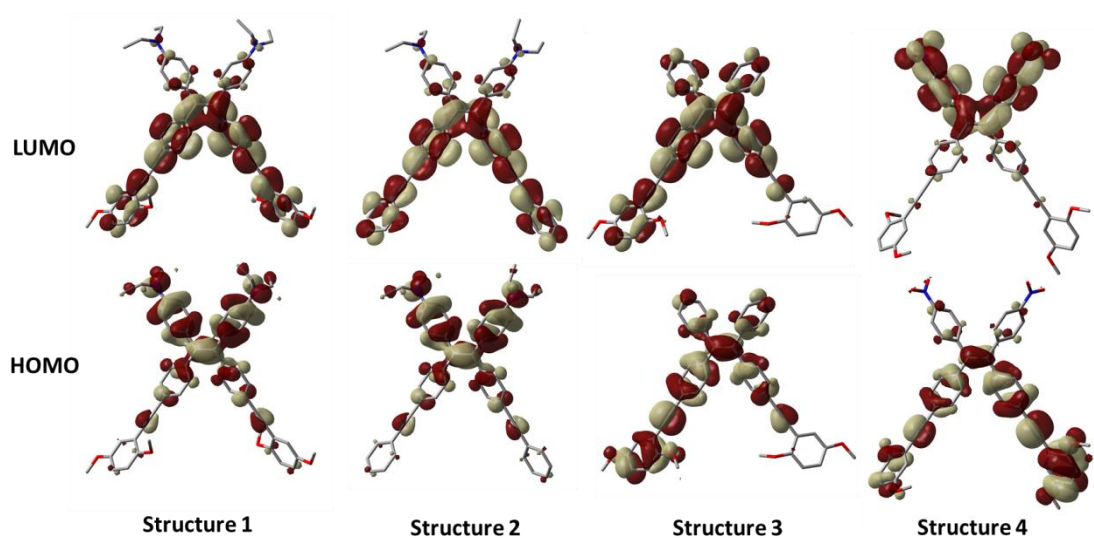


Figure 62. Molecular orbital amplitude plots of HOMO and LUMO calculated using DFT/B3LYP/6-311G. Reproduced with permission of ref. 129 © 2018, Wiley VCH.

Table 16. Quantum-chemical calculations utilizing DFT/B3LYP/6-311G.

Polymer	P1(eV)	P2(eV)	P3(eV)	P4(eV)
LUMO	-1.92	-1.93	-2.03	-3.29
HOMO	-4.47	-4.70	-5.36	-5.78
Gap	2.76	2.77	3.33	2.49

LUMO values of the analytes are calculated through DFT/B3LYP/6-311** level of theory and listed in Table 17. The LUMOs of **DNB**, **CDNB**, **TNT** and **PA** are lower in energy compared to the other ones, which accounts for their stronger tendency of electron transfer, resulting in a higher degree of quenching.

Table 17. LUMO Levels of the analytes calculated by DFT/B3LYP/6-311++G** level of theory.

Analyte	pNP	oCNB	oNA	mNA	mCNB	NB
LUMO (eV)	-2.42	-2.64	-2.67	-2.75	-2.90	-2.92
Analyte	oNP	DNT	DNB	CDNB	TNT	PA
LUMO (eV)	-3.19	-3.25	-3.45	-3.67	-3.92	-4.20

P1-P3 of course display a better quenching efficiency to all the analytes than **P4**, because interactions between the electron-donating amino groups in **P1-P3** are absent in **P4**.¹⁴⁷ Thus, the -NR₂-function on the side chain seems to be superior to the location of the amine directly on the backbone of the TPE polymer to construct efficient nitroarene sensors. Also **P3** has the most blue-shifted emission spectra, improving FRET-based fluorescent quenching with the blue-absorbing nitroarenes. The spectral overlap between the absorption spectra of the analytes and the emission spectra of polymers will influence the quenching performance. **P3**, with the most blue-shifted emission spectrum ($\lambda_{\max,em} = 513$ nm) has most overlap with the absorption of analytes (**P1**: 598 nm, **P2**: 590 nm; **P4**: 552 nm see Figure 63). The energy transfer between the analytes and **P3** is likely to contribute to the apparent strong quenching process. Quenching is probably due to electron and energy transfer between the analytes and polymers.

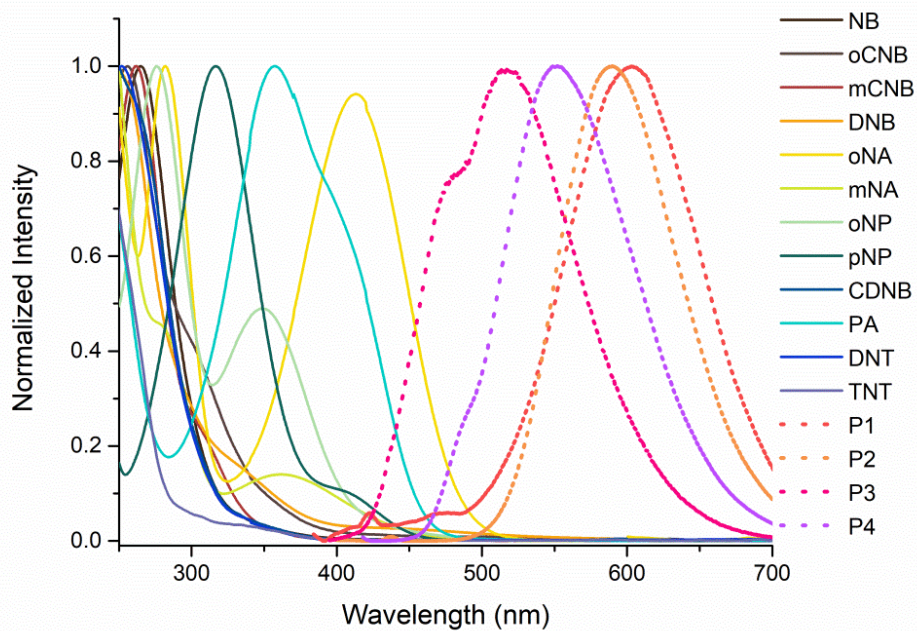


Figure 63. The normalized absorption spectra (full line) of the analytes and emission spectra (dotted line) of the polymers. Reproduced with permission of ref. 129 © 2018, Wiley VCH.

4.6 Discrimination of Nitroaromatics based on P1-P3

As **P4** is a weak sensor compared to **P1-P3**, discrimination was carried out by using **P1-P3**. As the polymers show different fluorescence quenching responses to the nitroaromatics, this system should discriminate nitroarene explosives. Therefore, the analytes (0.1 mM, 30 μ L) were added to the solution of polymers in water (1 μ M, 250 μ L, six repeats) and the fluorescent intensities were recorded before and after addition. The fluorescence changes give a specific response pattern of the polymers to the analytes as visualized by linear discriminant analysis (Figure 64a). Converting the training matrix of the data into canonical scores, three canonical factors (69%, 23%, 8%) were generated. A unique map of 12 clusters representing the analytes formed on the 2D score plot. Analytes are separated from each other indicating the performance of this four element sensor array (Figure 64b). The map can be divided into two parts on the x-axis. The left part consists of the low LUMO nitroarenes (LUMO < -3.40 eV), while the right part represents the analytes with relatively high LUMOs. The three-element sensor array **P1-P3** discriminates all of the analytes more effectively than our already reported four element TPE sensor array and the previous TPEPs, HCPs and PPEs.^{101, 118, 127}

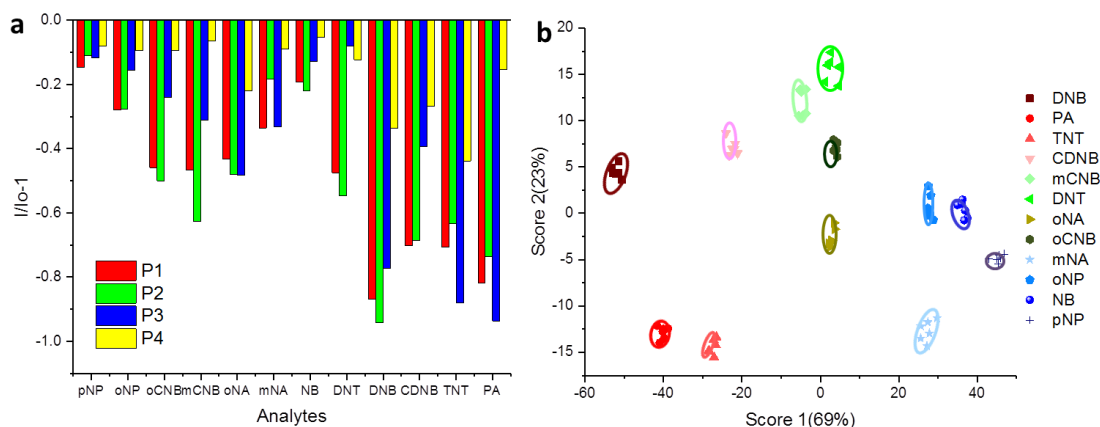


Figure 64. (a) Fluorescent response pattern ($I/I_0 - 1$) of **P1-P4** towards the analyte (in water) and (b) 2D canonical score plot of discriminant scores with 95% confidence ellipses, based on **P1-P3** against different analytes. Reproduced with permission of ref. 129 © 2018, Wiley VCH.

For our reported sensor, **TPEP-1**, the best sensor in **TPEPs**, the limit of detection (LOD) for **PA** is 0.24 μ M; **HCP-1-M**, the best in **HCPs**, the value is 0.28 μ M; and for **PPEs**, the LOD for **PA** is 4 μ M. The whole K_{sv} and LOD values of **P1-P4** compared to **TPEPs**, **HCPs** and

PPEs for **PA**, **TNT** and **DNB** is shown in Table 18 and 19. The sensitivities of **P1-P3** to these analytes are generally better than the previous sensors in chapter 2 and 3. The high quenching constants, less elements and well separated LDA map show this sensor array is an advanced effective, sensitive and selective tool to discriminate and detect nitroaromatics in aqueous phase.

Table 18. The K_{sv} of **F-TPEPs** compared to **TPEPs**, **HCPs** and **PPEs** for **PA**, **TNT** and **DNB**.

K_{sv}	PA	TNT	DNB
P1	63786	44935	41165
P2	58630	42571	62719
P3	187000	115000	58714
P4	6043	13607	9171
TPEP-1	47016	29869	55986
TPEP-2	26168	27560	24594
TPEP-3	43469	27643	35624
TPEP-4	30340	31263	32595
HCP-1-M	14468	7495	7208
HCP-2-M	11076	6157	5831
PPE-1-M	948	394	405
PPE-2-M	851	260	161

Table 19. The LOD values of **F-TPEPs** compared to **TPEPs**, **HCPs** and **PPEs** for **PA**, **TNT** and **DNB**.

LOD	PA (μM)	TNT (μM)	DNB (μM)
P1	0.34	0.49	0.53
P2	0.51	0.70	0.47
P3	0.14	0.22	0.44
P4	5.90	2.60	3.90
TPEP-1	0.24	0.38	0.20
TPEP-2	1.30	1.30	1.40

TPEP-3	0.29	0.45	0.35
TPEP-4	0.69	0.67	0.64
HCP-1-M	0.28	0.53	0.55
HCP-2-M	0.90	1.60	1.70
PPE-1-M	4.00	9.60	9.40
PPE-2-M	12.60	41.10	66.5

4.7 Conclusion

Four TPE-based polymers **F-TPEs** were synthesized displaying functional amino/nitro groups. The fluorescence of the TPE polymers with amino groups is pH-responsive. **P1** and **P2**, based on DEA-TPE, show similar trends for different pH values. Their emission intensity changes according to different pH because of a change in solubility but also the electronic Umpolung of an electron rich amine group into an electron accepting ammonium salt. The emission peaks blue-shift at pH 1; **P3** also shows a pH response, but only the intensity changes without color change suggesting that only AIE-effects play a role. **P4**, based on nitro-TPE, shows no response to pH, but it is solvatochromic. ICT and AIE affect the fluorescence performance in turn due to the acceptor-donor structure. AIE is responsible for the emission of the nanoscale aggregates. Contrary to **P4**, **P1-P3** detect and discriminate nitroaromatics very effectively. The enhanced sensitivities are owing to the functional electron-donating amino group.

Chapter 5. Summary and Outlook

In this chapter, a summary of the novel fluorescent polymers and their application as nitroaromatics sensor in aqueous phase will be given. Consequently, the prospect of the design of organic polymers and the expansion of these polymers will be discussed.

5.1 Summary

A series of novel structural motifs (truxene, tetraphenylethene) were utilized to construct new fluorescent polymers. The resulting polymers, with different building blocks or functional groups, have an effect on their optical and sensory properties. As shown in Figure 65, the work is based on regular **PPEs**. Evolution is realized through three approaches: Firstly, developing the linear structure into hyperbranched structures (**HCPs**, Chapter 2); Secondly, modifying the building blocks into more conjugated moiety TPE (**TPEPs**, Chapter 3); At last, further strengthening the superb polymers by introducing functional groups (**F-TPEPs**, Chapter 4). K_{sv} of the four systems polymers to PA in water are shown in Figure 65. The detecting power is highly enhanced by the three approaches.

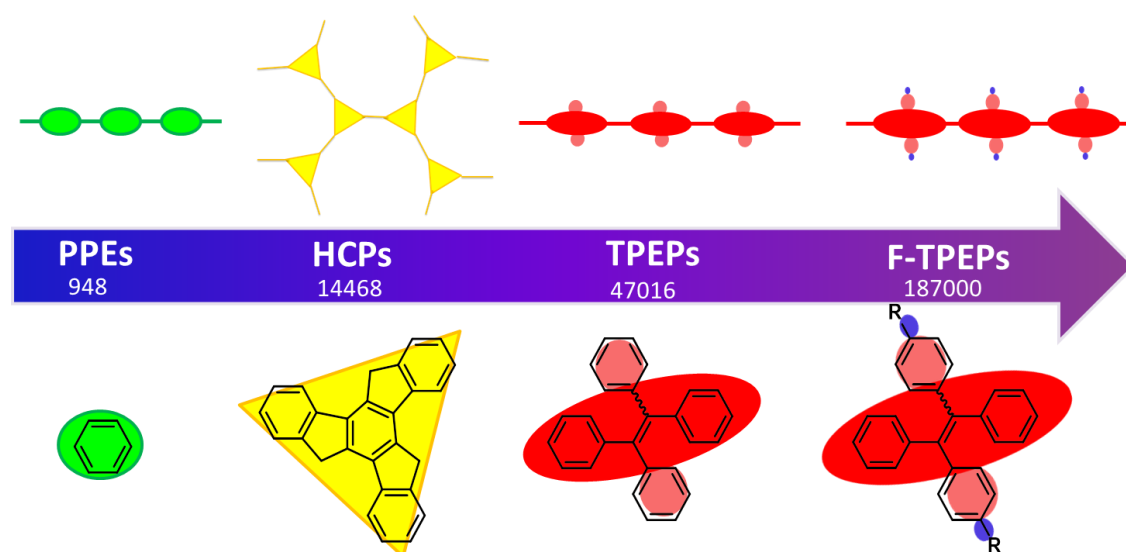


Figure 65. Illustration of the building blocks, constructed polymers and the best K_{sv} to PA in water.

HCPs with a truxene moiety reveal better sensing performance to the nitroaromatics compared to linear **PPEs**. To apply the polymers in aqueous phase, the amphiphilic **F-127** was adopted to cover the fluorescent polymers and form into fluorescent micelles. The

resulting micelles detect and discriminate nitroaromatics in water. This approach could increase the sensitivity to nitroaromatics in water.

Tetraphenylethene (TPE), with an aggregation-induced emission effect, was used to construct novel polymers (**TPEPs**). The emission of the TPE polymers increase under poor solvents compared with good solvents. Sensor arrays based on TPE polymers can detect and discriminate nitroaromatics in water and display excellent sensitivities to the nitroaromatics. Functional amino/nitro groups were also used to decorate the TPE polymers. The functional TPE polymers (**F-TPEPs**) demonstrate aggregate-enhanced emission effect, pH response or solvatochromic properties. The presence of amino groups enhances the sensing performance of TPE polymers for nitroaromatics.

The research also provides a new perspective for the design and construction of novel conjugated polymers for sensing purpose in water.

5.2 Outlook

The sensor or sensor array based on these functional, well-designed fluorescent polymers will have enhanced sensitivity, selectivity, high precision and fast response. The new progress on the fluorescent sensors will contribute to the detection and discrimination of structurally similar chemicals, analytes displaying similar properties or even component similar mixtures.

Besides smart tailoring of the polymers, practical application of these fluorescent materials could also be approached through a combination between the scientific and industry fields. Polymers with outstanding sensing capabilities could be produced in a large scale. Production processes are expected to be improved with high yield, environmental effect and low cost. The applications of fluorescent polymers in real-life still have a long way to go. The performance, the prepared procedure and the routes of applying the fluorescent polymer into commercial products are all very meaningful research topics. Application of the fluorescent substance in organic surrounding is not very convenient in reality. Thus, the sensors that could work in aqueous phase or well in the solid state are highly desired.

In this work, we have given three good examples about designing new functional fluorescent polymers and building effective sensor array on them. The excellent detective and discriminative power of the sensors are owing to the combination of several interactions, e.g. electrostatic interactions, π - π stacking, hydrophobic interactions, hydrogen bonding etc. Thus, in addition to the industry application, the deeper comprehension of the mechanism and interactions between polymers and analytes should also be emphasized. A better understanding of the working mechanism will surely help to broaden the further investigation and create better sensors.

Chapter 6. Experimental Section

6.1 General Remarks

Chemicals were either purchased from the chemical store at the Organisch-Chemisches Institute of the University of Heidelberg or from commercial laboratory suppliers. Chemicals were purchased from Sigma-Aldrich, Abcr or Acros. Reagents were used without further purification unless otherwise noted.

Solvents were purchased from the store of the Theoretikum or chemical store at the Organisch-Chemisches Institute of the University of Heidelberg and distilled prior use if necessary. All of the other absolute solvents were dried by an MB SPS-800 using drying columns.

Buffer solutions of pH 1 (HCl/KCl), pH 2 (KHPH/HCl), pH 3 (citric acid/NaOH/NaCl), pH 4 (citric acid/NaOH/NaCl), pH 5 (citric acid/NaOH), pH 6 (citric acid/NaOH), pH 7 (KH₂PO₄/Na₂HPO₄), pH 8 (borax/HCl), pH 9 KHPH/NaOH), pH 10 (borax/NaOH), pH 11 (boric acid/NaOH/KCl), pH 12 (Na₂HPO₄/NaOH), pH 13 (NaOH/KCl) were purchased from Sigma-Aldrich®.

Flash column chromatography was carried out using neutral silica gel S (0.032 mm-0.062 mm), purchased from Sigma Aldrich. Basic aluminum oxide, ranging 70-290 mesh (50-200 µm), was purchased from Sigma Aldrich and applied to separate the target molecules when necessary. As noted, Celite 545, coarse, (Fluka) was used for filtration.

Thin layer chromatography (TLC) was performed on Macherey & Nagel Polygram® SIL G/UV254 pre-coated plastic sheets. Components were visualized by observation under UV light (254 nm or 365 nm).

GC/MS chromatograms were recorded using a HP 5890 Series II Plus model, coupled with a HP 5972 Mass Selective Detector. As the capillary column, a HP 1 Crosslinked Methyl Silicone (25 m x 0.2 mm x 0.33 µm) was employed, with helium as carrier gas. The acquired data were analyzed using ACD/Labs Spectrus Processor 2012.

Gel Permeation Chromatography (GPC): Number-average molecular weight (M_n), weight-average molecular weight (M_w) and polydispersities (PDI, M_w/M_n) were determined by GPC

versus polystyrene standards. Measurements were carried out at room temperature in chloroform or THF with PSS-SDV columns (8.0 mm x 30.0 mm, 5 μm particles, 10^2 -, 10^3 - and 10^5 -Å pore size) on a Jasco PU-2050 GPC unit equipped with a Jasco UV-2075 UV-detector and a Jasco RI-2031 RI-detector. Data processing was done using PSS WinGPC Unity software.

Chemical formulas were drawn with CambridgeSoft ChemBioDraw Ultra (Version 14.0.0.117) for Windows.

Yields of polymers were determined on the basis of the formula weight of their shortest repeating unit. Negatively charged polymers were treated as the free acid, whereas for positively charged polymers the counter ion was taken into calculation.

^1H NMR spectra were recorded at room temperature on the following spectrometers: Bruker Avance III 300 (300 MHz), Bruker Avance III 400 (400 MHz) and Bruker Avance III 600 (600 MHz). The data were interpreted in first-order spectra. The spectra were recorded in CDCl_3 as indicated in each case. Chemical shifts are reported in δ units relative to the solvent residual peak¹⁴⁸ (CHCl_3 in CDCl_3 at $\delta_{\text{H}} = 7.26$ ppm, or TMS ($\delta_{\text{H}} = 0.00$ ppm)). The following abbreviations are used to indicate the signal multiplicity: s (singlet), d (doublet), t (triplet), q (quartet), quin (quintet), sext (sextet), dd (doublet of doublet), dt (doublet of triplet), ddd (doublet of doublet of doublet), etc., bs (broad signal), m (multiplet). Coupling constants (J) are given in Hz and refer to H, H-couplings.

^{13}C NMR spectra were recorded at room temperature on the following spectrometers: Bruker Avance III 300 (75 MHz), Bruker Avance III 400 (100 MHz) and Bruker Avance III 600 (150 MHz). The spectra were recorded in CDCl_3 as indicated in each case. Chemical shifts are reported in δ units relative to the solvent signal: CDCl_3 [$\delta_{\text{C}} = 77.16$ ppm (central line of the triplet)] or TMS ($\delta_{\text{C}} = 0.00$ ppm).¹⁴⁰ All NMR spectra were integrated and processed using Bruker's TopSpin Software.

High resolution mass spectra (HR-MS) were either recorded on the JEOL JMS-700 (EI^+), Bruker ApexQehybrid 9.4 T FT-ICR-MS (DART^+) or a Finnigan LCQ mass spectrometer at the Organisch-Chemisches Institut der Universität Heidelberg.

Elemental analyses were carried out at the Organisch-Chemisches Institut der Universität Heidelberg.

IR spectra were recorded on a JASCO FT/IR-4100. Substances were applied as a film. The obtained data were processed with the software JASCO Spectra Manage II.

Absorption spectra were recorded on a JASCO UV-VIS V-660 or JASCO UV-VIS V-670 and processed with the software JASCO Spectra Manage II. ASCII-files were exported and visualized by Origin.

Fluorescence spectra were recorded on a Jasco FP6500 spectrometer. Raw data were processed using JASCO Spectra Manage II. ASCII-files were exported and visualized with Origin.

Photographs of solutions were taken with a Canon EOS 7D camera equipped with an EF-S 60mm F/2.8 Macro lens. Solid state photographs were taken using a Samsung Galaxy S7.

Scanning electron microscopy (SEM) experiments were carried out with a Zeiss Ultra55 (Schröder Group, University of Heidelberg). Suspensions of the polymers in water were prepared by the same procedure. A 1ml droplet of each suspension was placed on a piece of plasma-cleaned silicon wafer and air dried. Samples were imaged in a FESEM (Ultra, Carl Zeiss Microscopy) at 1.5kV using SE and InLens detectors for secondary electrons. For improved statistics large areas of the samples were screened at low resolution using the Atlas 5 platform (Carl Zeiss Microscopy), then representative regions of interest scanned at 3 nm pixel size. All measurements were recorded with the Zeiss Smart SEM V05.04 software.

Fluorescence quantum yields (Φ) were obtained by the absolute method using an emission spectrometer equipped with an Ulbricht sphere. The system was calibrated with a primary light source.¹⁴¹ The procedure from Würth's group was used for substances with emission intensities ≥ 5000 counts, whereas the procedure of DeRose was used < 5000 counts, applying a filter ND 2.0. Given Φ for each sample are average values of at least three independent measurements.¹⁴²

Fluorescence lifetimes (τ) were acquired by an exponential fit according to the least mean square with commercially available software HORIBA Scientific Decay Data Analyses 6

(DAS6) version 6.4.4. The luminescence decays were recorded with a HORIBA Scientific Fluorocube single photon counting system operated with HORIBA Scientific Data Station version 2.2.

Fluorescent micelles preparation. Suspensions in water of F127 only (10 mg/ml), polymers only (0.5 μ M), and polymers (0.5 μ M) in F127 (10 mg/ml) were prepared by the same procedure: The polymers, dissolved in THF, were dropped into the micellar solution of F-127 in water. The mixtures were treated in an ultrasonic bath for 1 h, THF was removed by vacuum distillation, resulting in the final micellar preparations.¹¹⁵

Cyclic Voltammetry. The HOMO and LUMO of the polymers **TPEPs** in Chapter 3 were investigated by using cyclic voltammetry (CV). The CV experiments were carried out using a platinum working electrode with the film of polymers drop casting on the electrode surface, a platinum/titanium wire auxiliary electrode, a silver wire reference electrode, a 0.1M NBu₄PF₆ solution in degassed dry acetonitrile, and ferrocene/ ferrocenium as the reference redox system and internal standard (-4.8 eV). The scan rate is 50 mV/s.

Fluorescence response patterns were recorded using a CLARIOstar (firmware version 1.13) plate reader from BMG Labtech using the corresponding software (software version 5.20 R5). Data were analyzed with CLARIOstar MARS Data Analysis Software (software version 3.10 R5) from BMG Labtech. The polymers were dissolved in water to prepare stock solutions on the basis of their molecular weights. The resulting solutions were loaded into a 96-well plate (300 μ L microplate). The analyte was then added and the solutions were adjusted with buffer to the desired concentrations. The excitation wavelength was set according to the absorption wavelength of the used polymer or complex. The specific response for each analyte was measured six times and the peak values were obtained. These acquired data were used as the observables for the subsequent linear discriminant analysis.

Linear discriminant analysis (LDA) was carried out using the classical linear discriminant analysis method in SYSTAT (version 13.0). In LDA, all variables were used in the model (complete mode) and the tolerance was set as 0.001. The fluorescence response patterns were transformed into canonical patterns. The Mahalanobis distances of each individual pattern to

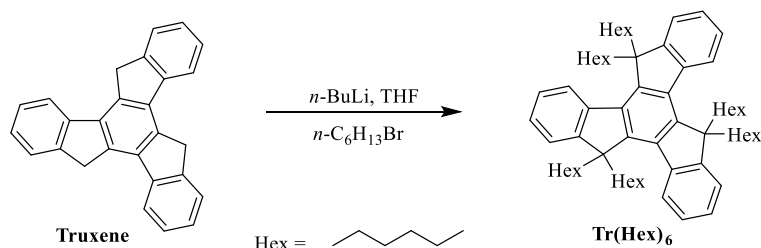
the centroid of each group in a multidimensional space were calculated and the assignment of the case was based on the shortest Mahalanobis distance.

Principal component analysis (PCA) is a mathematical transformation used to extract variance between entries in a data matrix by reducing the redundancy in the dimensionality of the data. It takes the data points for all analytes and generates a set of orthogonal eigenvectors (principal components, PCs) for maximum variance. PCA was carried out using XLSTAT (version 2016).

Graphs were visualized with Origin Pro 9.1.0 G (64 bit) SR2 and processed using Adobe ® Illustrator CS5 Version 15.0.2 for Windows or PowerPoint 2010 SP2.

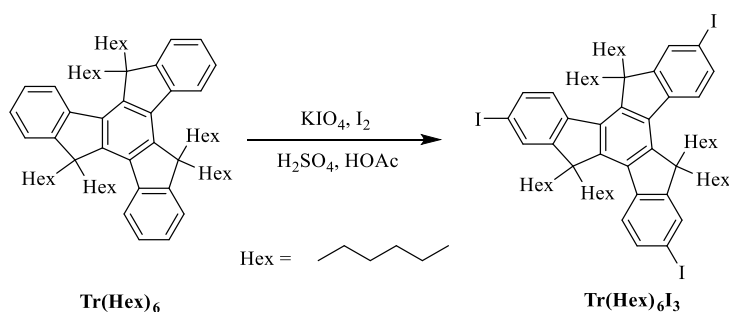
6.2 Synthesis Details and Analytical Data

6.2.1 Synthesis of HCPs and PPEs (Chapter 2)

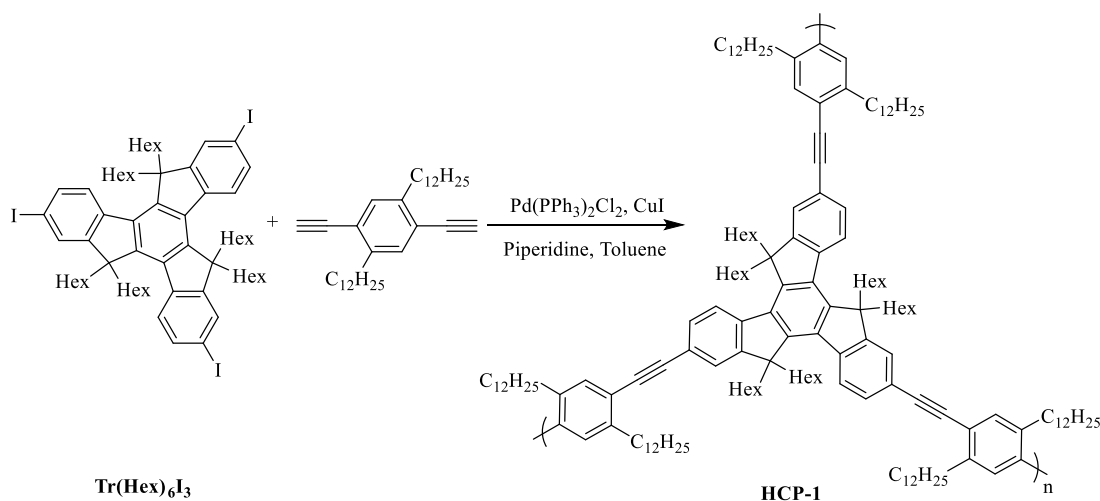


Truxene was synthesized according to the literature.¹⁵¹

Synthesis of Tr(Hex)₆: With vigorous stirring, 16.4 mL of *n*-BuLi (1.6 M, 10 equiv.) was added to a suspension of truxene (900 mg, 2.63 mmol) in 30 mL of anhydrous THF at -78 °C and the mixture was kept at this temperature over a period of 2 h. A solution of *n*-hexyl bromide (4.34 g, 10 equiv.) in THF was then added dropwisely. The reaction mixture was allowed slowly warm to room temperature and was stirred overnight. The mixture was then poured into 100 mL of saturated aqueous NaCl solution and the resulting solution was with stirred for 30 min. The mixture was exacted with ethyl acetate (2* 100 ml), and the combined organic phases were dried over MgSO₄, filtered and the solvent was removed in vacuum. The residue was purified by flash column chromatography using petroleum ether as eluent to afford Tr(Hex)₆ (1.95 g, 87%) as a light yellow solid. ¹H NMR (CDCl₃, 300 MHz): δ = 8.30-8.42 (d, 3H), 7.44- 7.49 (m, 3H), 7.31- 7.43 (m, 6H), 2.85- 3.06 (m, 6H), 1.96- 2.18 (m, 6H), 0.66- 1.00 (m, 36H), 0.54- 0.61 (m, 18H), 0.39- 0.51 (m, 12H). ¹³C NMR (CDCl₃, 100 MHz): δ = 153.8, 144.9, 140.5, 138.5, 126.5, 126.1, 124. 8 122.3, 55.8, 37.1, 31.6, 29.7, 24.0, 22.4, 14.0. HR-MS (DART⁺): m/z calcd. for C₆₃H₉₀ 846.70 [M+NH₄]⁺; found 847.11. C₆₃H₉₀: calcd. C 89.29, H 10.71, found C 89.32, H 10.96.

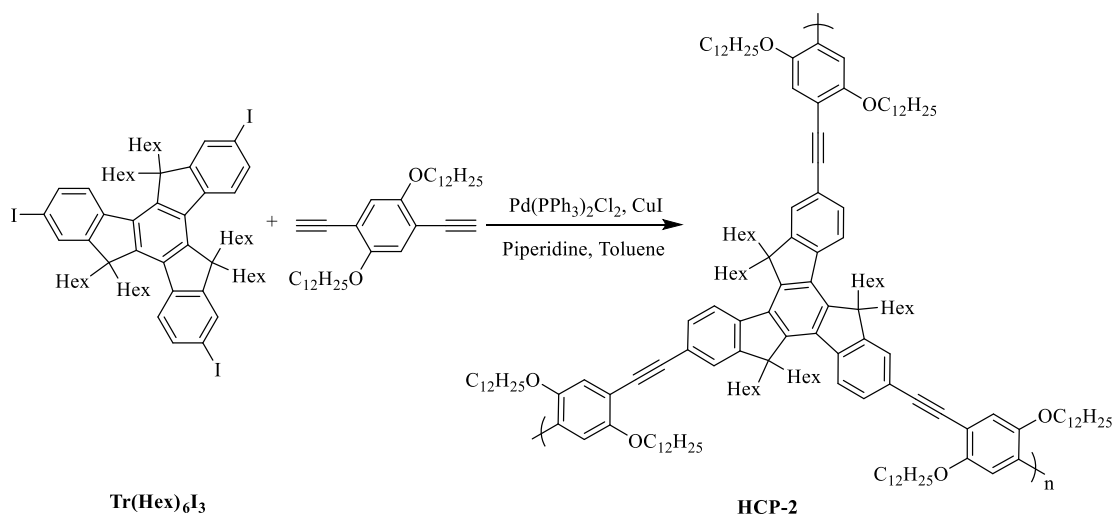


Synthesis of $\text{Tr}(\text{Hex})_6\text{I}_3$: A mixture of $\text{Tr}(\text{Hex})_6$ (500 mg, 0.59 mmol) and 10 mL of solvent ($\text{CH}_3\text{COOH}/\text{H}_2\text{SO}_4/\text{H}_2\text{O} = 100:40:3$) was heated to 60 °C with vigorous stirring, followed by adding 2 mL of CHCl_3 , KIO_4 (115 mg, 0.49 mmol, 0.83 equiv.), and I_2 (250 mg, 0.98 mmol, 1.66 equiv.). The mixture was stirred at 80 °C under nitrogen atmosphere. After the mixture cooled to room temperature, 100 mL of water was added. The resulting brown precipitate was filtered and purified by recrystallization three times from ethanol, to afford $\text{Tr}(\text{Hex})_6\text{I}_3$ as a white solid (480 mg, 66%). ^1H NMR (CDCl_3 , 300 MHz): $\delta = 8.00\text{--}8.10$ (d, 3H), 7.74– 7.78 (m, 3H), 7.68– 7.72 (m, 3H), 2.74– 2.94 (m, 6H), 1.88– 2.12 (m, 6H), 0.76– 1.05 (m, 36H), 0.56– 0.70 (m, 18H), 0.32– 0.55 (m, 12H). ^{13}C NMR (CDCl_3 , 100 MHz): $\delta = 155.9, 145.0, 139.6, 137.6, 135.3, 131.5, 126.3, 92.6, 55.9, 36.7, 31.4, 29.4, 23.9, 22.2, 13.8$.

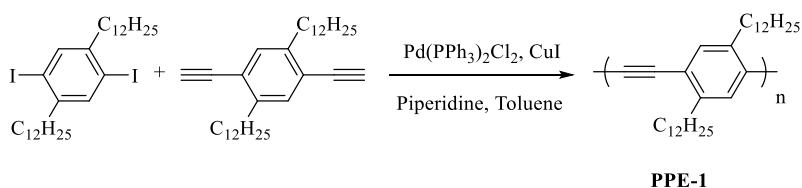


Synthesis of HCP-1: $\text{Tr}(\text{Hex})_6\text{I}_3$ (114 mg, 0.093 mmol) and 1,4-didodecyl-2,5-diethynylbenzene (65 mg, 0.140 mmol, 1.5 equiv.) were dissolved in a degassed mixture of catalyst stock solution (5 ml) with $\text{Pd}(\text{PPh}_3)_2\text{Cl}_2$ (0.01 equiv.) and CuI (0.01 equiv.). The catalyst stock solution was made of $\text{Pd}(\text{PPh}_3)_2\text{Cl}_2$ (6 mg, 9.3 μmol , 0.1 equiv.) and CuI (1.7 mg, 9.3 μmol , 0.1 equiv.) in 50 ml mixture of toluene/ piperidine (1:1) and degassed for 45

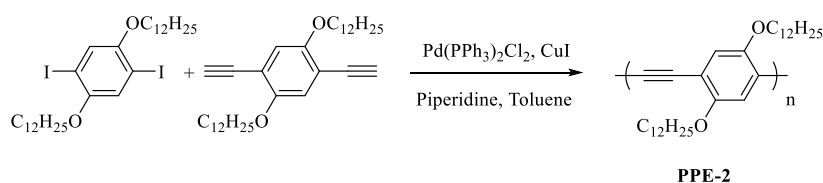
min. The mixture was stirred at room temperature for 48 h. Saturated NH_4Cl solution and CHCl_3 were added and the aqueous layer was extracted with CHCl_3 . The organic layers were dried over MgSO_4 , filtered and concentrated under vacuum. The raw product was dissolved in a small amount of CHCl_3 and slowly added to an excess of CH_3OH for precipitating, giving **HCP-1** as yellow solid (120 mg, 67%). ^1H NMR (CDCl_3 , 600 MHz): δ = 8.00- 8.40 (m, 3H), 7.69- 7.80 (m, 6H), 7.31- 7.49 (m, 4H), 2.60- 3.05 (m, 14H), 1.95- 2.10 (m, 6H), 1.64- 1.84 (m, 8H), 1.20- 1.40 (m, 72H), 0.78- 0.98 (m, 48H), 0.58- 0.70 (m, 18H), 0.36- 0.55 (m, 12H). Due to the poor solubility, a ^{13}C spectrum could not be obtained. IR (cm^{-1}): ν 2948, 2921, 2850, 1490, 1458, 1372, 1257, 1083, 1020, 888, 799, 721.



Synthesis of HCP-2: **HCP-2** was prepared through the same procedure as **HCP-1**. **Tr(Hex)₆I₃** (80 mg, 0.065 mmol) and 1,4-bis(dodecyloxy)-2,5-diethynylbenzene (48.5 mg, 0.098 mmol, 1.5 equiv.), $\text{Pd}(\text{PPh}_3)_2\text{Cl}_2$ (0.45 mg, 0.65 μmol , 0.01 equiv.) and CuI (0.125 mg, 0.65 μmol , equiv.) was used to get **HCP-2** as orange solid (80 mg, 62%). ^1H NMR (CDCl_3 , 600 MHz): δ = 8.00- 8.40 (m, 3H), 7.55- 7.80 (m, 6H), 6.97- 7.15 (m, 3H), 3.95- 4.20 (m, 6H), 2.78- 3.02 (m, 6H), 1.80- 2.20 (m, 12H), 1.20- 1.46 (m, 48H), 0.80- 1.00 (m, 45H), 0.57- 0.70 (m, 18H), 0.40- 0.55 (m, 12H). Due to the poor solubility, a ^{13}C spectrum could not be obtained. IR (cm^{-1}): ν 2954, 2947, 2921, 2852, 1502, 1464, 1376, 1215, 1022, 834, 804, 721.

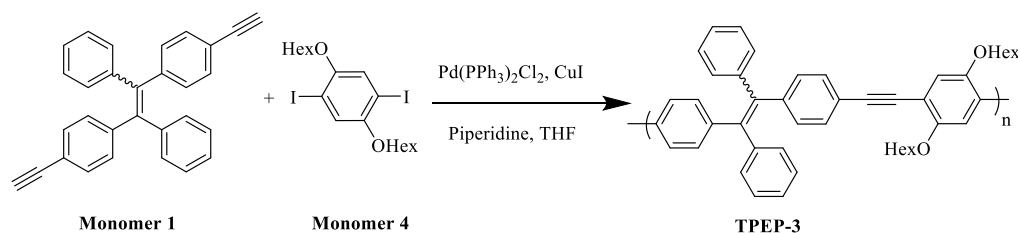


Synthesis of PPE-1: 1,4-Didodecyl-2,5-diodobenzene (1.00 g, 1.5 mmol) and 1,4-didodecyl-2,5-diethynylbenzene (694 mg, 1.5 mmol, 1 equiv.) were dissolved in toluene (5.0 mL) and piperidine (3.9 mL). After degassing the mixture for 45 min with N₂, 0.5 mL of a catalyst stock solution (3.0 μmol Pd(PPh₃)₂Cl₂, 6.0 μmol CuI, 5 mL piperidine) was added. The reaction mixture was heated up to 70 °C and stirred for 5 days. Saturated NH₄Cl solution and CHCl₃ were added and the aqueous layer was extracted with CHCl₃. The organic layers were dried over MgSO₄, filtered and concentrated under vacuum. The raw product was dissolved in a small amount of CHCl₃ and slowly added to an excess of CH₃OH twice and *n*-hexane twice for precipitating, giving **PPE-1** as an orange solid (1.440 g, 85%). ¹H NMR (CDCl₃, 400 MHz): δ = 7.14 (s, 2H), 2.80- 2.53 (m, 4H), 1.70- 0.90 (m, 40H), 0.80- 0.65 (m, 6H). Due to the poor solubility, a ¹³C spectrum could not be obtained. IR (cm⁻¹): ν 2917, 2849, 1502, 1465, 893, 886, 720.

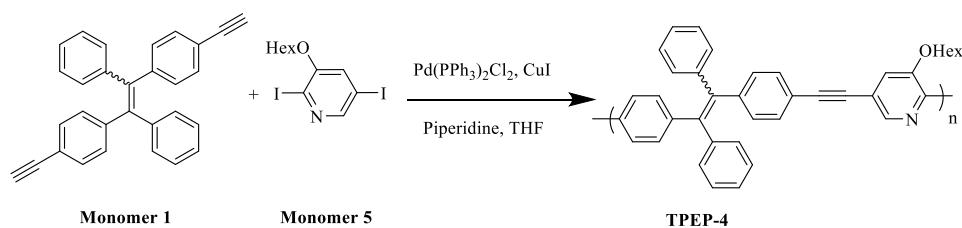


Synthesis of PPE-2: 1,4-Bis(dodecyloxy)-2,5-diodobenzene (858 mg, 1.5 mmol) and 1,4-bis(dodecyloxy)-2,5-diethynylbenzene (742 mg, 1.5 mmol) were dissolved in toluene (5.0 mL) and piperidine (3.9 mL). After degassing the mixture for 45 min with N₂, 0.5 mL of a catalyst stock solution (3.0 μmol Pd(PPh₃)₂Cl₂, 6.0 μmol CuI, 5 mL piperidine) was added. The reaction mixture was heated up to 70 °C and stirred for 5 days. Followed by same work up as **PPE-1**, an orange solid **PPE-2** was obtained (1.520 mg, 95%). ¹H NMR (CDCl₃, 400 MHz): δ = 7.01 (s, 2H), 4.10- 3.95 (m, 4H), 1.92- 1.78 (m, 4H), 1.60- 1.44 (m, 4H), 1.34- 1.21 (m, 32H), 0.90- 0.82 (m, 6H). Due to the poor solubility, a ¹³C spectrum could not be obtained. IR (cm⁻¹): ν 2919, 2850, 1514, 1468, 1428, 1388, 1277, 1213, 856, 720.

mg, 0.008 mmol, 0.02 equiv.) and CuI (1.5 mg, 0.008 mmol, 0.02 equiv.) were added and the mixture was stirred at room temperature for 48 h. **TPEP-2** was obtained as yellow solid (290 mg, 85%). ^1H NMR (CDCl_3 , 600 MHz): $\delta = 7.32\text{-}7.27$ (m, 2H), 7.25- 7.20 (m, 4H), 7.17- 7.10 (m, 6H), 7.07- 6.98 (m, 8H), 2.78- 2.73 (m, 4H), 1.68- 1.63 (m, 4H), 1.25- 1.32 (m, 12H), 0.86- 0.84 (m, 6H). Due to the poor solubility, a ^{13}C spectrum could not be obtained.



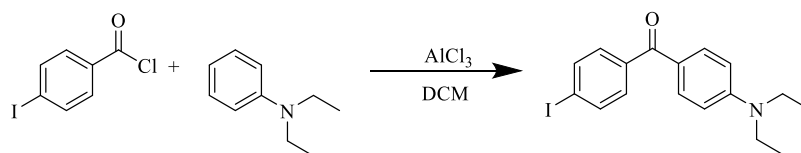
Synthesis of TPEP-3: **TPEP-3** was prepared through the same procedure as **TPEP-1**. Monomer 1 (70 mg, 0.18 mmol) and monomer 4 (98 mg, 0.18 mmol, 1.0 equiv.) were dissolved in a degassed mixture of THF/ piperidine/ CHCl_3 (1:1:1, 3 mL). $\text{Pd}(\text{PPh}_3)_2\text{Cl}_2$ (2.5 mg, 0.004 mmol, 0.02 equiv.) and CuI (1 mg, 0.004 mmol, 0.02 equiv.) were added, then the mixture was stirred at room temperature for 48 h. **TPEP-3** was obtained as yellow solid (140 mg, 83%). ^1H NMR (CDCl_3 , 600 MHz): $\delta = 7.20\text{-}6.60$ (m, 20H), 4.09- 3.62 (m, 4H), 1.90- 1.43 (m, 8H), 1.40- 1.20 (m, 8H), 0.90- 0.72 (m, 6H). Due to the poor solubility, a ^{13}C spectrum could not be obtained.



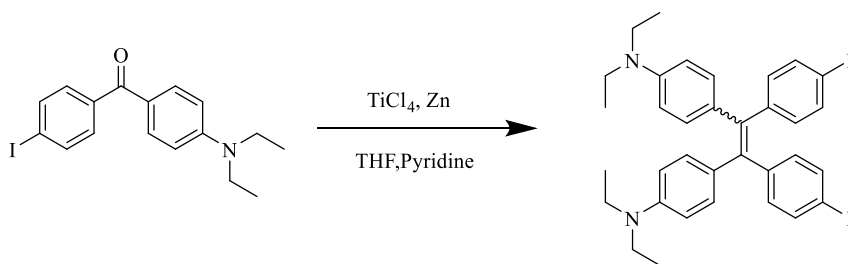
Synthesis of TPEP-4: **TPEP-4** was prepared through the same procedure as **TPEP-1**. Monomer 1 (85 mg, 0.22 mmol) and monomer 5 (75 mg, 0.22 mmol, 1.0 equiv.) were dissolved in a degassed mixture of THF/piperidine/ CHCl_3 (1:1:1, 3 mL). $\text{Pd}(\text{PPh}_3)_2\text{Cl}_2$ (3 mg, 0.005 mmol, 0.02 equiv.), and CuI (1 mg, 0.005 mmol, 0.02 equiv.) were added, then the mixture was stirred at room temperature for 48 h. **TPEP-4** was obtained as yellow solid (120 mg, 75%). ^1H NMR (CDCl_3 , 600 MHz): $\delta = 8.32\text{-}8.17$ (m, 1H), 7.40- 7.20 (m, 5H), 7.17- 7.07(m, 6H), 7.05- 6.93(m, 8H), 4.10- 4.00 (m, 2H), 1.93- 1.79 (m, 2H), 1.60- 1.44 (m, 2H),

1.39- 1.20 (m, 4H), 0.94- 0.83 (m, 3H). Due to the poor solubility, a ^{13}C spectrum could not be obtained.

6.2.3 Synthesis of F-TPEPs (Chapter 4)

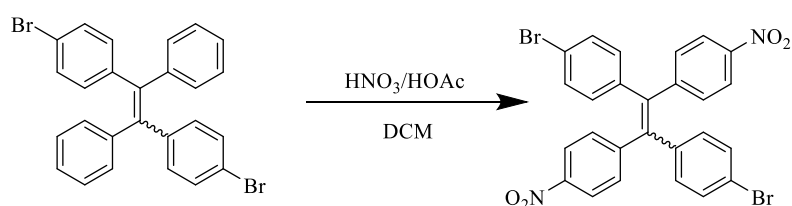


Synthesis of (4-(Diethylamino)phenyl)(4-iodophenyl)methanone: To a solution of 4-iodobenzoyl chloride (2.10 g, 7.88 mmol) and aluminum chloride (1.37 g, 10.3 mmol, 1.3 equiv.) in dichloromethane (50 mL), diethylaniline (1.41g, 9.46 mmol, 1.2 equiv.) was added. The resulting reaction mixture was stirred at room temperature for 3 h. The reaction mixture was quenched by adding saturated NH_4Cl solution and extracted with EtOAc and washed with brine, dried over Na_2SO_4 , and filtered. The solvent was concentrated under reduced pressure. Further purification was conducted by flash column chromatography (PE/ EA = 10:1). Crystallization from *n*-hexane gave the product as a yellow solid (440 mg, 15%). ^1H NMR (CDCl_3 , 300 MHz): δ = 7.83- 7.79 (m, 2 H), 7.76- 7.73 (m, 2 H), 7.46- 7.43 (m, 2 H), 6.67- 6.64 (m, 2 H), 3.48- 3.40 (m, 4H), 1.24- 1.20 (t, 6H). ^{13}C NMR (CDCl_3 , 100 MHz): δ = 151.38, 143.14, 138.96, 137.35, 133.11, 123.76, 115.13, 110.28, 44.92, 12.50.

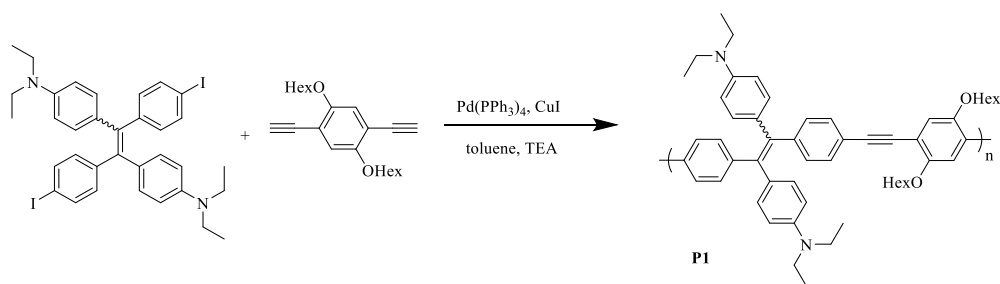


Synthesis of 4,4'-(1,2-bis(4-iodophenyl)ethene-1,2-diyl)bis(N,N-diethylaniline): (4-Diethyl-amino-phenyl)(4-iodophenyl)methanone (400 mg, 1.05 mmol) and Zn powder (138 mg, 2.11 mmol, 2.0 equiv.) were placed in a degassed flask. Dry THF (20 mL) was added and the mixture was cooled to $-78\text{ }^\circ\text{C}$. TiCl_4 (200 mg, 1.05 mmol, 1.0 equiv.) was added dropwise. The mixture was slowly warmed to room temperature and stirred for 0.5 h. Pyridine (0.05 mL) was then injected. After the mixture was heated to reflux overnight, the reaction was quenched with a 10% aqueous solution of K_2CO_3 . A large amount of water was added to the

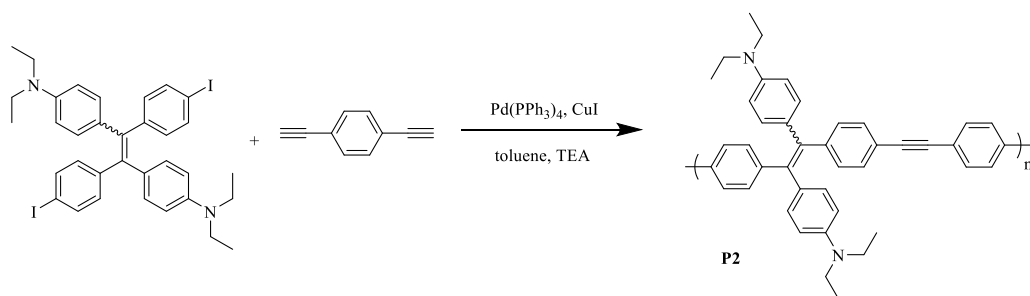
solution until the solid turned gray. The mixture was extracted with dichloromethane three times and the organic layers were combined and washed with brine twice. After evaporation of the solvent under reduced pressure, the crude product was purified by column chromatography on basic alumina by using a mixture of ethyl acetate/petrol ether = 1:3 as the eluent. And the product was washed with ethanol twice and dried over night to get yellow solid (120 mg, 31.5%) as a mixture of two isomers. $^1\text{H NMR}$ (CDCl_3 , 300 MHz): δ = 7.43-7.39 (m, 2H), 6.89- 6.85 (m, 4H), 6.49- 6.30 (m, 2H), 3.38- 3.20 (m, 4H), 1.16- 1.07 (m, 6H). HR-MS (DART⁺): m/z calcd. for $\text{C}_{34}\text{H}_{36}\text{I}_2\text{N}_2$ 726.10, found 727.10.



Synthesis of 1,2-Bis(4-bromophenyl)-1,2-diphenylethene: 1,2-Bis(4-bromophenyl)-1,2-diphenylethene was synthesized according to the literature.¹⁵⁵ 1,2-Bis(4-bromophenyl)-1,2-diphenylethene (500 mg, 1.02 mmol) was added to a solution of acetic acid (2 mL) in dichloromethane (30 mL) under vigorous stirring. Concentrated nitric acid (2.5 mL) was slowly dropped into the solution at 0 °C, then the reaction mixture was warmed to room temperature and continued to stir overnight. The reaction mixture was quenched with water before it was extracted with dichloromethane (3×50 mL). The combined organic layers were washed with a saturated brine solution and dried over anhydrous MgSO_4 . The solvent was evaporated to afford the crude product. The residue was purified by column chromatography (PE: EA = 3:1) and recrystallized from HOAc (10 mL) and dichloromethane (5 drops) to give the product as a yellow solid (430 mg, 73%). $^1\text{H NMR}$ (CDCl_3 , 300 MHz): δ = 8.05- 8.00 (m, 4 H), 7.34- 7.30 (m, 4 H), 7.19- 7.14 (m, 4 H), 6.87- 6.82 (m, 4 H). $^{13}\text{C NMR}$ (CDCl_3 , 100 MHz) δ = 148.7, 146.7, 144.0, 140.1, 137.6, 132.6, 131.8, 131.7, 123.6, 122.5. HR-MS (DART⁺): m/z calcd. for $\text{C}_{26}\text{H}_{16}\text{N}_2\text{O}_4\text{Br}_2$ 579.95, found 579.95. $\text{C}_{26}\text{H}_{16}\text{N}_2\text{O}_4\text{Br}_2$ calcd. C 53.82, H 2.78, N 4.83 found C 54.00, H 3.07, N 4.87.

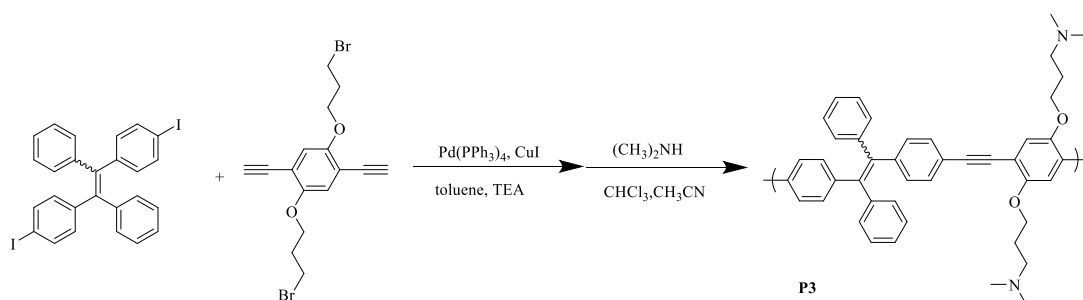


Synthesis of P1: 4,4'-(1,2-Bis(4-iodophenyl)ethene-1,2-diyl)bis(*N,N*-diethylaniline) (150 mg, 0.206 mmol) and 1,4-hexyloxy-2,5-diethynylbenzene (67 mg, 0.206 mmol, 1.0 equiv.) were dissolved in a degassed mixture of toluene/ triethylamine (TEA) (1:1, 5 mL). Pd(PPh₃)₄ (12 mg, 0.01 mmol, 0.05 equiv.) and CuI (2 mg, 0.01 mmol, 0.05 equiv) were added, then the mixture was stirred at 70 °C for 24 h. Saturated NH₄Cl solution and CHCl₃ were added and the aqueous layer was extracted with CHCl₃. The organic layers were dried over MgSO₄, filtered and concentrated under vacuum. The crude product was dissolved in a small amount of CHCl₃ and slowly added to an excess of CH₃OH and *n*-hexane for precipitating twice, to give **P1** as orange yellow solid (150 mg, 63%). ¹H NMR (CDCl₃, 300 MHz): δ = 7.30- 7.23 (m, 4H), 7.11- 7.01 (m, 4H), 6.97- 6.97(m, 2H), 6.89- 6.78 (m, 4H), 6.46- 6.37 (m, 4H), 4.04- 3.97 (m,4H), 3.34- 3.20 (m, 8H), 1.88- 1.74 (m, 4H), 1.58- 1.26 (m, 12H), 1.18- 1.10 (m, 12H), 0.93- 0.79 (m, 6H). Due to the poor solubility, a ¹³C NMR-spectrum could not be obtained. IR (cm⁻¹): ν 2926, 2863, 1603, 1512, 1354, 1263, 1194, 1148, 1071, 1031, 808, 697, 569, 518.

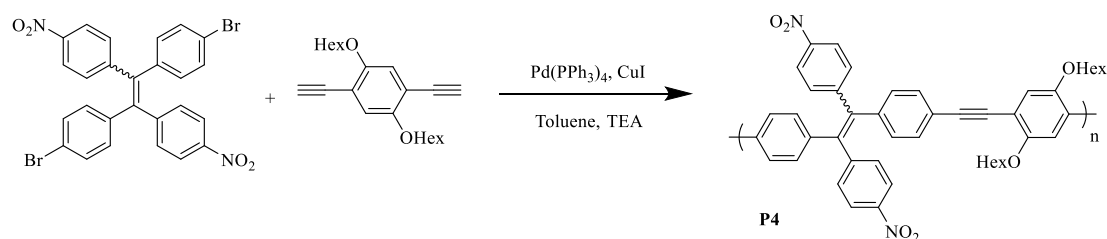


Synthesis of P2: 4,4'-(1,2-Bis(4-iodophenyl)ethene-1,2-diyl)bis(*N,N*-diethylaniline) (100 mg, 0.138 mmol) and 1,4-diethynylbenzene (17 mg, 0.138 mmol, 1.0 equiv.) were dissolved in a degassed mixture of toluene/TEA (1:1, 4 mL). Pd(PPh₃)₄ (8 mg, 0.007 mmol, 0.05 equiv.) and CuI (1 mg, 0.007 mmol, 0.05 equiv.) were added and the mixture was stirred at 80 °C for 24 h. Saturated NH₄Cl solution and CHCl₃ were added, the aqueous layer was extracted with

CHCl₃. The organic layers were dried over MgSO₄, filtered and concentrated under vacuum. The crude product was dissolved in small amount of CHCl₃ and slowly added to an excess of CH₃OH and hexane for precipitating to give **P2** as orange yellow solid (80 mg, 68%). ¹H NMR (CDCl₃, 300 MHz): δ = 7.44 (m, 4H), 7.30- 7.03 (m, 8H), 6.89- 6.78 (m, 4H), 6.45- 6.38 (m, 4H), 3.29 (m, 8H), 1.12 (m, 12H). Due to the poor solubility, ¹³C spectrum could not be obtained due to solubility reasons. IR (cm⁻¹): ν 2965, 2926, 1601, 1511, 1351, 1259, 1191, 1146, 1072, 1011, 795, 695, 538.



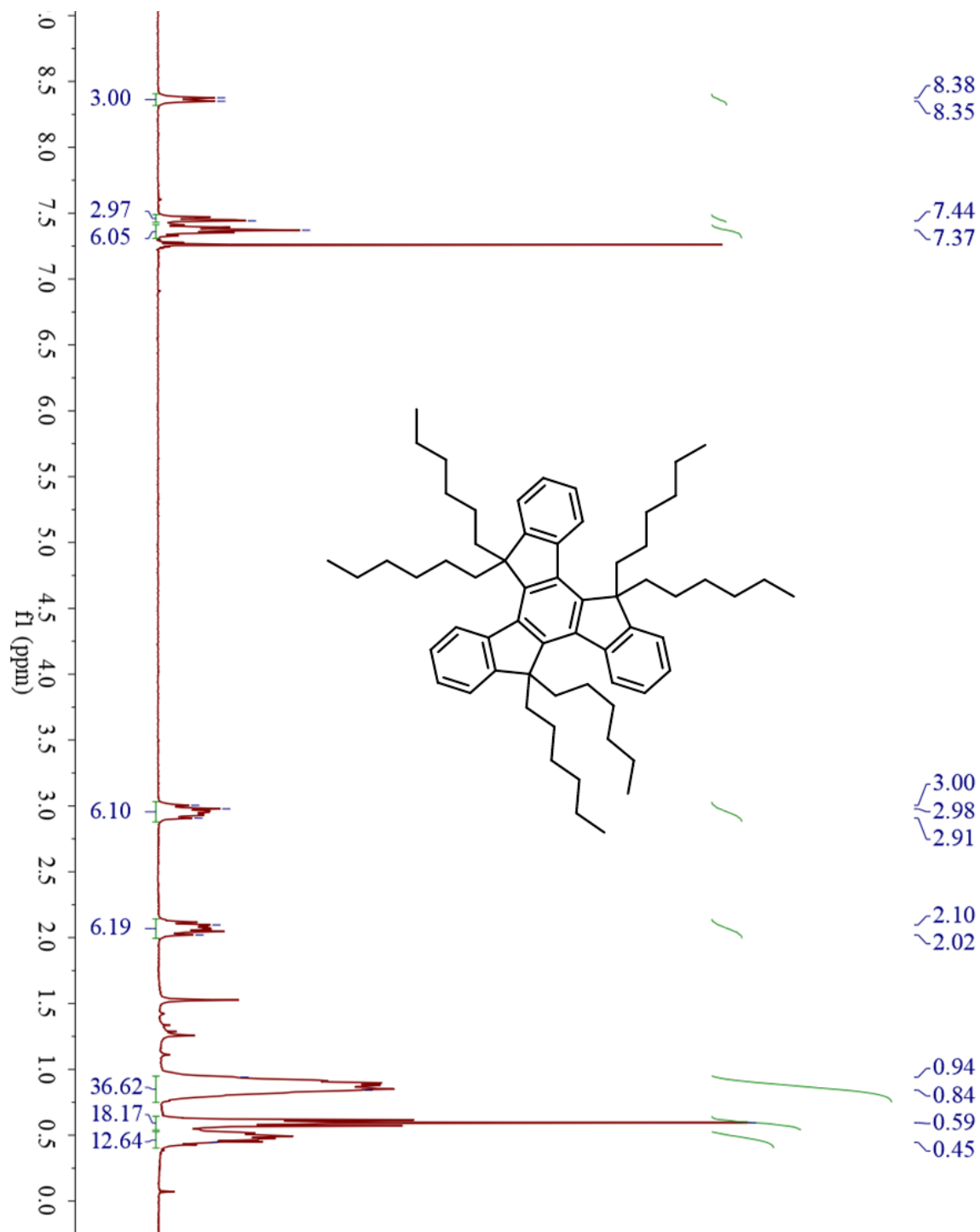
Synthesis of P3: 1,2-Bis(4-iodophenyl)-1,2-diphenylethene (140 mg, 0.263 mmol) and 1,4-bis(3-bromopropoxy)-2,5-diethynylbenzene (105 mg, 0.263 mmol, 1.0 equiv.) were dissolved in a degassed mixture of toluene/TEA (1:1, 4 mL). Pd(PPh₃)₄ (15 mg, 0.013 mmol, 0.05 equiv.) and CuI (2.5 mg, 0.013 mmol, 0.05 equiv.) were added and the mixture was stirred at 80 °C for 24 h. A saturated NH₄Cl solution and CHCl₃ were added and the aqueous layer was extracted with CHCl₃. The organic layers were dried over MgSO₄, filtered and concentrated under vacuum. Then the polymer was dissolved in degassed CH₃CN/CHCl₃ (5 mL/5 mL). Dimethylamine (5 mL) was added and reacted for 7 d under N₂ atmosphere at room temperature. After evaporation of the solvents, the crude product was dissolved in a small amounts of CHCl₃ and slowly added to an excess of CH₃OH to precipitate **P3** as orange yellow solid (95 mg, 39%). ¹H NMR (CDCl₃, 300 MHz): δ = 7.32- 7.22 (m, 6H), 7.17- 7.07 (m, 6H), 7.07- 6.97 (m, 8H), 4.06- 3.99 (m, 4H), 2.52- 2.47 (m, 4H), 2.26- 2.16 (m, 12 H), 2.03- 1.91 (m, 4H). Due to the poor solubility, a ¹³C NMR-spectrum could not be obtained.

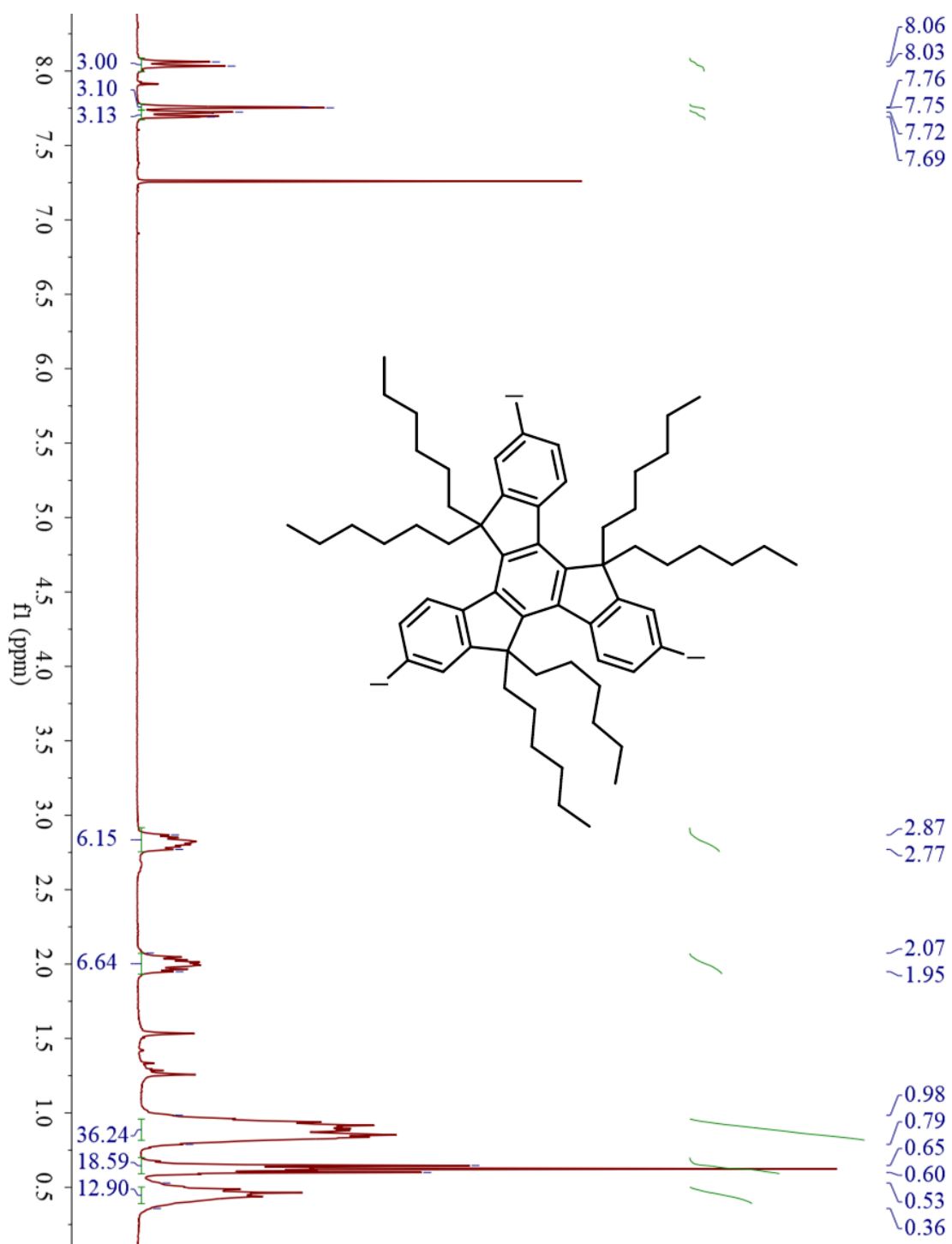


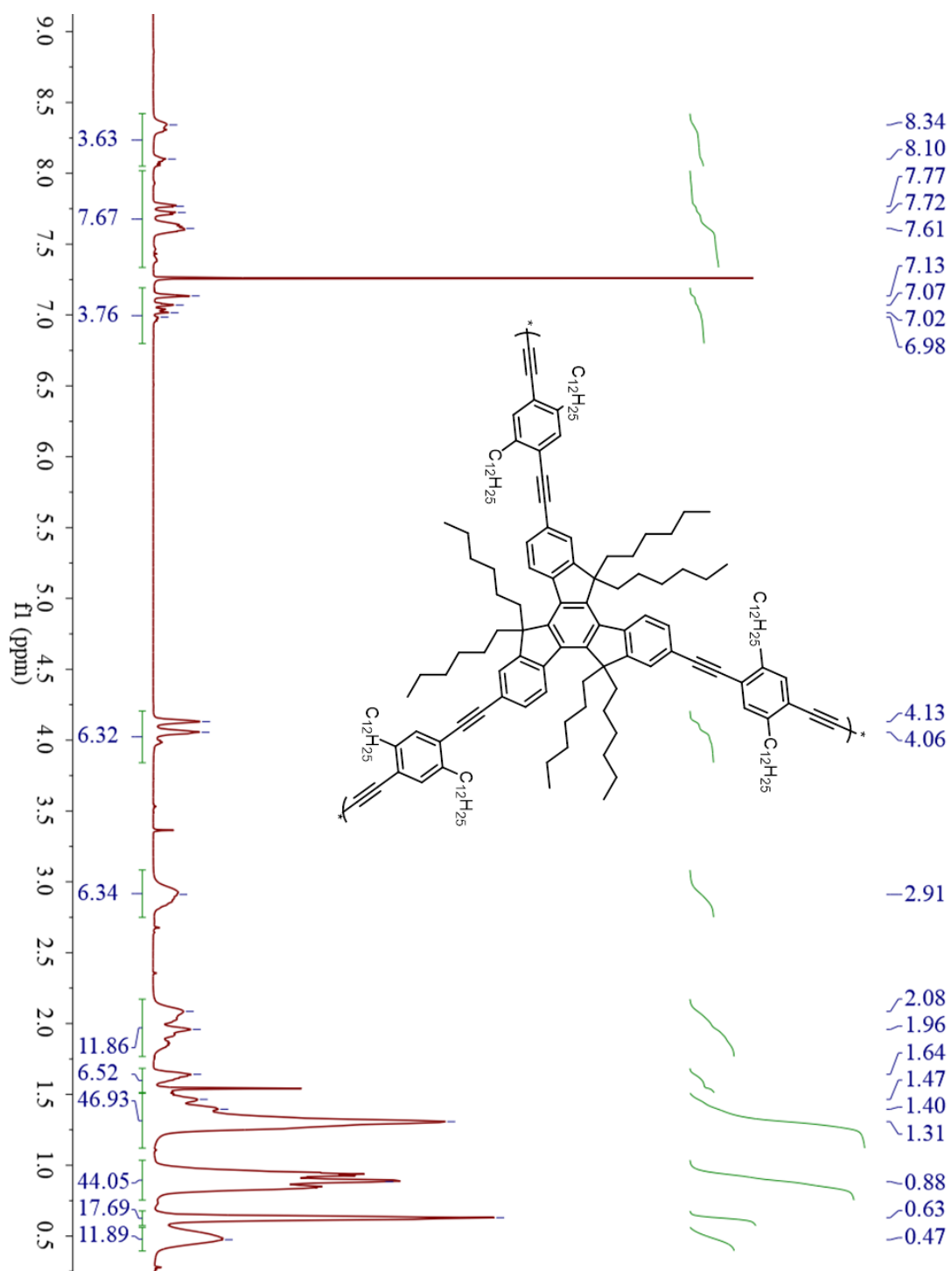
Synthesis of P4: 1,2-Bis(4-bromophenyl)-1,2-bis(4-nitrophenyl)ethene (100 mg, 0.170 mmol) and 1,4-hexyloxy-2,5-diethynylbenzene (57 mg, 0.170 mmol, 1 equiv.) were dissolved in a degassed mixture of toluene/TEA (1:1, 5 mL). Pd(PPh₃)₄ (12 mg, 0.01 mmol, 0.06 equiv.) and CuI (2 mg, 0.01 mmol, 0.06 equiv.) were added, then the mixture was stirred at 65 °C for 24 h. Saturated NH₄Cl solution and CHCl₃ were added and the aqueous layer was extracted with CHCl₃. The organic layers were dried over MgSO₄, filtered and concentrated under vacuum. The crude product was dissolved in a small amount of CHCl₃ and precipitated from CH₃OH and *n*-hexane to give **P4** as orange yellow solid (150 mg, 63%). ¹H NMR (CDCl₃, 300 MHz): δ = 8.05- 8.01 (m, 2H), 7.34- 7.31 (m, 2H), 7.23- 7.16 (m, 2H), 7.00- 6.84 (m, 4H), 4.04- 3.95 (m, 4H), 1.84- 1.73 (m, 4H), 1.43- 1.26 (m, 12H), 0.92- 0.88 (m, 6H). Due to the poor solubility, ¹³C-NMR spectrum could not be obtained. IR (cm⁻¹): ν 2926, 2858, 1594, 1515, 1384, 1340, 1273, 1211, 1106, 1014, 840, 803, 706, 476.

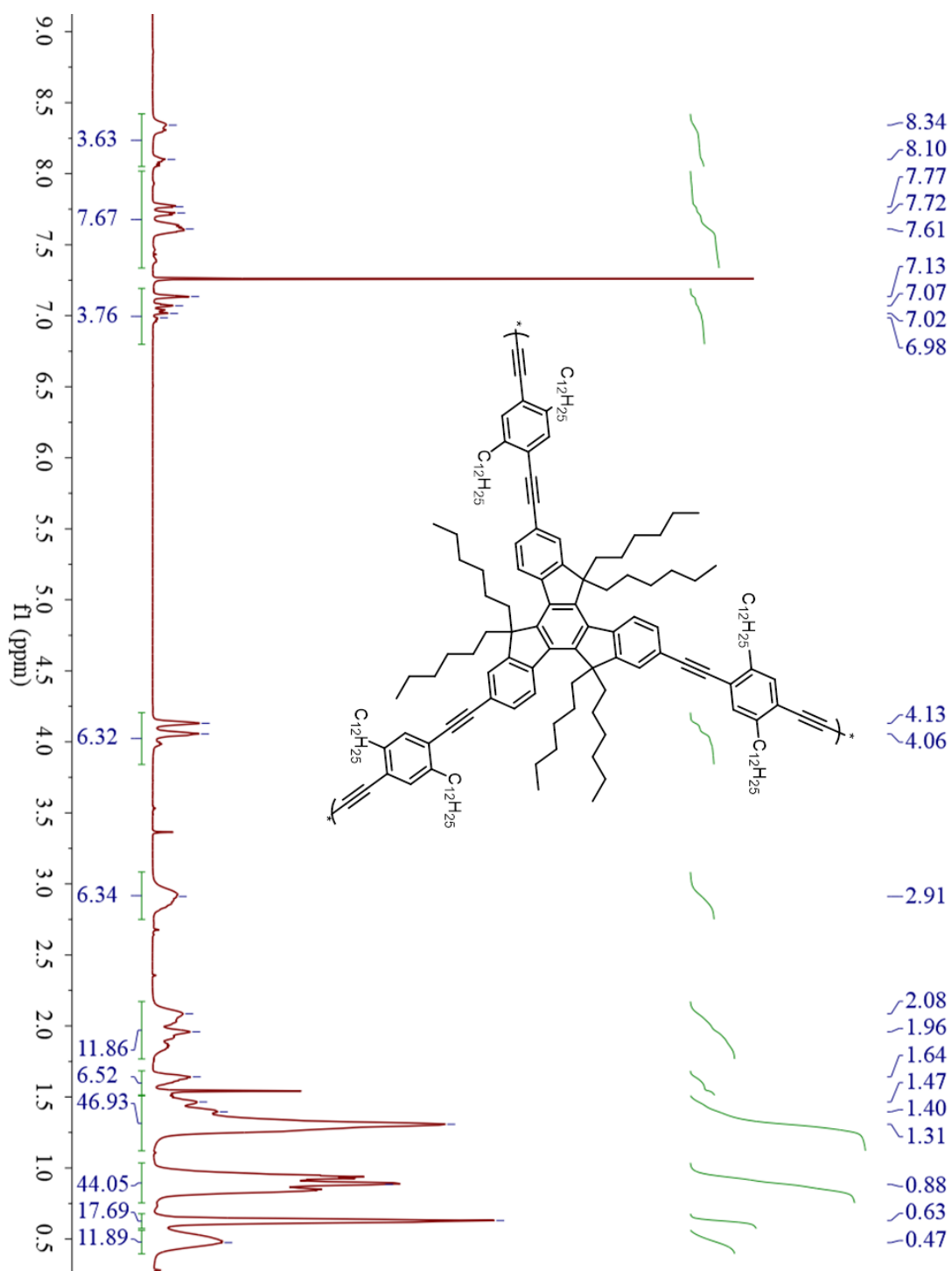
6.3 NMR Spectra

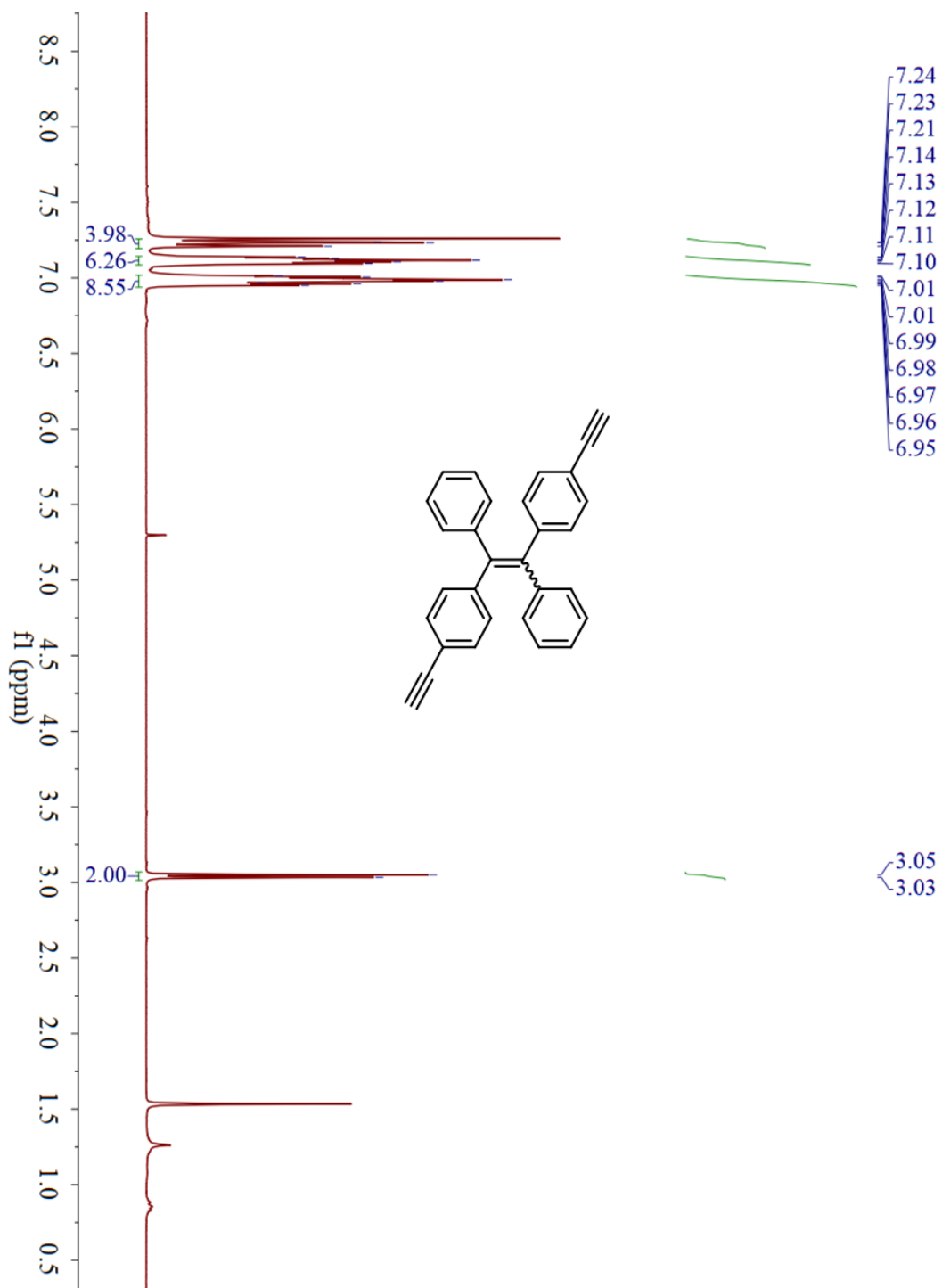
6.3.1 ^1H NMR spectra (Chapter 2)

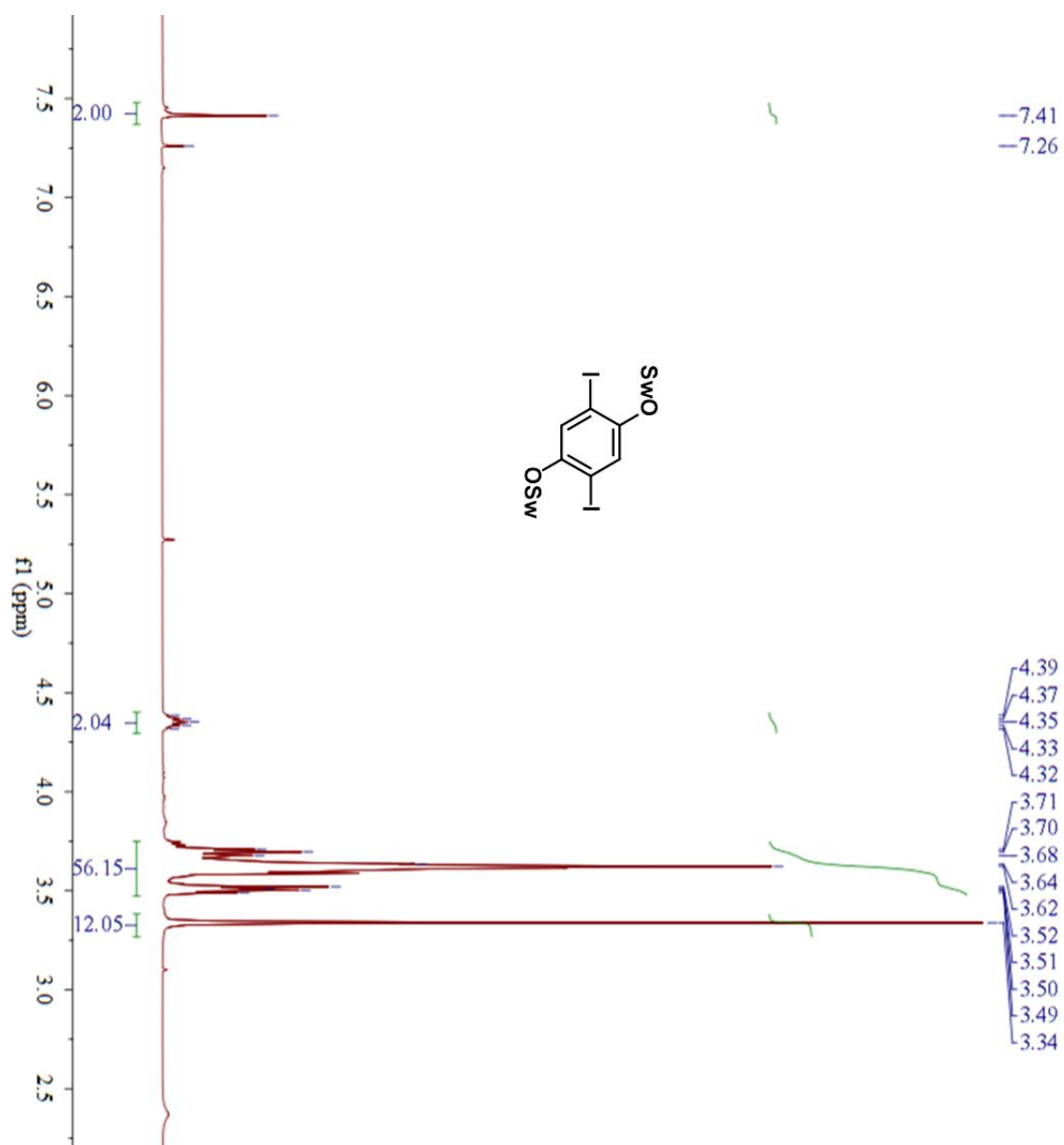


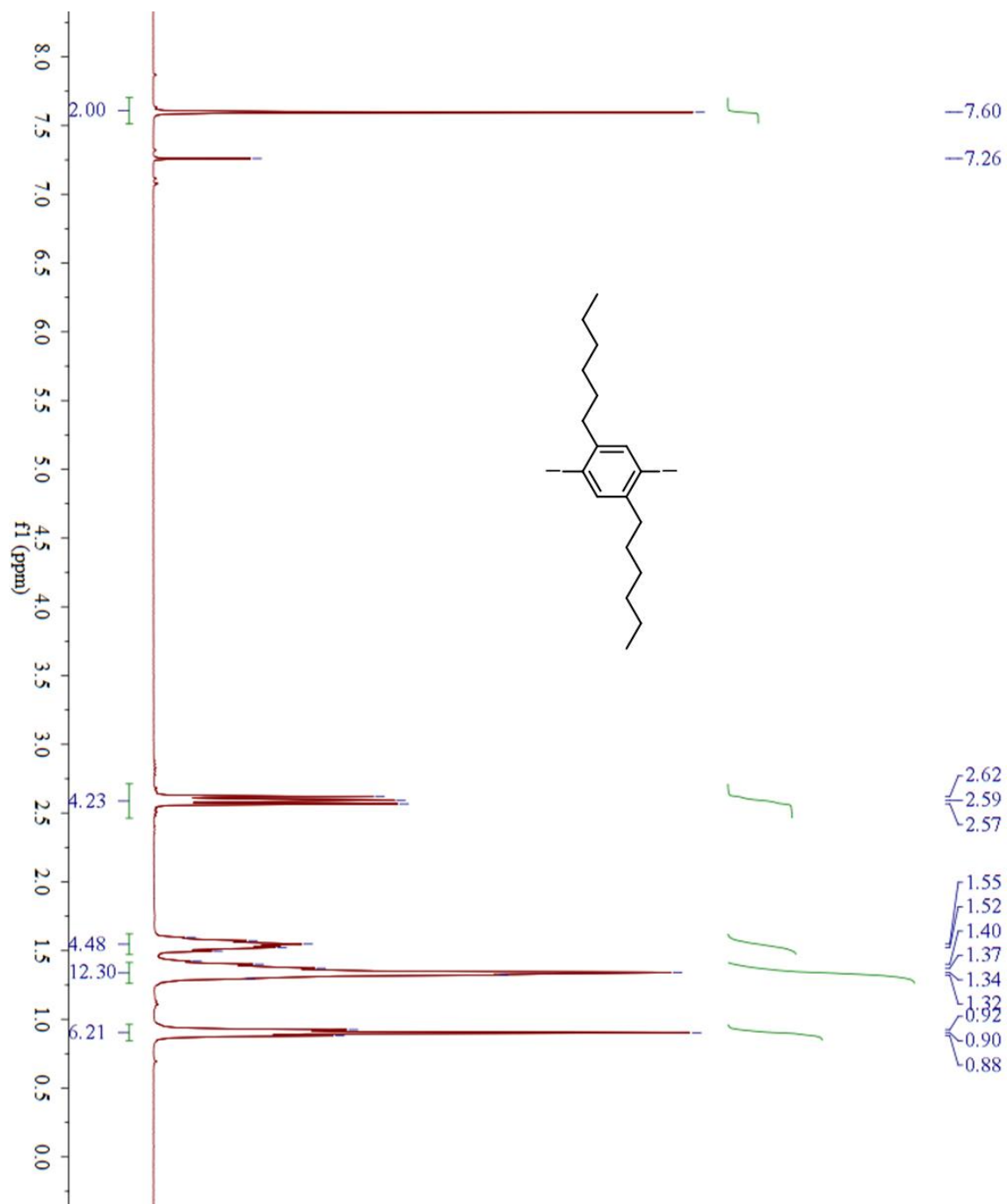


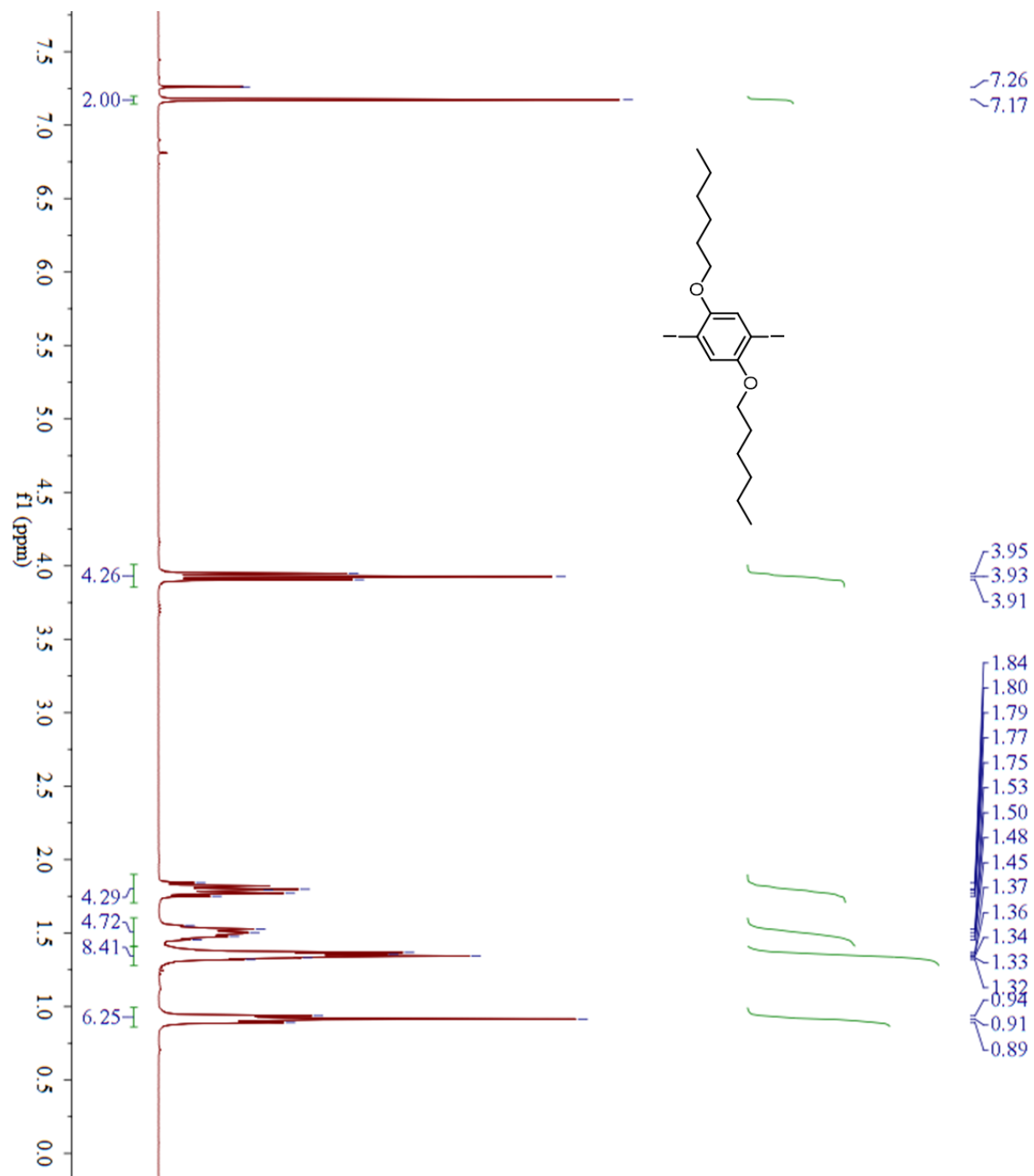


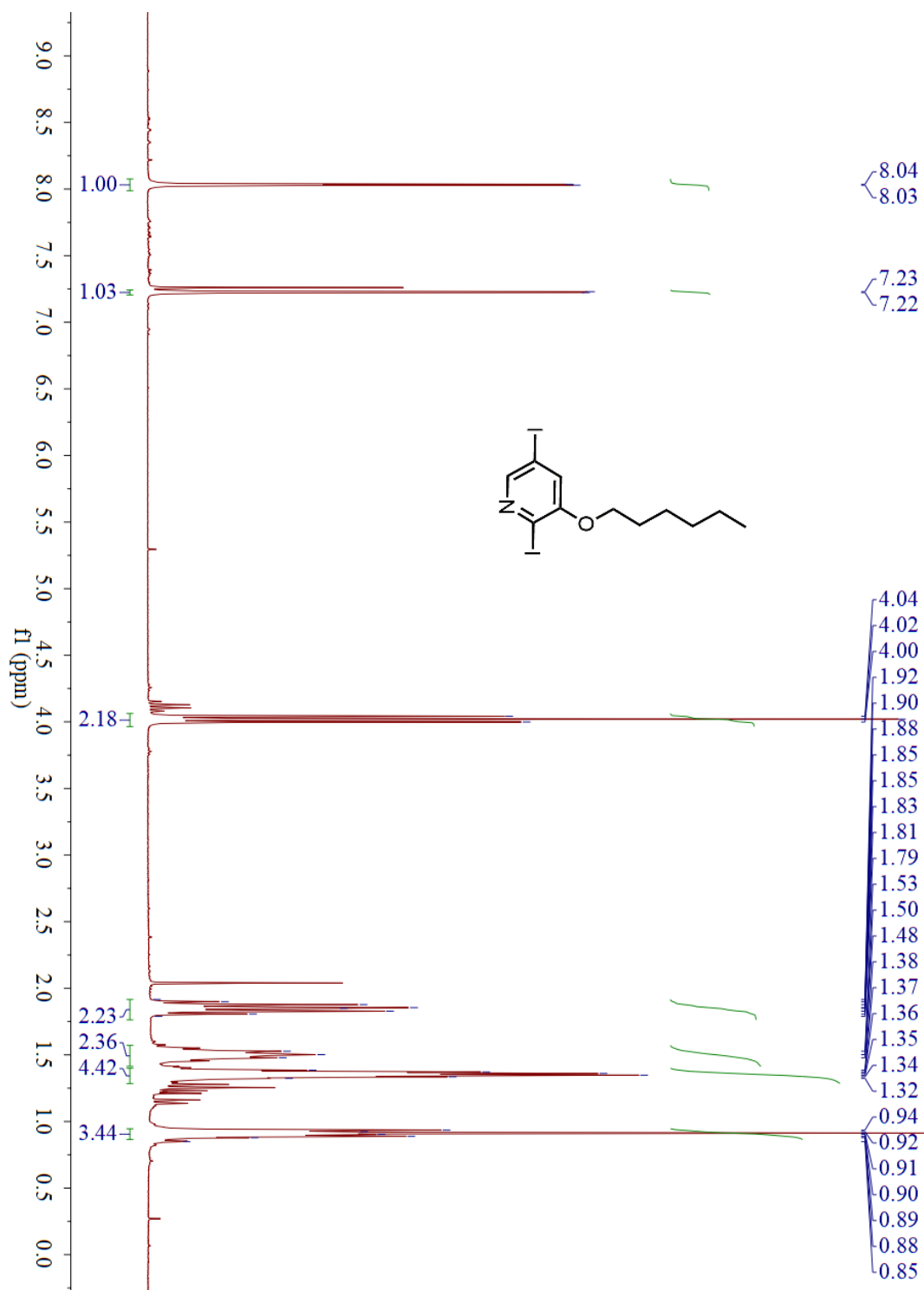


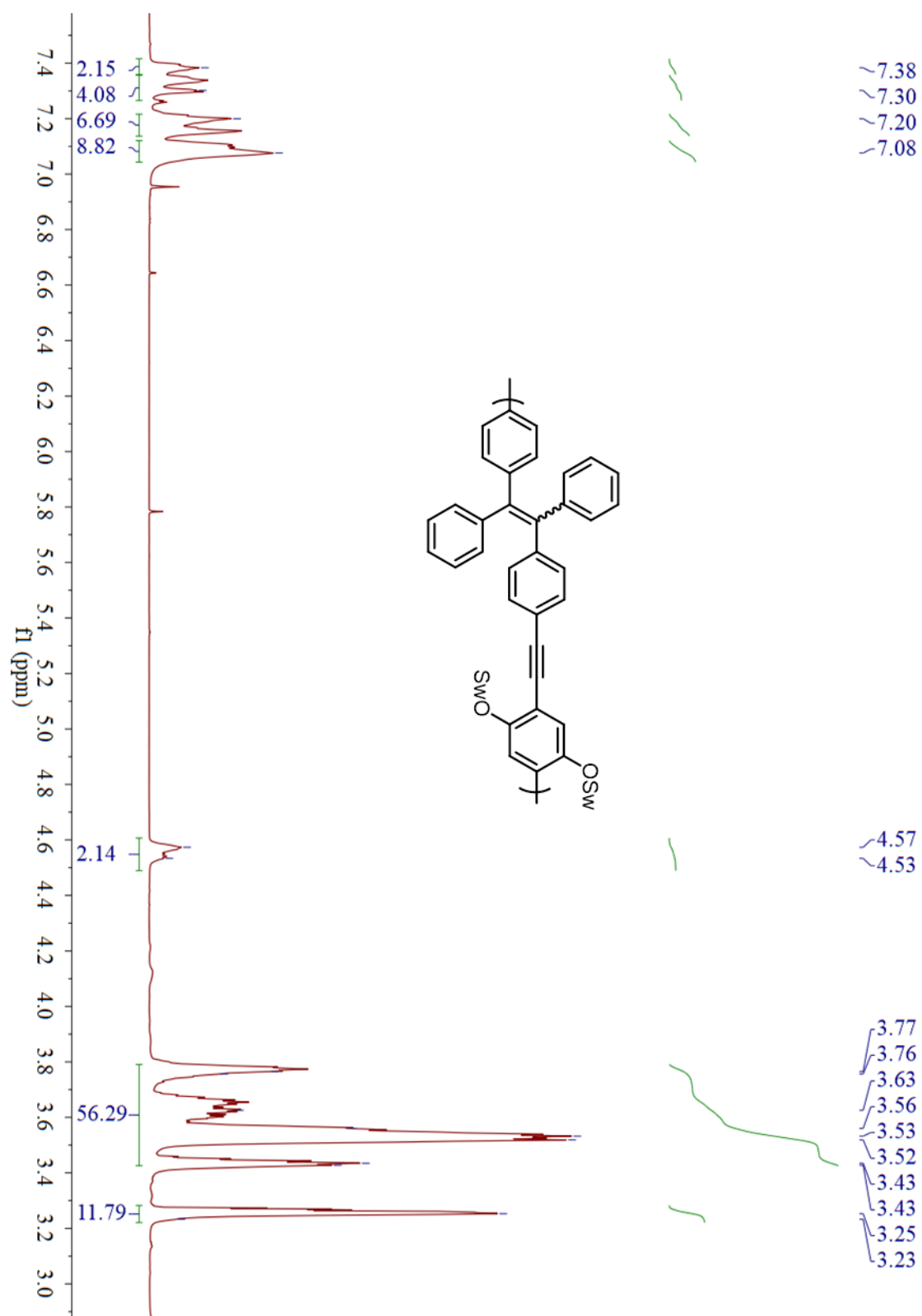
6.3.2 ^1H NMR spectra (Chapter 3)

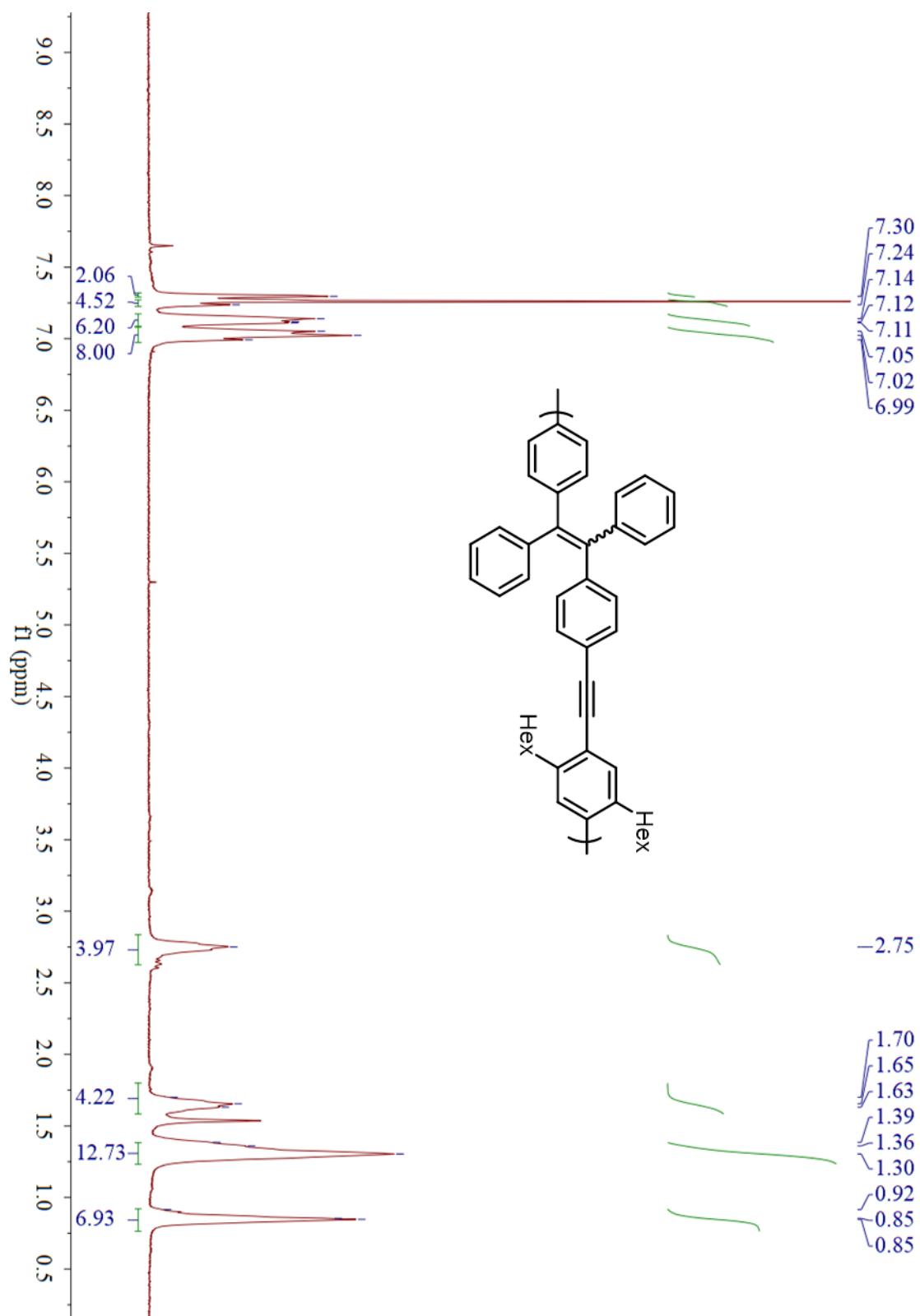


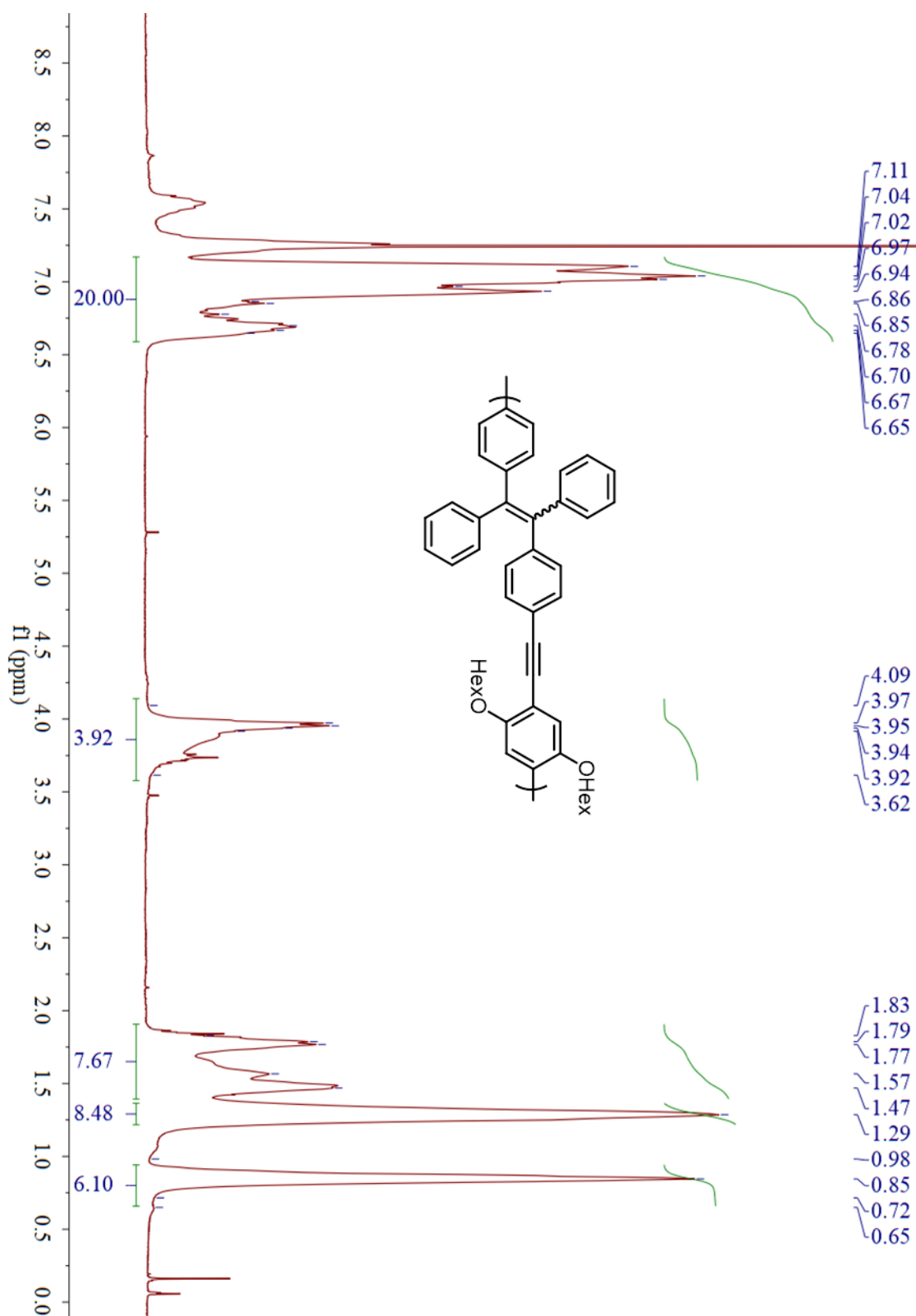
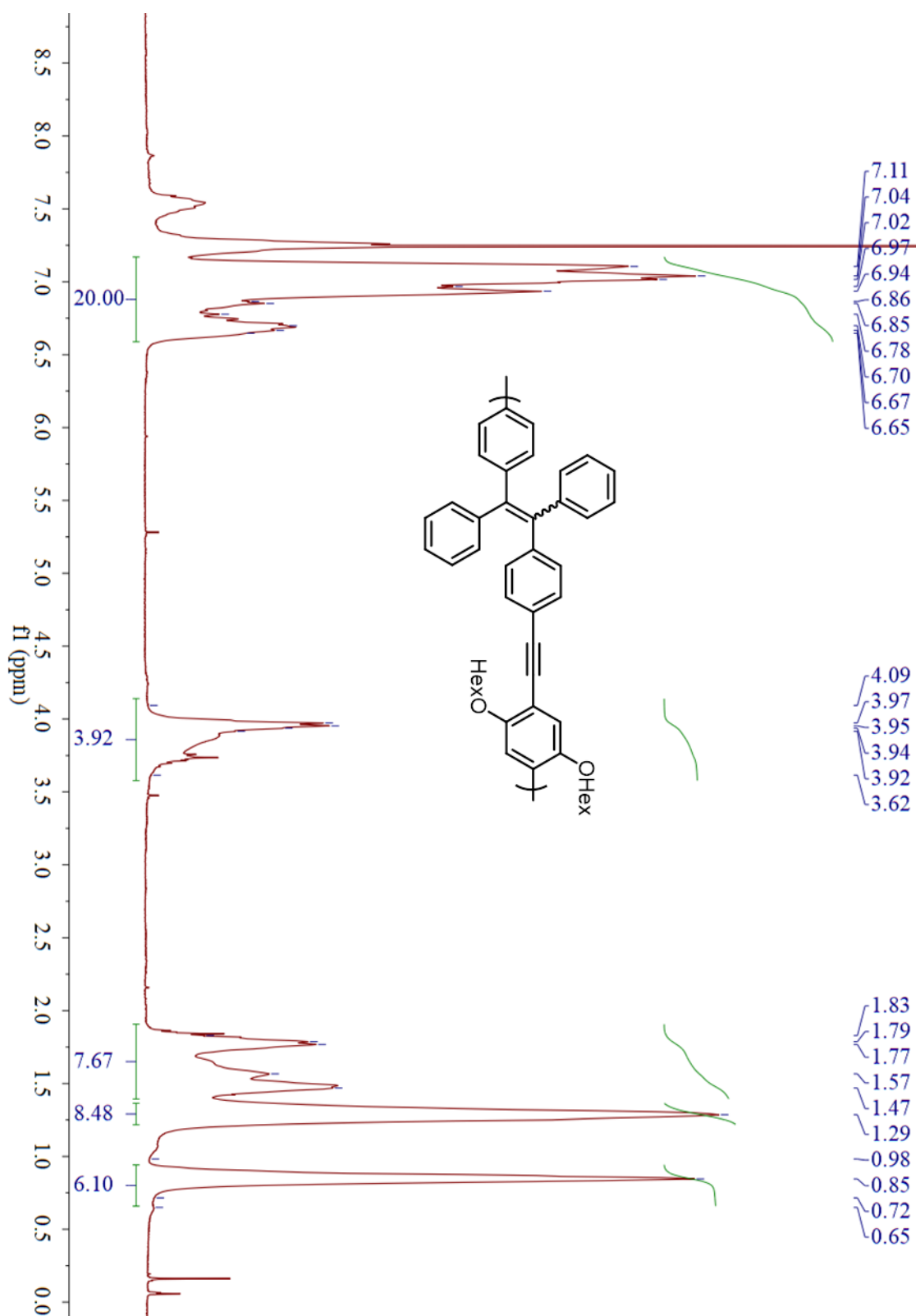


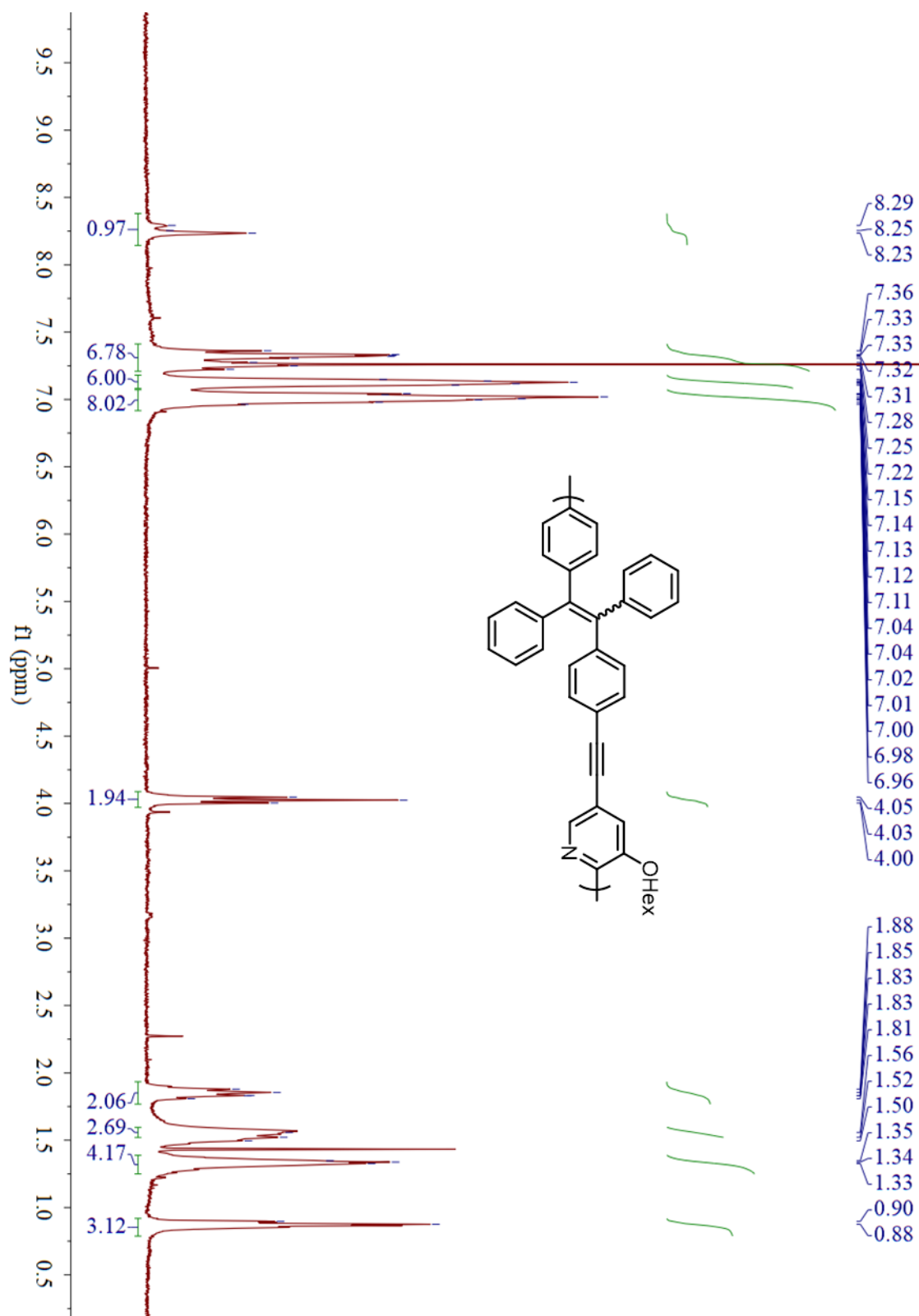


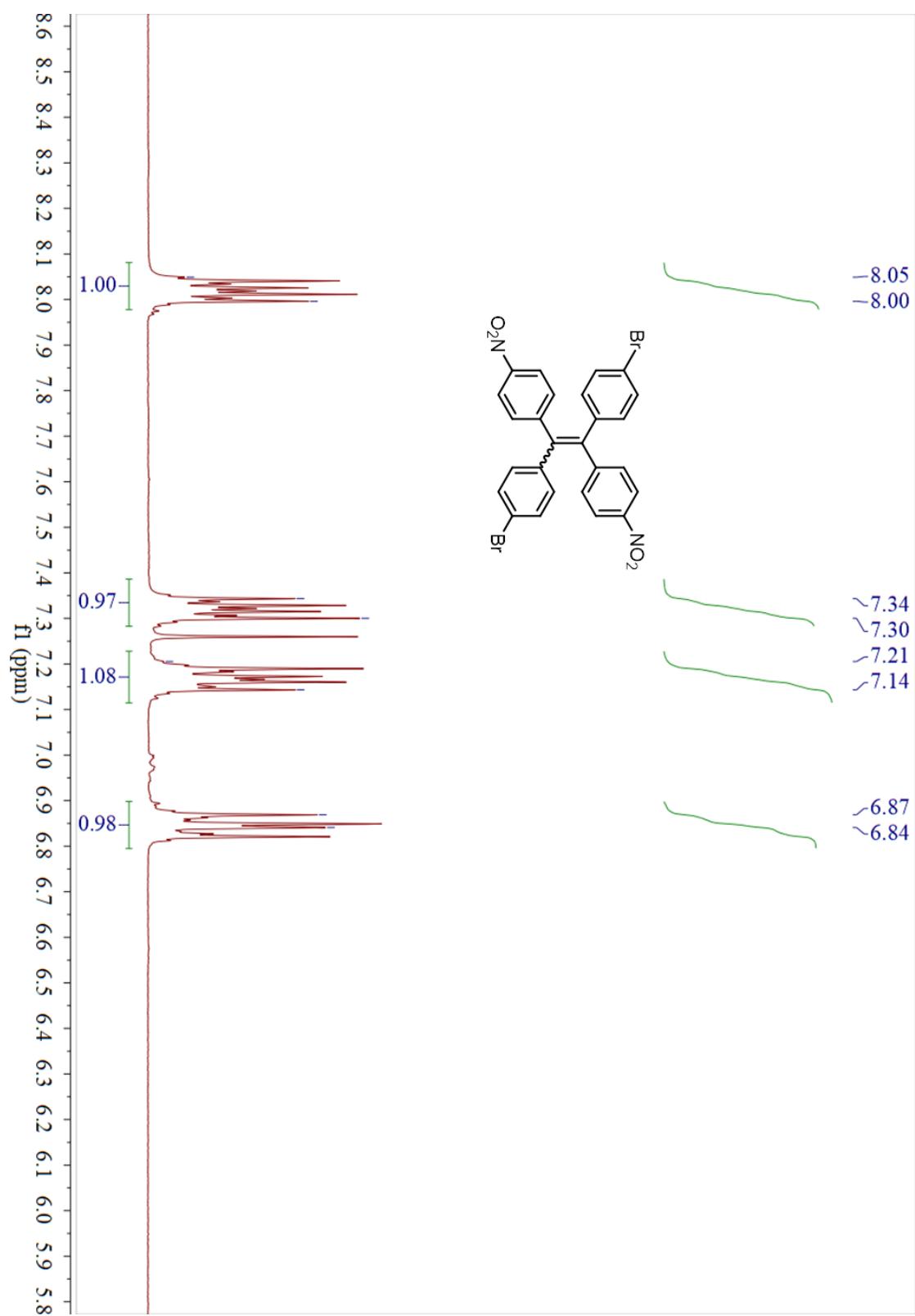


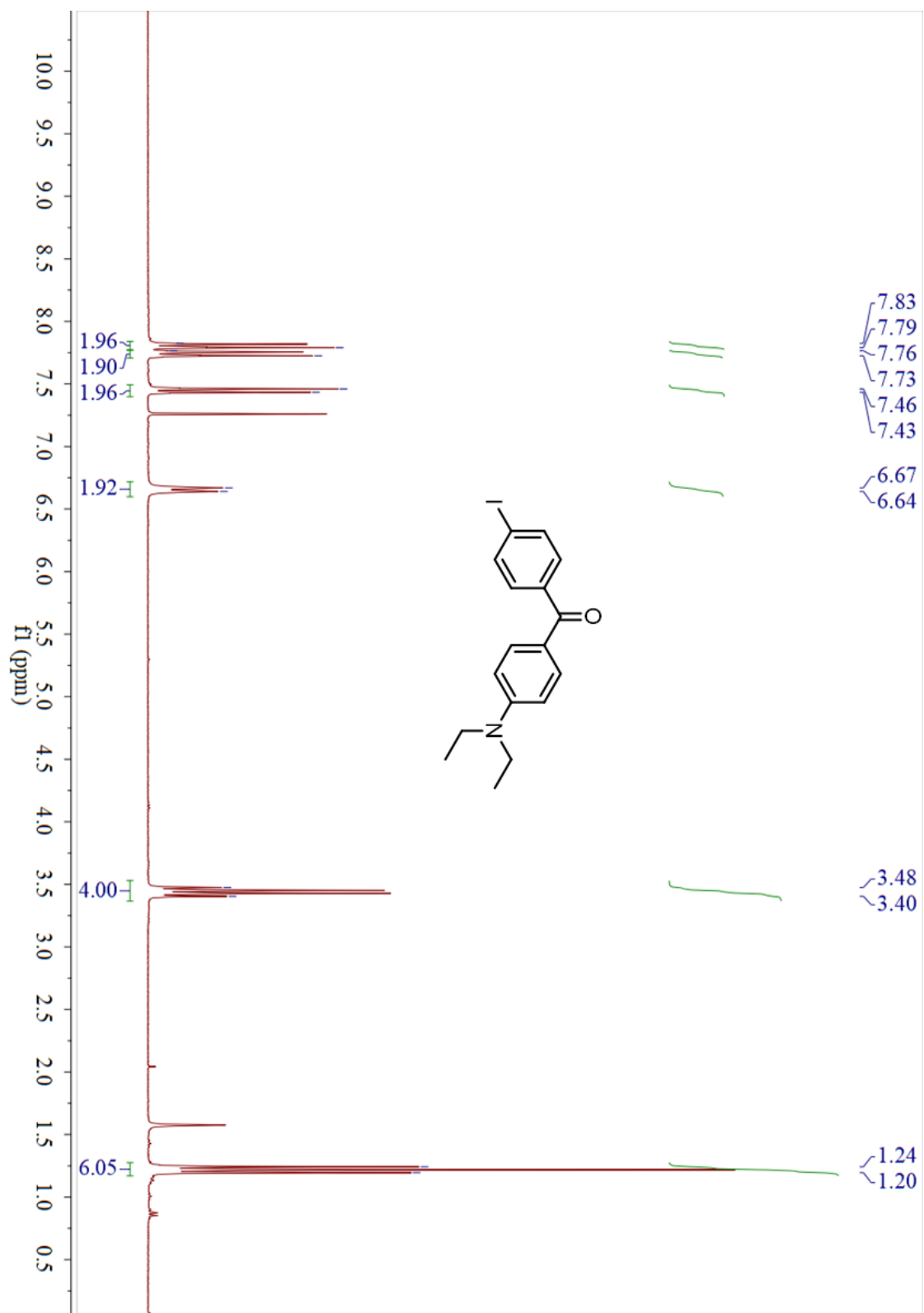


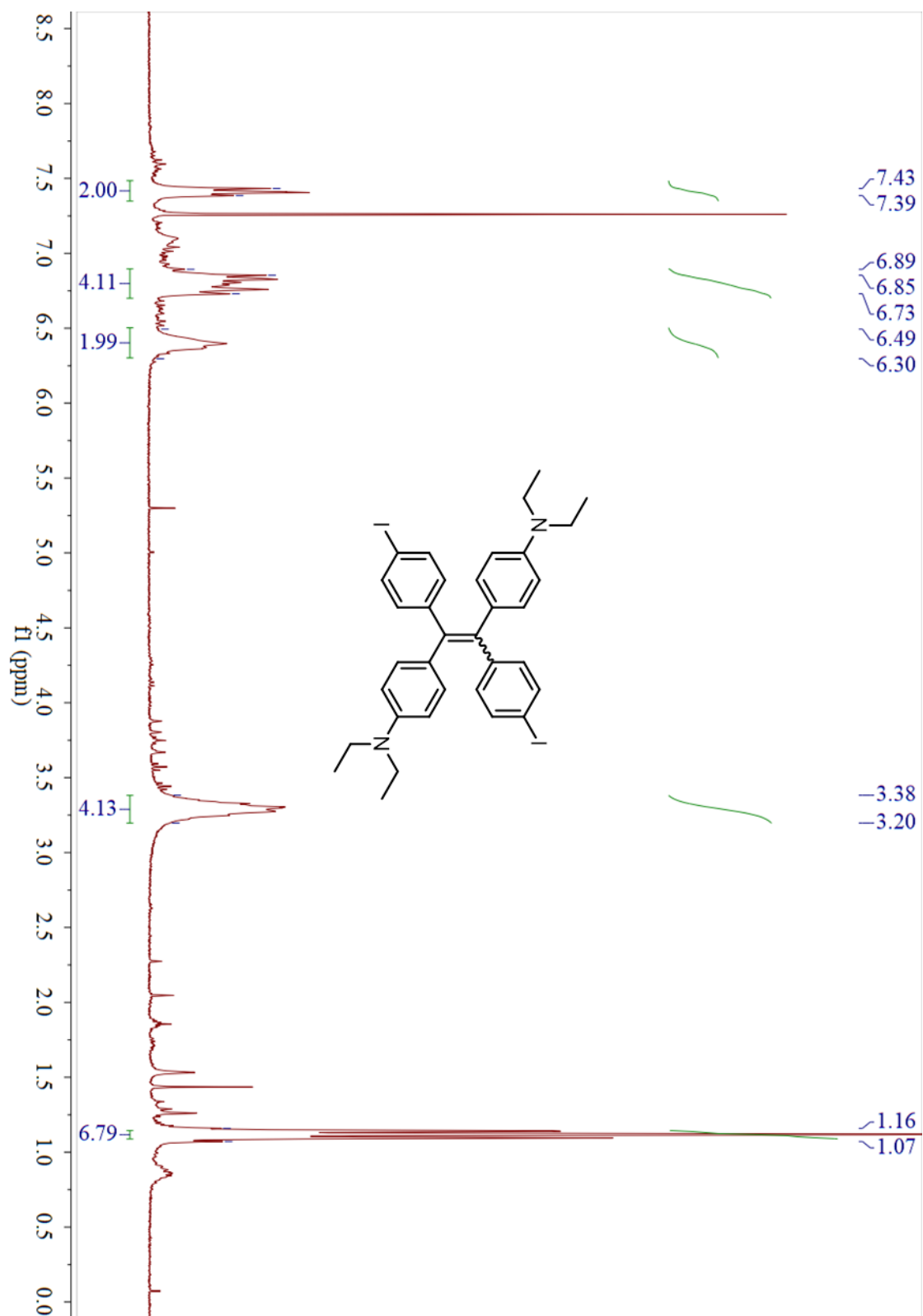


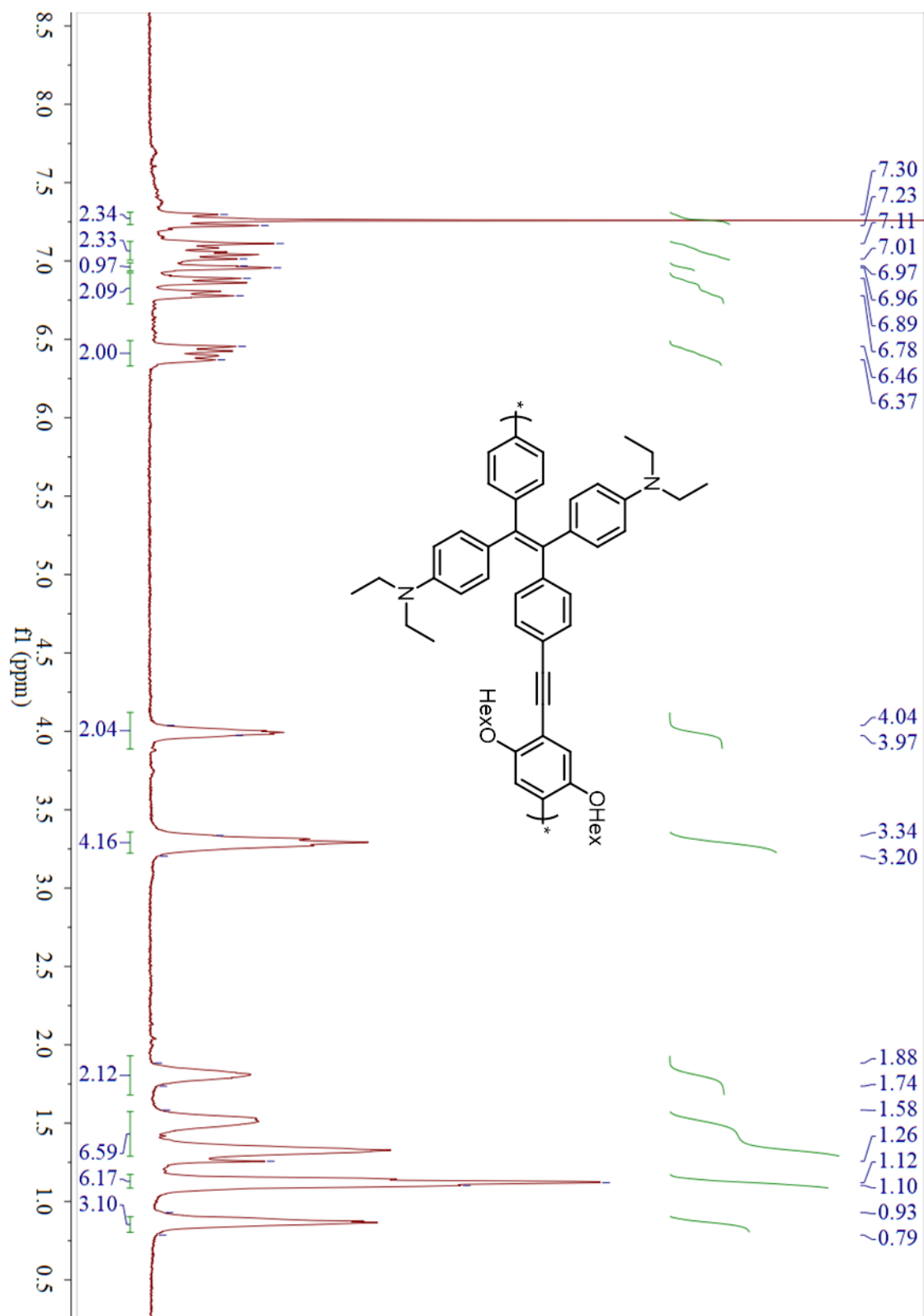


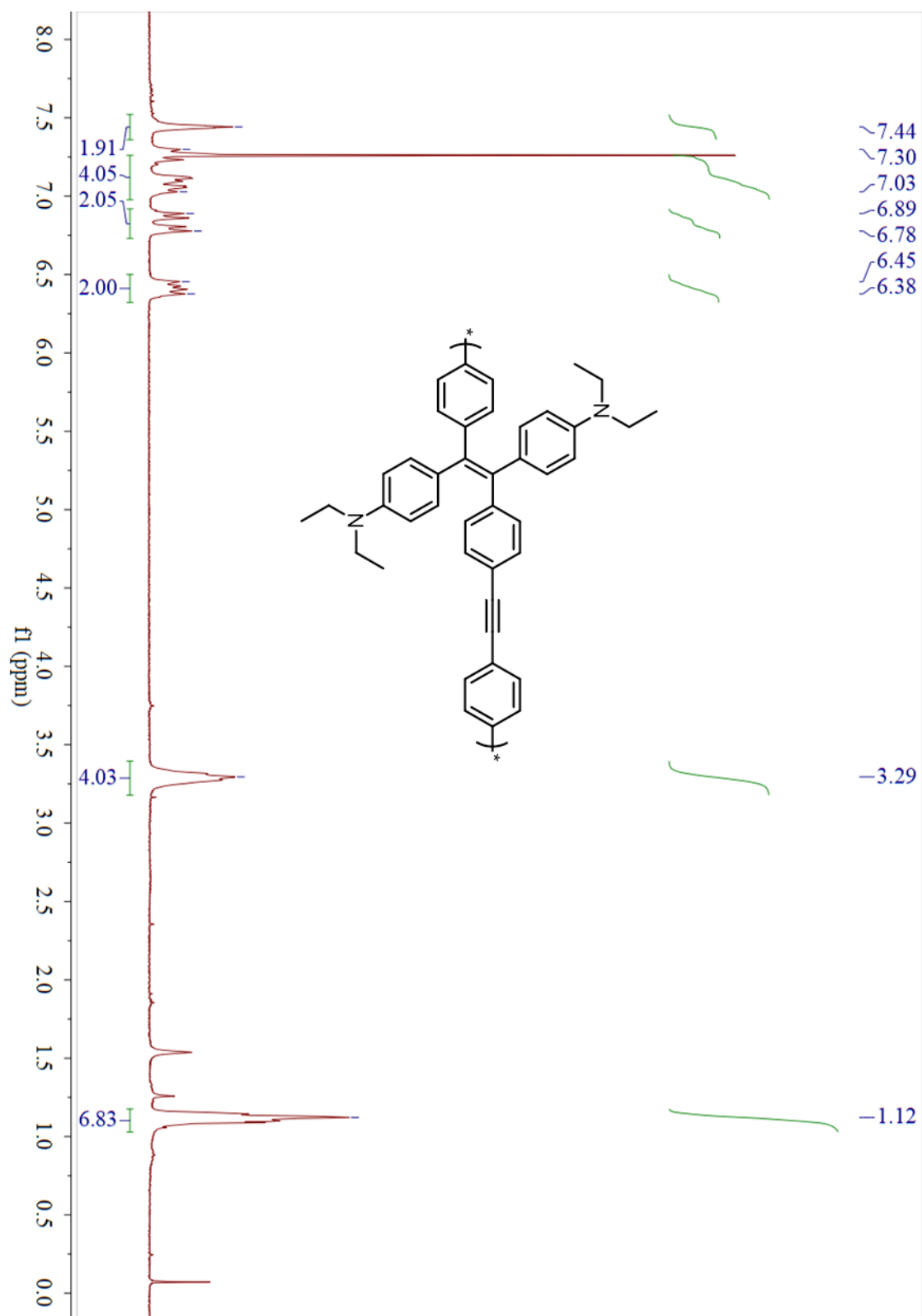


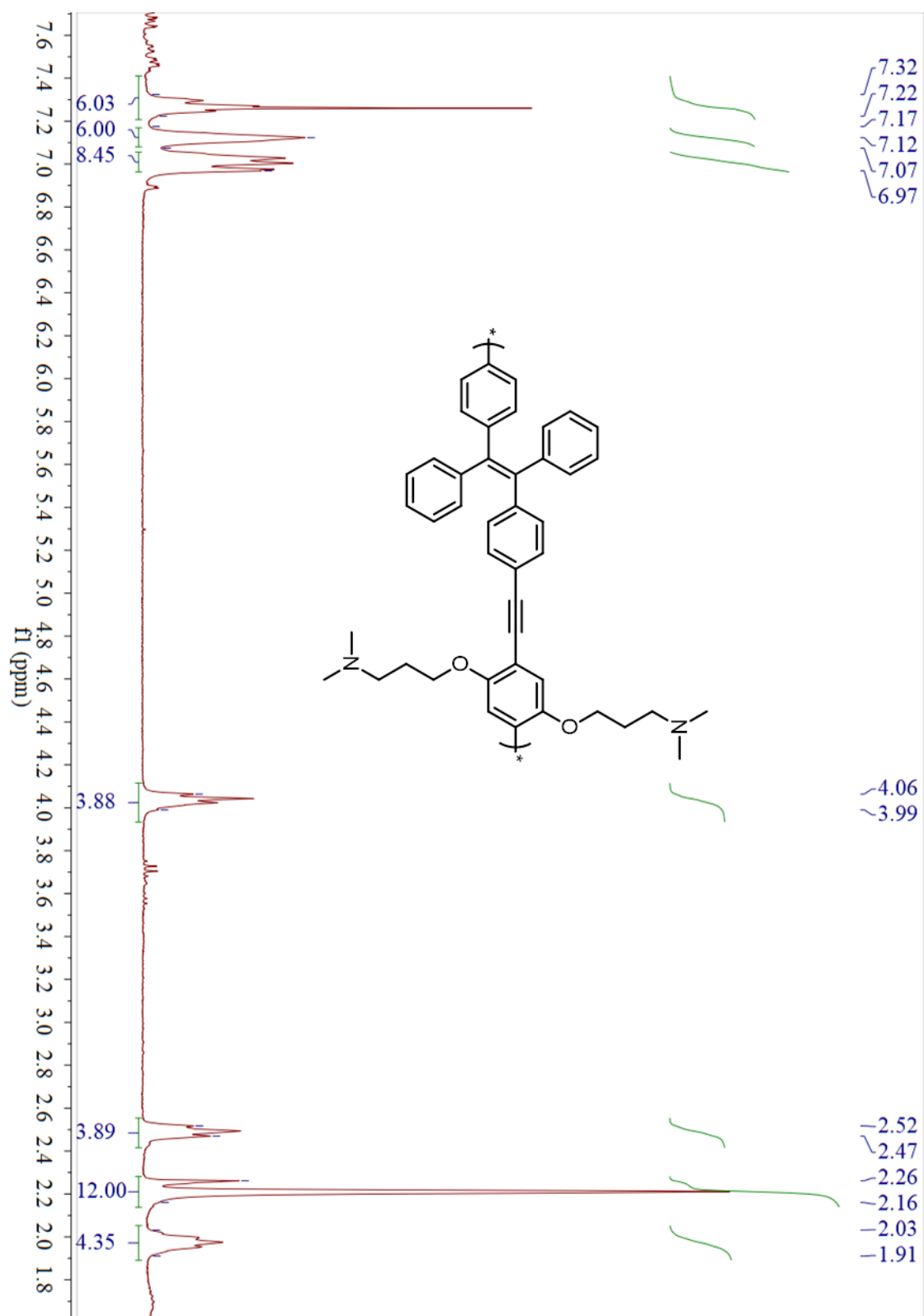
6.3.3 ^1H NMR spectra (Chapter 4)











6.4 Linear Discriminant Analysis

6.4.1 LDA Calculation (Chapter 2)

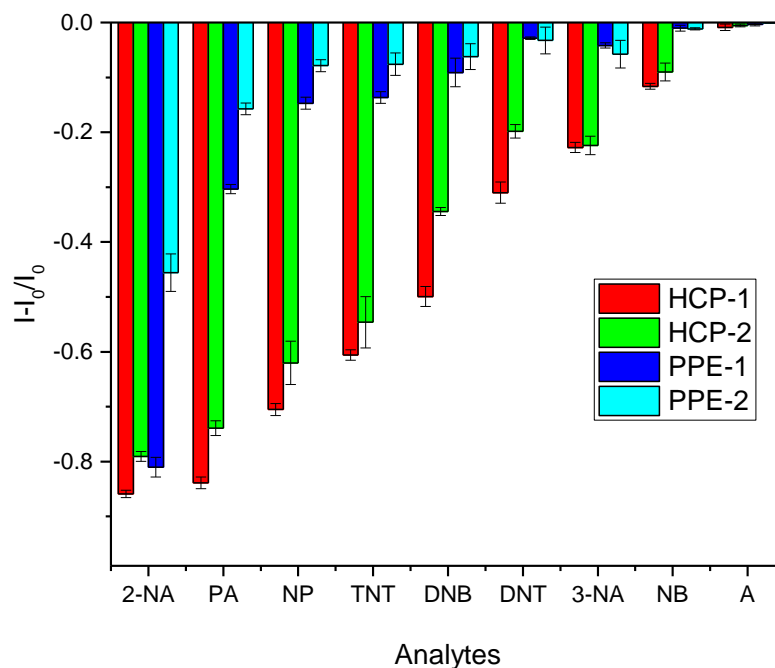


Figure 66. Fluorescence response pattern ($(I-I_0)/I_0$) obtained by **HCPs** and **PPEs** ($0.03 \mu\text{M}$) treated with analytes (0.3 mM).

Table 20. Training matrix of fluorescence response pattern from polymers ($0.03 \mu\text{M}$) against the nitroaromatic analytes (0.3 mM). LDA was carried out as described above resulting in the four factors of the canonical scores and group generation.

Analytes	Response patterns				LDA results				Group
	HCP-1	HCP-2	PPE-1	PPE-2	Factor1	Factor2	Factor3	Factor4	
2-NA	-0.86	-0.81	-0.83	-0.40	-58.84	21.16	0.14	0.55	1
2-NA	-0.85	-0.79	-0.84	-0.43	-58.12	23.11	0.93	0.00	1
2-NA	-0.86	-0.79	-0.81	-0.47	-56.63	21.22	3.31	-0.72	1
2-NA	-0.86	-0.79	-0.80	-0.48	-55.96	20.70	3.98	-0.85	1
2-NA	-0.87	-0.79	-0.83	-0.48	-58.20	22.23	3.16	-0.98	1
2-NA	-0.87	-0.78	-0.80	-0.47	-56.66	20.19	3.31	-1.22	1

3-NA	-0.22	-0.20	-0.03	-0.01	25.52	1.69	-1.27	1.04	2
3-NA	-0.22	-0.24	-0.04	-0.06	25.33	2.57	1.26	1.55	2
3-NA	-0.24	-0.22	-0.04	-0.08	24.48	2.19	1.63	0.41	2
3-NA	-0.23	-0.24	-0.04	-0.07	24.81	2.23	1.60	1.23	2
3-NA	-0.23	-0.23	-0.05	-0.06	24.23	2.90	0.77	1.11	2
3-NA	-0.23	-0.21	-0.05	-0.07	24.56	3.36	0.88	0.52	2
A	0.00	-0.01	0.00	-0.04	43.68	13.92	-0.50	0.78	3
A	0.00	-0.01	0.00	-0.01	43.26	13.44	-1.78	1.09	3
A	-0.01	0.00	0.00	-0.07	43.53	14.05	0.55	0.01	3
A	-0.01	-0.01	0.00	-0.06	43.30	13.74	0.28	0.36	3
A	-0.02	0.00	-0.01	-0.04	41.93	13.75	-1.07	0.12	3
A	-0.01	-0.01	0.00	-0.05	43.16	13.58	-0.15	0.46	3
DNB	-0.50	-0.34	-0.07	-0.05	4.34	-10.97	-0.58	-1.96	4
DNB	-0.47	-0.35	-0.08	-0.05	5.69	-8.95	-0.43	-1.02	4
DNB	-0.49	-0.34	-0.08	-0.04	4.33	-9.95	-1.18	-1.61	4
DNB	-0.52	-0.33	-0.08	-0.06	2.74	-10.97	-0.73	-2.72	4
DNB	-0.51	-0.35	-0.12	-0.08	1.37	-7.75	-0.46	-2.08	4
DNB	-0.51	-0.35	-0.13	-0.10	1.12	-6.75	0.15	-2.26	4
DNT	-0.28	-0.19	-0.03	-0.02	21.82	-0.98	-1.49	-0.64	5
DNT	-0.31	-0.22	-0.02	0.01	19.69	-4.07	-2.29	-0.28	5
DNT	-0.30	-0.20	-0.03	0.01	20.00	-2.60	-2.77	-0.53	5
DNT	-0.31	-0.20	-0.03	-0.05	20.19	-2.14	-0.29	-1.36	5
DNT	-0.32	-0.20	-0.03	-0.06	19.67	-2.48	0.06	-1.69	5
DNT	-0.34	-0.18	-0.03	-0.07	18.68	-3.01	0.00	-2.73	5
NB	-0.11	-0.08	-0.01	-0.07	35.72	8.56	0.76	-0.19	6
NB	-0.11	-0.10	-0.01	-0.05	35.26	7.94	0.23	0.51	6
NB	-0.12	-0.10	-0.02	-0.06	34.21	8.28	0.33	0.22	6

NB	-0.13	-0.09	-0.01	-0.08	34.46	7.58	1.19	-0.48	6
NB	-0.09	-0.09	-0.01	0.00	35.96	8.29	-1.91	1.22	6
NB	-0.14	-0.09	0.00	-0.04	33.77	5.76	-0.35	-0.33	6
NP	-0.72	-0.44	-0.13	-0.09	-13.60	-18.69	-0.55	-4.56	7
NP	-0.72	-0.62	-0.14	-0.08	-15.91	-20.88	1.65	0.05	7
NP	-0.71	-0.66	-0.15	-0.08	-16.15	-20.31	2.12	1.29	7
NP	-0.70	-0.67	-0.15	-0.07	-15.73	-20.12	1.94	1.87	7
NP	-0.69	-0.66	-0.15	-0.09	-14.70	-19.15	2.71	1.63	7
NP	-0.69	-0.66	-0.16	-0.07	-15.51	-18.80	1.61	1.87	7
PA	-0.84	-0.76	-0.54	-0.17	-44.95	-0.41	-3.15	1.19	8
PA	-0.84	-0.73	-0.56	-0.16	-45.88	1.24	-4.55	0.61	8
PA	-0.84	-0.74	-0.55	-0.16	-45.44	0.41	-4.14	0.83	8
PA	-0.86	-0.74	-0.55	-0.14	-47.03	-0.90	-5.16	0.59	8
PA	-0.83	-0.73	-0.56	-0.15	-45.36	1.57	-4.89	0.94	8
PA	-0.83	-0.73	-0.56	-0.16	-45.22	1.73	-4.47	0.83	8
TNT	-0.59	-0.57	-0.14	-0.08	-6.94	-13.67	1.91	1.68	9
TNT	-0.62	-0.55	-0.13	-0.08	-8.19	-15.54	1.59	0.49	9
TNT	-0.62	-0.54	-0.14	-0.08	-8.63	-14.71	1.18	0.27	9
TNT	-0.60	-0.56	-0.13	-0.07	-7.11	-14.86	1.48	1.28	9
TNT	-0.61	-0.55	-0.14	-0.09	-7.93	-14.21	1.85	0.64	9
TNT	-0.61	-0.56	-0.14	-0.08	-8.16	-14.52	1.58	0.99	9

Table 21. Detection and identification of nine unknown samples using LDA training matrix from our polymer sensor array. All unknown samples could be assigned to the corresponding clusters defined by the training matrix according to their shortest mahalanobis distance. The jackknifed classification matrix with cross-validation reveals a 100% accuracy.

Unknown	Response patterns				LDA results				Analyte	
	HCP-1	HCP-2	PPE-1	PPE-2	Factor1	Factor2	Factor3	Factor4	Group	Verification
1	-0.49	-0.35	-0.07	-0.05	4.9069	-10.62	-0.344	-1.491	4	DNB
1	-0.48	-0.35	-0.09	-0.06	4.6439	-8.61	-0.331	-1.309	4	DNB
1	-0.51	-0.36	-0.07	-0.04	3.3656	-11.92	-0.774	-1.583	4	DNB
1	-0.51	-0.33	-0.12	-0.09	1.6936	-7.289	-0.354	-2.684	4	DNB
2	-0.27	-0.18	-0.02	-0.02	23.098	-1.007	-1.319	-0.7	5	DNT
2	-0.31	-0.22	-0.03	-0.02	19.583	-2.917	-1.253	-0.559	5	DNT
2	-0.29	-0.20	-0.02	-0.03	21.745	-2.142	-0.735	-0.747	5	DNT
2	-0.33	-0.22	-0.04	-0.06	18.303	-2.596	0.047	-1.378	5	DNT
3	-0.70	-0.65	-0.14	-0.10	-14.6	-20.02	3.146	1.032	7	NP
3	-0.71	-0.64	-0.15	-0.08	-15.97	-20.01	1.803	0.797	7	NP
3	-0.70	-0.69	-0.16	-0.07	-16.44	-19.74	2.007	2.394	7	NP
3	-0.71	-0.68	-0.14	-0.11	-15.38	-20.81	3.971	1.455	7	NP
4	-0.21	-0.22	-0.05	-0.02	25.077	3.4033	-0.938	1.716	2	3-NA
4	-0.23	-0.24	-0.05	-0.04	23.863	2.4283	0.073	1.567	2	3-NA
4	-0.24	-0.20	-0.04	-0.08	24.661	2.4928	1.311	-0.088	2	3-NA
4	-0.23	-0.25	-0.04	-0.03	24.161	1.4412	0.053	1.887	2	3-NA
5	0.00	0.00	0.00	-0.04	43.768	14.069	-0.656	0.532	3	A
5	0.00	-0.01	0.00	-0.04	43.677	13.918	-0.496	0.781	3	A
5	-0.01	-0.01	0.00	-0.05	43.162	13.581	-0.15	0.458	3	A
5	-0.01	0.00	0.00	-0.01	42.694	13.094	-2.019	0.616	3	A
6	-0.82	-0.74	-0.55	-0.18	-43.85	1.7198	-3.123	1.069	8	PA
6	-0.85	-0.71	-0.54	-0.19	-44.87	0.1629	-3.17	-0.474	8	PA

6	-0.83	-0.76	-0.56	-0.14	-45.77	0.9628	-4.842	1.784	8	PA
6	-0.84	-0.73	-0.57	-0.16	-46.4	1.9132	-4.794	0.643	8	PA
7	-0.59	-0.57	-0.14	-0.08	-6.938	-13.67	1.905	1.68	9	TNT
7	-0.62	-0.55	-0.13	-0.08	-8.191	-15.54	1.591	0.488	9	TNT
7	-0.62	-0.54	-0.14	-0.08	-8.629	-14.71	1.184	0.27	9	TNT
7	-0.60	-0.56	-0.13	-0.07	-7.112	-14.86	1.485	1.281	9	TNT
8	-0.86	-0.80	-0.80	-0.41	-57.03	19.433	1.149	0.107	1	2-NA
8	-0.89	-0.80	-0.83	-0.48	-59.6	21.091	3.155	-1.177	1	2-NA
8	-0.85	-0.78	-0.82	-0.47	-56.41	22.541	2.979	-0.719	1	2-NA
8	-0.86	-0.77	-0.83	-0.45	-57.78	22.553	1.637	-0.954	1	2-NA
9	-0.08	-0.13	-0.02	-0.06	36.561	9.8162	1.13	1.854	6	NB
9	-0.09	-0.10	-0.01	-0.03	36.29	8.615	-0.464	1.161	6	NB
9	-0.09	-0.12	-0.01	-0.05	36.387	8.6331	0.71	1.454	6	NB
9	-0.10	-0.09	0.00	-0.05	36.535	7.9099	0.398	0.456	6	NB

Canonical Scores Plot

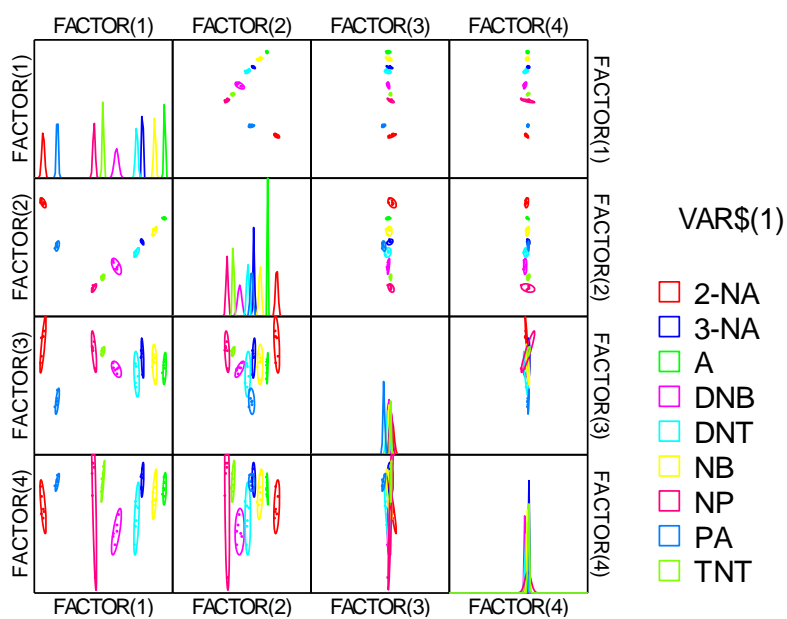


Figure 67. Correlations of canonical fluorescence response patterns from sensor array the HCPs and PPEs against nine aromatic analytes.

6.4.2 LDA Calculation (Chapter 3)

Table 22. Training matrix of fluorescence response pattern from polymers (1 μM) against fourteen nitroaromatic analytes at a concentration of 0.1 mM. LDA was carried out as described above resulting in the four factors of the canonical scores and group generation.

Analytes	Response patterns				LDA results			
	TPEP-1	TPEP-2	TPEP-3	TPEP-4	Score1	Score2	Score3	Score4
NB	-0.15	-0.03	-0.11	-0.04	70.30	-4.28	3.05	-2.03
NB	-0.13	-0.05	-0.13	-0.03	69.62	-2.44	4.76	-0.99
NB	-0.13	-0.03	-0.12	-0.03	70.97	-3.01	4.58	-2.02
NB	-0.16	-0.03	-0.13	-0.03	69.31	-2.51	2.74	-2.25
NB	-0.14	-0.05	-0.12	-0.03	69.32	-3.12	3.85	-0.37
NB	-0.16	-0.05	-0.13	-0.03	68.93	-2.95	3.12	-0.73
2,4-DNT	-0.60	-0.42	-0.72	-0.35	-12.27	13.42	2.32	-3.93
2,4-DNT	-0.54	-0.47	-0.73	-0.35	-13.22	13.67	6.29	-0.39
2,4-DNT	-0.60	-0.43	-0.73	-0.35	-12.80	13.99	2.41	-3.59
2,4-DNT	-0.60	-0.46	-0.73	-0.34	-13.48	14.44	2.10	-0.76
2,4-DNT	-0.60	-0.48	-0.72	-0.35	-14.76	13.32	2.62	1.12
2,4-DNT	-0.60	-0.43	-0.71	-0.35	-11.52	12.96	1.95	-2.77
2,6-DNT	-0.60	-0.39	-0.62	-0.25	0.48	13.52	-2.99	0.50
2,6-DNT	-0.58	-0.40	-0.61	-0.25	1.77	12.44	-2.12	1.70
2,6-DNT	-0.58	-0.39	-0.63	-0.27	-0.37	12.56	-1.22	-0.17
2,6-DNT	-0.61	-0.37	-0.63	-0.27	-0.57	12.95	-2.85	-1.58
2,6-DNT	-0.60	-0.41	-0.62	-0.27	-0.97	12.38	-2.24	1.21
2,6-DNT	-0.59	-0.39	-0.63	-0.27	-0.96	13.19	-1.84	0.11
oNA	-0.75	-0.36	-0.40	-0.38	2.78	-9.05	-14.72	2.00
oNA	-0.75	-0.35	-0.38	-0.37	4.90	-9.90	-15.12	1.61
oNA	-0.74	-0.37	-0.39	-0.38	3.06	-9.95	-13.76	2.53

oNA	-0.74	-0.37	-0.42	-0.37	2.24	-7.03	-13.35	1.69
oNA	-0.75	-0.37	-0.42	-0.37	1.59	-7.81	-13.71	2.17
oNA	-0.74	-0.36	-0.41	-0.36	3.50	-7.13	-13.91	2.13
mNA	-0.43	-0.20	-0.22	-0.23	38.13	-10.77	-4.64	0.63
mNA	-0.44	-0.19	-0.24	-0.22	37.81	-8.31	-4.99	-0.27
mNA	-0.42	-0.20	-0.23	-0.24	36.95	-9.99	-3.87	0.47
mNA	-0.40	-0.18	-0.23	-0.22	39.95	-9.19	-3.24	-0.26
mNA	-0.45	-0.19	-0.26	-0.24	35.37	-8.80	-4.64	-1.74
mNA	-0.41	-0.21	-0.24	-0.24	35.89	-9.71	-2.59	0.55
oDNB	-0.89	-0.59	-0.80	-0.72	-52.90	-5.97	-2.73	-5.57
oDNB	-0.90	-0.58	-0.80	-0.72	-53.08	-6.39	-3.27	-5.94
oDNB	-0.89	-0.58	-0.80	-0.72	-52.47	-5.81	-2.66	-6.04
oDNB	-0.90	-0.58	-0.80	-0.71	-52.01	-5.18	-3.34	-6.20
oDNB	-0.90	-0.61	-0.81	-0.72	-54.45	-5.74	-2.72	-4.00
oDNB	-0.89	-0.59	-0.80	-0.72	-52.90	-6.01	-3.04	-5.13
mDNB	-0.39	-0.27	-0.47	-0.21	22.87	6.91	3.86	-1.77
mDNB	-0.41	-0.25	-0.46	-0.22	23.00	5.80	2.48	-3.35
mDNB	-0.37	-0.27	-0.48	-0.23	22.29	6.49	5.40	-2.31
mDNB	-0.39	-0.26	-0.48	-0.22	22.44	7.48	4.36	-3.03
mDNB	-0.42	-0.26	-0.48	-0.21	22.45	7.45	1.89	-2.93
mDNB	-0.43	-0.28	-0.48	-0.19	22.21	8.45	1.08	-0.89
oCNB	-0.39	-0.22	-0.38	-0.12	35.17	7.00	-1.17	0.61
oCNB	-0.42	-0.20	-0.37	-0.13	35.36	5.69	-3.18	-1.31
oCNB	-0.40	-0.22	-0.37	-0.12	35.33	6.32	-1.94	0.53
oCNB	-0.39	-0.21	-0.35	-0.13	36.45	4.03	-1.68	0.62
oCNB	-0.42	-0.22	-0.36	-0.12	35.82	5.56	-3.04	0.73
oCNB	-0.48	-0.22	-0.37	-0.13	32.87	5.46	-6.18	0.17

mCNB	-0.50	-0.37	-0.59	-0.16	11.15	17.23	-0.70	3.64
mCNB	-0.49	-0.38	-0.60	-0.16	10.35	18.26	0.31	3.27
mCNB	-0.50	-0.38	-0.60	-0.16	9.89	17.67	-0.04	3.39
mCNB	-0.52	-0.39	-0.59	-0.18	8.80	15.51	-0.68	3.89
mCNB	-0.52	-0.38	-0.61	-0.17	8.72	17.58	-0.83	3.33
mCNB	-0.50	-0.38	-0.62	-0.16	9.35	19.17	0.25	2.70
oNP	-0.40	-0.34	-0.43	-0.30	17.18	-1.67	4.90	2.43
oNP	-0.42	-0.35	-0.43	-0.31	15.40	-2.80	3.99	2.44
oNP	-0.39	-0.35	-0.44	-0.31	15.94	-1.67	5.84	2.54
oNP	-0.41	-0.35	-0.44	-0.29	15.84	-0.65	4.13	3.18
oNP	-0.42	-0.35	-0.43	-0.33	14.61	-3.67	4.59	1.84
oNP	-0.41	-0.35	-0.44	-0.31	15.42	-1.88	4.83	2.03
pNP	-0.32	-0.20	-0.21	-0.35	35.78	-18.07	4.51	-2.51
pNP	-0.32	-0.20	-0.25	-0.34	33.81	-15.04	5.35	-3.60
pNP	-0.32	-0.23	-0.21	-0.32	35.75	-17.07	3.48	0.86
pNP	-0.30	-0.22	-0.21	-0.33	36.19	-16.82	4.90	-0.50
pNP	-0.30	-0.20	-0.21	-0.35	35.90	-18.49	5.58	-1.94
pNP	-0.33	-0.22	-0.20	-0.34	35.78	-18.56	2.94	-0.20
CDNB	-0.78	-0.63	-0.84	-0.57	-45.88	6.23	1.25	1.25
CDNB	-0.78	-0.62	-0.83	-0.60	-46.53	3.35	1.54	0.11
CDNB	-0.79	-0.64	-0.84	-0.59	-47.67	4.68	1.48	0.62
CDNB	-0.78	-0.63	-0.84	-0.60	-46.94	4.14	1.99	0.39
CDNB	-0.80	-0.64	-0.82	-0.58	-45.94	4.28	0.07	2.07
CDNB	-0.80	-0.63	-0.85	-0.56	-46.18	6.71	0.34	1.07
TNT	-0.74	-0.70	-0.71	-0.76	-50.94	-15.00	5.70	4.48
TNT	-0.74	-0.70	-0.71	-0.76	-50.78	-15.08	5.41	4.81
TNT	-0.75	-0.70	-0.73	-0.78	-53.29	-15.31	6.03	3.79

TNT	-0.75	-0.69	-0.72	-0.79	-52.39	-15.82	5.93	2.78
TNT	-0.74	-0.71	-0.72	-0.79	-53.38	-15.95	6.81	4.18
TNT	-0.74	-0.72	-0.71	-0.79	-52.93	-16.80	6.50	5.33
PA	-0.90	-0.70	-0.91	-0.69	-62.78	2.57	-0.34	-0.12
PA	-0.89	-0.70	-0.91	-0.72	-63.67	0.40	0.53	-0.84
PA	-0.90	-0.70	-0.90	-0.72	-64.22	-0.02	0.05	-0.99
PA	-0.90	-0.69	-0.91	-0.72	-63.43	0.65	0.17	-1.38
PA	-0.90	-0.70	-0.90	-0.73	-64.98	-1.01	0.36	-0.77
PA	-0.89	-0.68	-0.90	-0.74	-64.31	-1.47	0.72	-2.34

Canonical Scores Plot

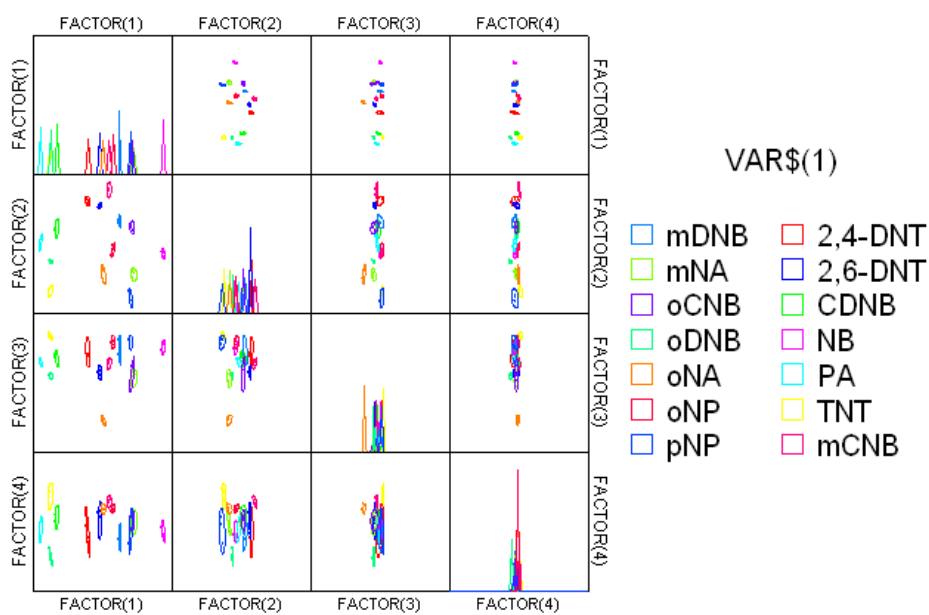


Figure 68. Correlations of canonical fluorescence response patterns from **TPEPs** sensor array against nine aromatic analytes.

6.4.3 LDA Calculation (Chapter 4)

Table 23. Training matrix of fluorescence response patterns from **F-TPEPs** (1 μM) against twelve nitroaromatic analytes at a concentration of 0.1 mM. LDA was carried out as described above resulting in the four factors of the canonical scores and group generation.

Analytes	Response patterns				LDA results			
	P1	P2	P3	P4	Score1	Score2	Score3	Score4
PA	-0.80	-0.73	-0.93	-0.15	-39.16	-11.08	-12.45	2.43
PA	-0.82	-0.74	-0.94	-0.16	-40.54	-11.47	-12.28	1.45
PA	-0.81	-0.74	-0.94	-0.15	-40.44	-11.14	-12.43	1.64
PA	-0.82	-0.73	-0.94	-0.13	-40.24	-11.96	-14.41	1.18
PA	-0.84	-0.73	-0.94	-0.17	-41.30	-12.65	-12.69	-0.41
PA	-0.83	-0.75	-0.93	-0.15	-41.98	-10.75	-12.97	1.16
NB	-0.19	-0.23	-0.11	-0.05	36.28	1.46	0.51	2.07
NB	-0.19	-0.20	-0.12	-0.05	37.55	-0.44	-0.52	1.37
NB	-0.18	-0.22	-0.14	-0.05	36.95	0.30	0.49	3.10
NB	-0.20	-0.24	-0.14	-0.03	34.96	1.10	-1.39	3.16
NB	-0.19	-0.21	-0.14	-0.07	36.74	-0.83	0.90	1.75
NB	-0.20	-0.23	-0.12	-0.08	36.13	0.81	2.43	1.70
TNT	-0.70	-0.63	-0.86	-0.44	-26.17	-14.67	10.85	-0.32
TNT	-0.71	-0.62	-0.89	-0.44	-26.79	-16.78	10.16	-1.18
TNT	-0.69	-0.63	-0.88	-0.43	-26.36	-15.47	10.60	0.48
TNT	-0.73	-0.63	-0.88	-0.44	-28.09	-16.00	9.62	-1.41
TNT	-0.69	-0.65	-0.89	-0.44	-26.86	-15.03	11.75	1.13
TNT	-0.72	-0.64	-0.89	-0.43	-28.04	-16.02	9.33	-0.83
mNA	-0.31	-0.17	-0.29	-0.06	29.61	-10.64	-6.82	-3.08
mNA	-0.32	-0.19	-0.33	-0.08	27.32	-11.23	-5.54	-2.31
mNA	-0.34	-0.17	-0.32	-0.08	27.71	-12.36	-6.57	-4.14

mNA	-0.34	-0.20	-0.37	-0.10	25.50	-13.02	-5.28	-2.68
mNA	-0.35	-0.17	-0.34	-0.10	27.11	-13.80	-5.76	-4.48
mNA	-0.35	-0.20	-0.34	-0.12	25.60	-11.92	-3.34	-3.64
oNA	-0.43	-0.48	-0.45	-0.22	3.78	-2.31	5.52	2.78
oNA	-0.44	-0.48	-0.44	-0.22	3.67	-1.65	5.79	2.47
oNA	-0.43	-0.48	-0.51	-0.22	2.74	-4.25	5.98	4.26
oNA	-0.43	-0.48	-0.50	-0.21	2.95	-3.66	5.01	4.16
oNA	-0.43	-0.49	-0.51	-0.22	2.32	-3.86	5.67	4.47
oNA	-0.43	-0.48	-0.49	-0.23	3.01	-3.62	6.35	3.47
mCNB	-0.47	-0.61	-0.30	-0.08	-3.83	11.18	-2.62	3.87
mCNB	-0.49	-0.63	-0.27	-0.06	-5.35	13.89	-3.49	3.68
mCNB	-0.45	-0.63	-0.29	-0.07	-3.81	13.70	-1.53	6.01
mCNB	-0.47	-0.64	-0.29	-0.06	-5.05	13.61	-2.87	5.49
mCNB	-0.46	-0.63	-0.35	-0.06	-4.69	11.01	-2.80	6.59
mCNB	-0.47	-0.63	-0.35	-0.06	-5.63	10.99	-2.90	6.38
oCNB	-0.46	-0.50	-0.22	-0.09	4.25	8.04	-3.43	-0.92
oCNB	-0.46	-0.50	-0.24	-0.10	4.03	7.19	-2.41	-0.75
oCNB	-0.46	-0.49	-0.25	-0.10	4.28	6.43	-2.74	-0.59
oCNB	-0.46	-0.50	-0.24	-0.13	3.93	7.24	-0.39	-0.49
oCNB	-0.47	-0.50	-0.25	-0.08	3.25	7.32	-4.52	-0.44
oCNB	-0.46	-0.51	-0.24	-0.07	3.19	8.45	-4.05	0.16
DNB	-0.86	-0.92	-0.77	-0.32	-50.59	3.39	2.27	0.76
DNB	-0.87	-0.94	-0.75	-0.34	-51.39	5.20	4.02	0.70
DNB	-0.86	-0.94	-0.78	-0.34	-51.49	3.96	4.04	1.02
DNB	-0.86	-0.95	-0.79	-0.32	-52.20	3.95	2.87	1.76
DNB	-0.88	-0.95	-0.77	-0.33	-53.08	4.63	2.68	0.87
DNB	-0.88	-0.95	-0.78	-0.36	-52.75	3.83	4.49	0.46

DNT	-0.47	-0.53	-0.06	-0.10	4.62	15.99	-1.26	-3.38
DNT	-0.48	-0.55	-0.04	-0.12	2.61	17.47	-0.32	-4.03
DNT	-0.47	-0.52	-0.09	-0.13	4.63	13.81	-0.06	-3.67
DNT	-0.48	-0.56	-0.08	-0.14	1.85	15.93	0.91	-3.30
DNT	-0.47	-0.56	-0.08	-0.13	2.41	16.31	0.67	-2.52
DNT	-0.47	-0.56	-0.15	-0.13	1.14	14.14	1.05	-1.07
2NP	-0.31	-0.26	-0.12	-0.12	27.44	0.45	0.73	-3.46
2NP	-0.27	-0.29	-0.15	-0.09	28.20	1.86	0.66	0.51
2NP	-0.27	-0.30	-0.14	-0.08	27.55	2.94	0.45	0.62
2NP	-0.28	-0.27	-0.18	-0.06	27.81	0.25	-1.84	0.35
2NP	-0.29	-0.27	-0.16	-0.11	27.87	-0.27	0.58	-1.20
2NP	-0.27	-0.27	-0.19	-0.11	28.88	-0.89	1.83	0.45
4NP	-0.18	-0.12	-0.12	-0.08	43.03	-5.04	0.76	-0.91
4NP	-0.15	-0.10	-0.09	-0.10	46.11	-5.19	2.68	-1.32
4NP	-0.15	-0.11	-0.11	-0.10	45.66	-4.88	2.97	-0.35
4NP	-0.13	-0.10	-0.11	-0.08	47.01	-4.74	2.91	0.89
4NP	-0.13	-0.12	-0.16	-0.05	45.52	-5.53	0.60	2.59
4NP	-0.15	-0.11	-0.12	-0.07	45.13	-5.04	0.68	0.24
CDNB	-0.70	-0.67	-0.39	-0.27	-21.07	6.24	1.80	-6.33
CDNB	-0.70	-0.68	-0.38	-0.27	-21.69	7.26	1.85	-5.84
CDNB	-0.70	-0.69	-0.40	-0.26	-22.45	6.77	1.36	-5.60
CDNB	-0.69	-0.68	-0.40	-0.26	-21.97	6.68	1.84	-5.26
CDNB	-0.70	-0.69	-0.43	-0.26	-23.22	6.08	1.60	-4.96
CDNB	-0.72	-0.70	-0.37	-0.28	-24.02	8.33	2.44	-6.77

Canonical Scores Plot

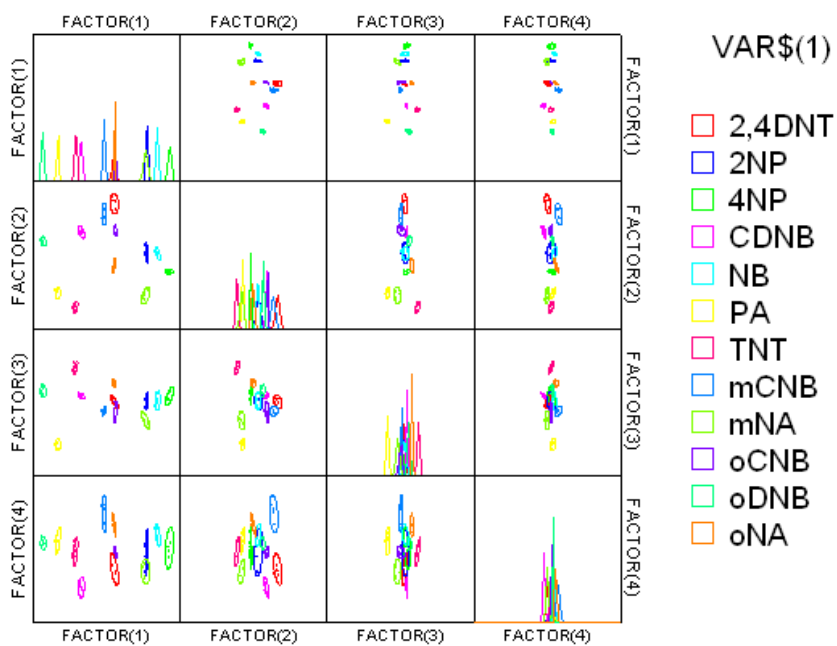


Figure 69. Correlations of canonical fluorescence response patterns from sensor array **F-TPEPs** against twelve aromatic analytes.

References

1. Thomas, S. W.; Joly, G. D.; Swager, T. M., *Chem. Rev.* **2007**, *107*, 1339-1386.
2. Wang, Y.; Zhu, Y.; Xie, G.; Zhan, H.; Yang, C.; Cheng, Y., *J. Mater. Chem. C* **2017**, *5*, 10715-10720.
3. Stolz, S.; Petzoldt, M.; Kotadiya, N.; Rödlmeier, T.; Eckstein, R.; Freudenberg, J.; Bunz, U. H. F.; Lemmer, U.; Mankel, E.; Hamburger, M.; Hernandez-Sosa, G., *J. Mater. Chem. C* **2016**, *4*, 11150-11156.
4. Bender, M.; Schelkle, K. M.; Jürgensen, N.; Schmid, S.; Hernandez-Sosa, G.; Bunz, U. H. F., *Macromolecules* **2016**, *49*, 2957-2961.
5. Nikolka, M.; Nasrallah, I.; Rose, B.; Ravva, M. K.; Broch, K.; Sadhanala, A.; Harkin, D.; Charmet, J.; Hurhangee, M.; Brown, A.; Illig S.; Too, P.; Jongman, J.; McCulloch, I.; Bredas, J. -L.; Siringhaus, H., *Nat. Mater.* **2017**, *16*, 356.
6. Günes, S.; Neugebauer, H.; Sariciftci, N. S., *Chem. Rev.* **2007**, *107*, 1324-1338.
7. Erb, T.; Zhokhavets, U.; Gobsch, G.; Raleva, S.; St ühn, B.; Schilinsky, P.; Waldauf, C.; Brabec, C. J., *Adv. Funct. Mater.* **2005**, *15*, 1193-1196.
8. Han, J.; Cheng, H.; Wang, B.; Braun, M. S.; Fan, X.; Bender, M.; Huang, W.; Domhan, C.; Mier, W.; Lindner, T.; Seehafer, K.; Wink, M.; Bunz, U. H. F., *Angew. Chem. Int. Ed* **2017**, *129*, 15448-15453.
9. Han, J.; Wang, B.; Bender, M.; Seehafer, K.; Bunz, U. H. F., *ACS Appl. Mater. Interfaces* **2016**, *8*, 20415-20421.
10. Bunz, U. H. F.; Rotello, V. M., *Angew. Chem. Int. Ed* **2010**, *49*, 3268-3279.
11. Waltman, R.; Bargon, J., *Can. J. Chem.* **1986**, *64*, 76-95.
12. Sadki, S.; Schottland, P.; Brodie, N.; Sabouraud, G., *Chem. Soc. Rev.* **2000**, *29*, 283-293.
13. Toshima, N.; Hara, S., *Prog. Polym. Sci.* **1995**, *20*, 155-183.
14. Kovacic, P.; Kyriakis, A., *J. Am. Chem. Soc.* **1963**, *85*, 454-458.
15. Cheng, Y.-J.; Luh, T.-Y., *J. Organomet. Chem.* **2004**, *689*, 4137-4148.
16. Cheng, Y.-J.; Yang, S.-H.; Hsu, C.-S., *Chem. Rev.* **2009**, *109*, 5868-5923.
17. Stille, J. K., *Angew. Chem. Int. Ed* **1986**, *25*, 508-524.
18. Sonogashira, K., *J. Organomet. Chem.* **2002**, *653*, 46-49.
19. Tamao, K.; Sumitani, K.; Kumada, M., *J. Am. Chem. Soc.* **1972**, *94*, 4374-4376.
20. Yamamoto, T.; Maruyama, T.; Zhou, Z.-H.; Ito, T.; Fukuda, T.; Yoneda, Y.; Begum, F.; Ikeda, T.; Sasaki, S.; Takezoe, H.; Fukuda, A.; Kubota K., *J. Am. Chem. Soc.* **1994**, *116*, 4832-4845.
21. Feng, X.; Liu, L.; Wang, S.; Zhu, D., *Chem. Soc. Rev.* **2010**, *39*, 2411-2419.
22. Yoshii, R.; Hirose, A.; Tanaka, K.; Chujo, Y., *J. Am. Chem. Soc.* **2014**, *136*, 18131-18139.

-
23. Adhikari, B.; Majumdar, S., *Prog. Polym. Sci.* **2004**, *29*, 699-766.
 24. Banica, F.-G., *Chemical Sensors and Biosensors: Fundamentals and Applications*. John Wiley & Sons: **2012**.
 25. Rodionova, O. Y.; Houmøller, L. P.; Pomerantsev, A. L.; Geladi, P.; Burger, J.; Dorofeyev, V. L.; Arzamastsev, A. P., *Anal. Chim. Acta* **2005**, *549*, 151-158.
 26. Kumar, B.; Baldi, A., *Curr. Drug Saf.* **2016**, *11*, 112-120.
 27. Hu, Z.; Deibert, B. J.; Li, J., *Chem. Soc. Rev.* **2014**, *43*, 5815-5840.
 28. Andrew, T. L.; Swager, T. M., *J. Am. Chem. Soc.* **2007**, *129*, 7254-7255.
 29. Albrecht, M.; Gossage, R. A.; Lutz, M.; Spek, A. L.; van Koten, G., *Chem. Eur. J.* **2000**, *6*, 1431-1445.
 30. Aragay, G.; Merkoç, A. J., *Electrochim. Acta* **2012**, *84*, 49-61.
 31. Alloway, B. J., *Heavy metals in soils* **2013**, *22*, 11-50.
 32. Chouteau, C.; Dzyadevych, S.; Durrieu, C.; Chovelon, J.-M., *Biosens. Bioelectron.* **2005**, *21*, 273-281.
 33. Rakow, N. A.; Suslick, K. S., *Nature* **2000**, *406*, 710.
 34. Zhang, C.; Suslick, K. S., *J. Agric. Food Chem.* **2007**, *55*, 237-242.
 35. Feng, L.; Musto, C. J.; Kemling, J. W.; Lim, S. H.; Suslick, K. S., *Chem. Commun.* **2010**, *46*, 2037-2039.
 36. Swager, T. M., *Acc. Chem. Res.* **1998**, *31*, 201-207.
 37. Liu, S.; Tian, J.; Wang, L.; Zhang, Y.; Qin, X.; Luo, Y.; Asiri, A. M.; Al-Youbi, A. O.; Sun, X., *Adv. Mater.* **2012**, *24*, 2037-2041.
 38. Liu, X.; Tang, Y.; Wang, L.; Zhang, J.; Song, S.; Fan, C.; Wang, S., *Adv. Mater.* **2007**, *19*, 1471-1474.
 39. Stringer, R. C.; Gangopadhyay, S.; Grant, S., *Anal. Chem.* **2010**, *82*, 4015-4019.
 40. Li, C.; Numata, M.; Takeuchi, M.; Shinkai, S., *Angew. Chem. Int. Ed* **2005**, *117*, 6529-6532.
 41. Chen, Z.; Wu, P.; Cong, R.; Xu, N.; Tan, Y.; Tan, C.; Jiang, Y., *ACS Appl. Mater. Interfaces* **2015**, *8*, 3567-3574.
 42. Whitcombe, M. J.; Chianella, I.; Larcombe, L.; Piletsky, S. A.; Noble, J.; Porter, R.; Horgan, A. *Chem. Soc. Rev.* **2011**, *40*, 1547-1571.
 43. You, C.-C.; Miranda, O. R.; Gider, B.; Ghosh, P. S.; Kim, I.-B.; Erdogan, B.; Krovi, S. A.; Bunz, U. H. F.; Rotello, V. M., *Nat. Nanotechnol.* **2007**, *2*, 318.
 44. Gaylord, B. S.; Heeger, A. J.; Bazan, G. C., *PNAS* **2002**, *99*, 10954-10957.
 45. Liu, B.; Bazan, G. C., *Chem. Mater.* **2004**, *16*, 4467-4476.

-
46. Han, J.; Bender, M.; Seehafer, K.; Bunz, U. H. F., *Angew. Chem. Int. Ed* **2016**, *55*, 7689-7692.
47. Han, J.; Ma, C.; Wang, B.; Bender, M.; Bojanowski, M.; Hergert, M.; Seehafer, K.; Herrmann, A.; Bunz, U. H. F., *Chem* **2017**, *2*, 817-824.
48. Hagihara, S.; Tanaka, H.; Matile, S., *J. Am. Chem. Soc.*, **2008**, *130*, 5656-5657.
49. Bender, M.; Bojanowski, N. M.; Seehafer, K.; Bunz, U. H. F., *Chem. Eur. J.* **2018**, *24*, 13102-13105.
50. Han, J.; Wang, B.; Bender, M.; Kushida, S.; Seehafer, K.; Bunz, U. H. F., *ACS Appl. Mater. Interfaces* **2016**, *9*, 790-797.
51. Han, J.; Wang, B.; Bender, M.; Pfisterer, J.; Huang, W.; Seehafer, K.; Yazdani, M.; Rotello, V. M.; Rotello, C. M.; Bunz, U. H. F., *Polym. Chem.* **2017**, *8*, 2723-2732.
52. Kim I-B.; Dunkhorst A.; Gilbert J.; Bunz, U. H. F., *Macromolecules* **2005**, *38*, 4560-4562.
53. Rochat, S.; Swager, T. M., *Angew. Chem. Int. Ed* **2014**, *53*, 9792-9796.
54. Wang, F.; Gu, H.; Swager, T. M., *J. Am. Chem. Soc.* **2008**, *130*, 5392-5393.
55. Askim, J. R.; Mahmoudi, M.; Suslick, K. S., *Chem. Soc. Rev.* **2013**, *42*, 8649-8682.
56. Zhou, H.; Baldini, L.; Hong, J.; Wilson, A. J.; Hamilton, A. D., *J. Am. Chem. Soc.* **2006**, *128*, 2421-2425.
57. Carey, J. R.; Suslick, K. S.; Hulkower, K. I.; Imlay, J. A.; Imlay, K. R.; Ingison, C. K.; Ponder, J. B.; Sen, A.; Wittrig, A. E., *J. Am. Chem. Soc.* **2011**, *133*, 7571-7576.
58. Liu, Y.; Minami, T.; Nishiyabu, R.; Wang, Z.; Anzenbacher Jr, P., *J. Am. Chem. Soc.* **2013**, *135*, 7705-7712.
59. Minami, T.; Esipenko, N. A.; Akdeniz, A.; Zhang, B.; Isaacs, L.; Anzenbacher Jr, P., *J. Am. Chem. Soc.* **2013**, *135*, 15238-15243.
60. Wright, A. T.; Anslyn, E. V., *Chem. Soc. Rev.* **2006**, *35*, 14-28.
61. Diehl, K. L.; Anslyn, E. V., *Chem. Soc. Rev.* **2013**, *42*, 8596-8611.
62. Miranda, O. R.; You, C.-C.; Phillips, R.; Kim, I.-B.; Ghosh, P. S.; Bunz, U. H. F.; Rotello, V. M., *J. Am. Chem. Soc.* **2007**, *129*, 9856-9857.
63. Gemperline, P., *Practical Guide to Chemometrics*. CRC press: **2006**.
64. Li, Z.; Askim, J. R.; Suslick, K. S., *Chem. Rev.* **2019**, *119*, 231-292.
65. Janzen, M. C.; Ponder, J. B.; Bailey, D. P.; Ingison, C. K.; Suslick, K. S., *Anal. Chem.* **2006**, *78*, 3591-3600.
66. Mungkarndee, R.; Techakriengkrai, I.; Tumcharern, G.; Sukwattanasinitt, M., *Food Chem.* **2016**, *197*, 198-204.
67. Wang, B. H.; Han, J. S.; Bender, M.; Hahn, S.; Seehafer, K.; Bunz, U. H. F., *Acs Sens.* **2018**, *3*, 504-511.

-
68. Neilson, A.; Allard, A., *The Handbook of Environmental Chemistry. Part J. PAHs and Related Compounds* **1998**, 1-80.
69. Rickert, D. E., *Toxicity of Nitroaromatic Compounds*. CRC Press: **1985**.
70. Isayev, O.; Rasulev, B.; Gorb, L.; Leszczynski, J., *Mol. Divers.* **2006**, *10*, 233-245.
71. Donlon, B. A.; Razo-Flores, E.; Field, J. A.; Lettinga, G., *Appl. Environ. Microbiol.* **1995**, *61*, 3889-3893.
72. Purohit, V.; Basu, A. K., *Chem. Res. Toxicol.* **2000**, *13*, 673-692.
73. Wu, J. T.; Tan, C. Y.; Chen, Z. F.; Chen, Y. Z.; Tan, Y.; Jiang, Y. Y., *Analyst* **2016**, *141*, 3242-3245.
74. Håkansson, K.; Coorey, R. V.; Zubarev, R. A.; Talrose, V. L.; Håkansson, P., *J. Mass Spectrom.* **2000**, *35*, 337-346.
75. Moore, D. S.; Scharff, R. J., *Anal. Bioanal. Chem.* **2009**, *393*, 1571-1578.
76. Sylvia, J. M.; Janni, J. A.; Klein, J.; Spencer, K. M., *Anal. Chem.* **2000**, *72*, 5834-5840.
77. Hallowell, S. F., *Talanta* **2001**, *54*, 447-458.
78. Eiceman, G.; Stone, J., *Anal. Chem* **2004**, *76*, 390-397.
79. Deshmukh, A.; Bandyopadhyay, S.; James, A.; Patra, A., *J. Mater. Chem. C* **2016**, *4*, 4427-4433.
80. Sohn, H.; Sailor, M. J.; Magde, D.; Trogler, W. C., *J. Am. Chem. Soc.* **2003**, *125*, 3821-3830.
81. Yang, J. S.; Swager, T. M., *J. Am. Chem. Soc.* **1998**, *120*, 5321-5322.
82. McQuade, D. T.; Pullen, A. E.; Swager, T. M., *Chem. Rev.* **2000**, *100*, 2537-2574.
83. McNeil, A. J.; Muller, P.; Whitten, J. E.; Swager, T. M., *J. Am. Chem. Soc.* **2006**, *128*, 12426-12427.
84. Levine, M.; Song, I.; Andrew, T. L.; Kool, S. E.; Swager, T. M., *J. Polym. Sci. A* **2010**, *48*, 3382-3391.
85. Tsuchihara, K.; Masuda, T.; Higashimura, T., *J. Am. Chem. Soc.* **1991**, *113*, 8548-8549.
86. Albert, K. J.; Walt, D. R., *Anal. Chem.* **2000**, *72*, 1947-1955.
87. Yang, J. S.; Swager, T. M., *J. Am. Chem. Soc.* **1998**, *120*, 11864-11873.
88. Saxena, A.; Fujiki, M.; Rai, R.; Kwak, G., *Mater.* **2005**, *17*, 2181-2185.
89. McGill, R. A.; Mlsna, T. E.; Chung, R.; Nguyen, V. K.; Stepnowski, J.; Abraham, M. H.; Kobrin, P. H., *SPIE* **1998**, 384-390.
90. Singh, S., *J. Hazard. Mater.* **2007**, *144*, 15-28.
91. Chen, J.; Law, C. C.; Lam, J. W.; Dong, Y.; Lo, S. M.; Williams, I. D.; Zhu, D.; Tang, B. Z., *Chem. Mater.* **2003**, *15*, 1535-1546.

-
92. Qin, A.; Lam, J. W.; Tang, L.; Jim, C. K.; Zhao, H.; Sun, J.; Tang, B. Z., *Macromolecules* **2009**, *42*, 1421-1424.
93. Wu, J.; Liu, W.; Ge, J.; Zhang, H.; Wang, P., *Chem. Soc. Rev.* **2011**, *40*, 3483-3495.
94. Sun, X.; Wang, Y.; Lei, Y., *Chem. Soc. Rev.* **2015**, *44*, 8019-8061.
95. Förster, T., *Naturwissenschaften* **1946**, *6*, 166-175.
96. Nagarkar, S. S.; Desai, A. V.; Ghosh, S. K., *Chem. Commun.* **2014**, *50*, 8915-8918.
97. Sapsford, K. E.; Berti, L.; Medintz, I. L., *Angew. Chem. Int. Ed* **2006**, *45*, 4562-4589.
98. Kim, J. S.; Quang, D. T., *Chem. Rev.* **2007**, *107*, 3780-3799.
99. You, L.; Zha, D.; Anslyn, E. V., *Chem. Rev.* **2015**, *115*, 7840-7892.
100. Xu, Y.; Li, B.; Li, W.; Zhao, J.; Sun, S.; Pang, Y., *Chem. Commun.* **2013**, *49*, 4764-4766.
101. Huang, W.; Smarsly, E.; Han, J.; Bender, M.; Seehafer, K.; Wacker, I.; Schröder, R. R.; Bunz, U. H. F., *ACS Appl. Mater. Interfaces* **2017**, *9*, 3068-3074.
102. Long, Y.; Chen, H.; Yang, Y.; Wang, H.; Yang, Y.; Li, N.; Li, K.; Pei, J.; Liu, F., *Macromolecules* **2009**, *42*, 6501-6509.
103. Goubard, F.; Dumur, F., *RSC Adv.* **2015**, *5*, 3521-3551.
104. Huang, C.; Fu, W.; Li, C.-Z.; Zhang, Z.; Qiu, W.; Shi, M.; Heremans, P.; Jen, A. K.-Y.; Chen, H., *J. Am. Chem. Soc.* **2016**, *138*, 2528-2531.
105. Cao, X.-Y.; Zhang, W.-B.; Wang, J.-L.; Zhou, X.-H.; Lu, H.; Pei, J., *J. Am. Chem. Soc.* **2003**, *125*, 12430-12431.
106. Cao, X.-Y.; Zhou, X.-H.; Zi, H.; Pei, J., *Macromolecules* **2004**, *37*, 8874-8882.
107. Sonogashira, K.; Tohda, Y.; Hagihara, N., *Tetrahedron Lett.* **1975**, *16*, 4467-4470.
108. Nagarkar, S. S.; Joarder, B.; Chaudhari, A. K.; Mukherjee, S.; Ghosh, S. K., *Angew. Chem. Int. Ed* **2013**, *52*, 2881-2885.
109. Nagarkar, S. S.; Desai, A. V.; Ghosh, S. K., *Chem. Commun.* **2014**, *50*, 8915-8918.
110. Hu, Z.; Lustig, W. P.; Zhang, J.; Zheng, C.; Wang, H.; Teat, S. J.; Gong, Q.; Rudd, N. D.; Li, J., *J. Am. Chem. Soc.* **2015**, *137*, 16209-16215.
111. Xu, B.; Wu, X.; Li, H.; Tong, H.; Wang, L., *Macromolecules* **2011**, *44*, 5089-5092.
112. Zong & Chen, Y., *Analyst* **2016**, *141*, 3242-3245.
113. Germain, M. E.; Knapp, M. J., *J. Am. Chem. Soc.* **2008**, *130*, 5422-5423.
114. Tian, J.; Chen, H.; Zhuo, L.; Xie, Y.; Li, N.; Tang, B. Z. *Chem. Eur. J.* **2011**, *17*, 6626-6634.
115. Liang, Z.; Chen, H.; Wang, X.; Sun, R., *Dyes Pigm.* **2016**, *125*, 367-374.
116. Rainò G.; Stöferle, T.; Park, C.; Kim, H. C.; Chin, I. J.; Miller, R. D.; Mahrt, R. F., *Adv. Mater.* **2010**, *22*, 3681-3684.
117. Chowdhury, A.; Mukherjee, P. S., *J. Org. Chem.* **2015**, *80*, 4064-4075.

-
118. Huang, W.; Bender, M.; Seehafer, K.; Wacker, I.; Schröder, R. R.; Bunz, U. H. F., *Macromolecules* **2018**, *51*, 1345-1350.
119. Hong, Y.; Lam, J. W.; Tang, B. Z., *Chem. Soc. Rev.* **2011**, *40*, 5361-5388.
120. Luo, J.; Xie, Z.; Lam, J. W.; Cheng, L.; Chen, H.; Qiu, C.; Kwok, H. S.; Zhan, X.; Liu, Y.; Zhu, D., *Chem. Commun.* **2001**, *27*, 1740-1741.
121. Yang, Z.; Qin, W.; Leung, N. L.; Arseneault, M.; Lam, J. W.; Liang, G.; Sung, H. H.; Williams, I. D.; Tang, B. Z., *J. Mater. Chem. C* **2016**, *4*, 99-107.
122. Sun, N.; Su, K.; Zhou, Z.; Yu, Y.; Tian, X.; Wang, D.; Zhao, X.; Zhou, H.; Chen, C., *ACS Appl. Mater. Interfaces* **2018**, *10*, 16105-16112.
123. Zhao, E.; Chen, Y.; Wang, H.; Chen, S.; Lam, J. W.; Leung, C. W.; Hong, Y.; Tang, B. Z., *ACS Appl. Mater. Interfaces* **2015**, *7*, 7180-7188.
124. Liu, X.; Liang, G., *Chem. Commun.* **2017**, *53*, 1037-1040.
125. Hong, Y.; Chen, S.; Leung, C. W. T.; Lam, J. W. Y.; Liu, J.; Tseng, N.-W.; Kwok, R. T. K.; Yu, Y.; Wang, Z.; Tang, B. Z., *ACS Appl. Mater. Interfaces* **2011**, *3*, 3411-3418.
126. Bender, M.; Seehafer, K.; Findt, M.; Bunz, U. H. F., *RSC Adv.* **2015**, *5*, 96189-96193.
127. Wang, B.; Han, J.; Bender, M.; Seehafer, K.; Bunz, U. H. F., *Macromolecules* **2017**, *50*, 4126-4131.
128. Zhao, D.; Swager, T. M., *Macromolecules* **2005**, *38*, 9377-9384.
129. Huang, W.; Bender, M.; Seehafer, K.; Wacker, I.; Schröder, R. R.; Bunz, U. H. F., *Macromol. Rapid Commun.* **2018**, 1800774.
130. Xu, B.; Chi, Z.; Zhang, J.; Zhang, X.; Li, H.; Chen, C.; Liu, S.; Zhang Y.; Xu, J., *Chem. Commun.* **2011**, *47*, 11080-11082
131. Li, H.; Chi, Z.; Xu, B.; Zhang, X.; Li, X.; Liu, S.; Zhang Y.; Xu, J., *J. Mater. Chem.* **2011**, *21*, 3760-3767.
132. Zhang, X.; Chi, Z.; Zhang, J.; Li, H.; Xu, B.; Li, X.; Liu, S.; Zhang Y.; Xu, J., *J. Phys. Chem. B* **2011**, *115*, 7606-7611.
133. Xu, B.; Xie, M.; He, J.; Xu, B.; Chi, Z.; Tian, W.; Jiang, L.; Zhao, F.; Liu, S.; Zhang, Y.; Xu Z.; Xu, J., *Chem. Commun.* **2013**, *49*, 273-275.
134. Chi, Z.; Zhang, X.; Xu, B.; Zhou, X.; Ma, C.; Zhang, Y.; Liu, S.; Xu, J., *Chem. Soc. Rev.* **2012**, *41*, 3878-3896.
135. Zhao, Z.; Chen, S.; Lam, J. W.; Lu, P.; Zhong, Y.; Wong, K. S.; Tang, B. Z. *Chem. Commun.* **2010**, *46*, 2221-2223.
136. Zhao, N.; Yang, Z.; Lam, J. W.; Sung, H. H.; Xie, N.; Chen, S.; Su, H.; Gao, M.; Williams, D.; Wong, K. S.; Tang, B. Z., *Chem. Commun.* **2012**, *48*, 8637-8639.
137. Chen, Y.; Han, H.; Tong, H.; Chen, T.; Wang, H.; Ji, J.; Jin, Q., *ACS Appl. Mater. Interfaces* **2016**, *8*, 21185-21192.

-
138. Joarder, B.; Desai, A. V.; Samanta, P.; Mukherjee, S.; Ghosh, S. K., *Chem. Eur. J.* **2015**, *21*, 965-969.
139. Germain, M. E.; Knapp, M. J., *J. Am. Chem. Soc.* **2008**, *130*, 5422-5423.
140. Amaro, M.; Filipe, H. A.; Ramalho, J. P.; Hof, M.; Loura, L. M., *Phys. Chem. Chem. Phys.* **2016**, *18*, 7042-7054.
141. Kim, H. W.; Choi, M. G.; Park, H.; Lee, J. W.; Chang, S.-K., *RSC Adv.* **2015**, *5*, 4623-4627.
142. Onoda, M.; Uchiyama, S.; Santa, T.; Imai, K., *Luminescence* **2002**, *17*, 11-14.
143. Qin, W.; Li, K.; Feng, G.; Li, M.; Yang, Z.; Liu, B.; Tang, B. Z., *Adv. Funct. Mater.* **2014**, *24*, 635-643.
144. Grabowski, Z. R.; Rotkiewicz, K.; Rettig, W., *Chem. Rev.* **2003**, *103*, 3899-4032.
145. Cogan, S.; Zilberg, S.; Haas, Y., *J. Am. Chem. Soc.* **2006**, *128*, 3335-3345.
146. Yang, Z.; Qin, W.; Lam, J. W.; Chen, S.; Sung, H. H.; Williams, I. D.; Tang, B. Z., *Chem. Sci.* **2013**, *4*, 3725-3730.
147. Yang, J.-S.; Swager, T. M., *J. Am. Chem. Soc.* **1998**, *120*, 11864-11873.
148. Fulmer, G. R.; Miller, A. J.; Sherden, N. H.; Gottlieb, H. E.; Nudelman, A.; Stoltz, B. M.; Bercaw, J. E.; Goldberg, K. I., *Organometallics* **2010**, *29*, 2176-2179.
149. DeRose, P. C.; Early, E. A.; Kramer, G. W., *Rev. Sci. Instrum.* **2007**, *78*, 033107.
150. Würth, C.; Grabolle, M.; Pauli, J.; Spieles, M.; Resch-Genger, U., *Nat. Protoc.* **2013**, *8*, 1535-1550.
151. Gómez-Lor, B.; Frutos, Ó. d.; Ceballos, P. A.; Granier, T.; Echavarren, A. M., *Eur. J. Org. Chem.* **2001**, *11*, 2107-2114.
152. He, L.; Liu, X.; Liang, J.; Cong, Y.; Weng, Z.; Bu, W., *Chem. Commun.* **2015**, *51*, 7148-7151.
153. Seehafer, K.; Bender, M.; Schwaebel, S. T.; Bunz, U. H. F., *Macromolecules* **2014**, *47*, 7014-7020.
154. Jester, S.-S.; Idelson, A.; Schmitz, D.; Eberhagen, F.; Höger, S., *Langmuir* **2011**, *27*, 8205-8215.
155. Huang, J.; Jiang, Y.; Yang, J.; Tang, R.; Xie, N.; Li, Q.; Kwok, H. S.; Tang, B. Z.; Li, Z., *J. Mater Chem. C* **2014**, *2*, 2028-2036.

Eidesstattliche Versicherung gemäß § 8 der Promotionsordnung
der Naturwissenschaftlich-Mathematischen Gesamtfakultät der
Universität Heidelberg

Bei der eingereichten Dissertation zu dem Thema

**„Novel Conjugated Polymers: Synthesis and Application as Sensor Arrays for Detection
and Discrimination of Nitroaromatics“**

handelt es sich um meine eigenständig erbrachte Leistung.

Ich habe nur die angegebenen Quellen und Hilfsmittel benutzt und mich keiner unzulässigen Hilfe Dritter bedient. Insbesondere habe ich wörtlich oder sinngemäß aus anderen Werken übernommene Inhalte als solche kenntlich gemacht.

Die Arbeit oder Teile davon habe ich bislang nicht an einer Hochschule des In- oder Auslands als Bestandteil einer Prüfungs- oder Qualifikationsleistung vorgelegt.

Die Richtigkeit der vorstehenden Erklärung bestätige ich.

Die Bedeutung der eidesstaatlichen Versicherung und die strafrechtlichen Folgen einer unrichtigen oder unvollständig eidesstattlichen Versicherung sind mir bekannt.

Ich versichere an Eides statt, dass ich nach bestem Wissen die reine Wahrheit erkläre und nichts verschwiegen habe.

Ort und Datum

Unterschrift